Effect of planetary gearboxes on the dynamics of rotating systems

Ali Tatar

A thesis submitted to Imperial College London for the degree of Doctor of Philosophy

Department of Mechanical Engineering

Imperial College London

November 2019

To my family,

“Every conclusion will open

A new intro in your life

Which is an endless while loop”

Mr. Ali Tatar

“I'm free to say whatever I

Whatever I like

If it's wrong or right, it's alright”

Mr. Noel Gallagher

Declaration of originality

I hereby declare that the contents of this thesis are entirely my own work. Any additional sources of information have been duly cited in the thesis. This PhD research project has been carried out in the Dynamics Group of the Department of Mechanical Engineering at Imperial College London and funded by the Republic of Turkey, Ministry of National Education. This thesis is original and has not been submitted for any other degree or qualification in this, or any other university. Some parts of this thesis have been used in the following publications in which I am the first author.

- Tatar, A., Schwingshackl, C.W. and Friswell, M.I., 2019. Dynamic behaviour of three-dimensional planetary geared rotor systems. Mechanism and Machine Theory, 134, pp.39-56.

- Tatar, A., Salles, L., Haslam, A.H. and Schwingshackl, C.W., 2019. Comparison of Computational Generalized and Standard Eigenvalue Solutions of Rotating Systems. In Topics in Modal Analysis & Testing, Volume 9 (pp. 187-194). Springer, Cham.

- Tatar, A. and Schwingshackl, C.W., 2018, June. Effect of a Planetary Gearbox on the Dynamics of a Rotor System. In ASME Turbo Expo 2018: Turbomachinery Technical Conference and Exposition. American Society of Mechanical Engineers Digital Collection.

Ali Tatar

November 2019

Copyright declaration

Acknowledgement

Foremost, I would like to gratefully offer my thanks to my supervisor Dr Christoph Schwingshackl for providing the opportunity to carry out this PhD research and his invaluable support during my stay at Imperial College London.

I wish to express my gratitude to Professor Michael Friswell for sharing his great knowledge in rotor dynamics and vibration fields with me, the highly valued technical discussions and his useful comments and suggestions on my research.

I am also thankful to Professor Norbert Hoffmann and Dr Loic Salles for sharing their great theoretical knowledge and ideas related to this PhD research project with me.

A special thanks is extended to undergraduate and graduate supervisor Professor Kenan Yüce Şanlıtürk who encouraged me to do my PhD at Imperial College London.

I would like to thank all members of Dynamics Group of the Department of Mechanical Engineering, in which a warm thank you goes to Mr Peter Higgs who always offered his best advice for finding solutions to various issues we have encountered.

I would like to thank my close friends, who always supported me with their sincere intent. It is impossible to forget their supports at times of low ebb and struggles.

This PhD study was funded by the Republic of Turkey, Ministry of National Education. I am grateful to the Turkish Government for providing financial support.

Last but not least, I wish to express my deepest gratitude to my family and Savas family for always believing in me. I will never forget their dedicated unwavering support and patience during my studies at times of joy or sadness. Without their supreme altruism, love and care, this thesis would not have been possible.

Ali Tatar

November 2019

Abstract

The coupled dynamic behaviour of planetary geared rotor systems is much less well understood compared to the classical geared rotor systems. For a better understanding, this research project investigates the coupled dynamic behaviour of planetary geared rotor systems and how the planetary gearbox parameters affect their global dynamics. In the numerical study, a six degrees of freedom hybrid dynamic model of a planetary geared rotor system is created in the recently developed "GEAROT" rotor dynamics software by considering gyroscopic effects. Based on the modal analysis results of the hybrid dynamic model, the vibration modes are classified as coupled torsional-axial, lateral and gearbox for the helical gear configuration, and torsional, axial, lateral and gearbox for the spur one. Modal energy analysis is used to quantify the coupling level between the shafts and planetary gearbox, which highlights the effect of a planetary gearbox on the dynamic behaviour of a rotating system. An extensive planetary gearbox parameter study including gear contact, gearbox mass and support, and planet gear parameters is conducted using the hybrid dynamic model to investigate the parameter effects on the modal behaviour of planetary geared rotors. The sensitivity of planetary geared rotor vibration modes to the gearbox parameters is determined by computing the frequency shifts and comparing the mode shapes between the two extreme cases. In the experimental study, free-free impact hammer tests are carried out on a planetary geared rotor assembly to validate the numerical modal analyses results in "GEAROT". On the basis of both experimental and numerical modal analysis of planetary geared rotors, the lateral vibration modes are identified as "in phase" and "out of phase". Briefly, the numerically identified lateral modal behaviour of planetary geared rotor systems is successfully validated with the experimental modal analysis results.

Table of contents

List of tables

List of figures

Nomenclature

Symbols

q	Generalized coordinates
ξ	Natural coordinates
d	Diameter of shaft
l_e	Length of a beam element
ρ_e	Material density of beam elements
A_e	Cross-sectional area of beam elements
I_e	Second moment of area of beam elements
J_e	Polar moment of area of beam elements
E_e	Elasticity modulus of beam elements
G_e	Shear modulus of beam elements
ν_e	Poisson`s ratio
α_1, α_2	Proportional damping constants
N	Number of planets
r_c	Radius of carrier
m	Mass
I_d	Diametral mass moment of inertia
I_p	Polar mass moment of inertia
$\boldsymbol{\Omega}$	Rotating speed of elements
k_x	Support bearing stiffness in x direction
k_y	Support bearing stiffness in y direction
k_z	Support bearing stiffness in z direction
k_{Q_x}	Support bearing stiffness in Q_x direction
k_{Q_y}	Support bearing stiffness in Q_y direction
k_{Q_z}	Support bearing stiffness in Q_z direction
c_x	Support bearing damping in x direction
c_y	Support bearing damping in y direction
c_z	Support bearing damping in z direction
c_{Q_x}	Support bearing damping in Q_x direction
c_{Q_y}	Support bearing damping in Q_y direction
c_{Q_z}	Support bearing damping in Q_z direction
T	Kinetic energy
V	Potential energy
L	Total energy
ε	Modal energy ratio

Subscripts

$h = r, c, s$	Central member index
r	Ring gear
c	Carrier
s	Sun gear
p	Planet gear

Abbreviations

FRF	Frequency response function
DOF	Degree of freedom
SDOF	Single degree of freedom
MDOF	Multi-degrees of freedom
BW	Backward whirling
FW	Forward whirling
LAPACK	Linear algebra package
SEP	Standard eigenvalue problem
GEP	Generalized eigenvalue problem
PTM	Purely torsional model
TTM	Torsional-transverse model
TDM	Three-dimensional model
rpm	Revolution per minute
MAC	Modal assurance criteria
ICP	Integrated circuit piezoelectric

Chapter 1

1 Introduction

1.1 Background and motivation

Rotating machinery vibration has always become a significant engineering problem in industries such as automotive, aerospace, turbomachinery and wind power etc. For optimum system performance, safety and customer satisfaction, the manufacturers aim to reduce the noise and vibration of their rotating machine products. Therefore, they conduct extensive numerical and experimental studies before mass production so as to predict the dynamic behaviour of the rotating machines accurately. So far, a good understanding of underlying physics of rotating systems has been achieved, including gyroscopic moments, centrifugal and unbalance forces. Rotor dynamic modelling approaches such as rigid and flexible disks, bearings and shafts, linear and nonlinear bearing stiffness and damping, asymmetric and symmetric rotor geometries, and vibrational behaviour of rotor systems in terms of uncoupled and coupled lateral, torsional and axial vibrations have been investigated in detail and shown by many basic rotor dynamics books [1–5].

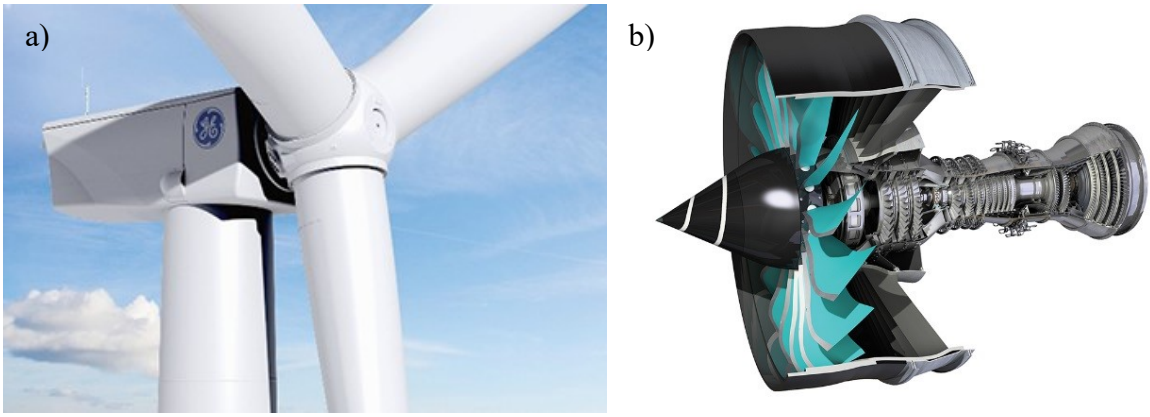

Figure 1.1: Planetary gearbox applications, a) wind turbine [Source: General Electric], b) geared turbofan engine [Source: Rolls-Royce plc].

A new trend couples rotating shafts with large planetary gearboxes in high power rotating machinery applications such as wind turbines and geared turbofan engines as seen in Figure 1.1. Planetary gearboxes are widely seen in rotating systems because of their compactness, higher speed ratio, load sharing and power transmission capacity, and lower stress, vibration and noise advantages [6,7]. On the other hand, installation of a planetary gearbox into a rotating system introduces coupled dynamic problems which includes the dynamics of the gearbox and whole rotor system. The planetary gearbox can affect the global dynamic behaviour of the rotor system with its mass and inertia, stiffness and damping, and gyroscopic moments. As a result, it changes the modal properties of the global rotor system in terms of natural frequencies, mode shapes, frequency response functions and modal damping. Moreover, the planetary gearbox can become a new source of vibration by introducing new vibration excitations into the global rotor system. These are known as internal vibration excitations due to transmission error, manufacturing error, tooth profile modifications and time-varying mesh stiffness, and external vibration excitations due to the unbalanced rotating gear wheels, geometric eccentricities, and torque/speed fluctuations of gears [8–10]. Briefly, a planetary gearbox may have both positive and negative effects on the dynamic response of the global rotor system in terms of mechanical vibration.

A large amount of research has been conducted on planetary gearbox dynamics to investigate the modal behaviour of planetary gears, the linear and nonlinear vibrations of the gears inside the planetary gearbox with the effects of internal and external excitations, and loss of tooth contact [6,7,10]. Overall, good progress has been made in understanding the linear and nonlinear dynamics of the planetary gearbox. A considerable amount of research has also been done for understanding the dynamic behaviour of geared rotor systems [9,11,12]. However, there is little work to understand the dynamic behaviour of planetary geared rotor systems since the complex interaction between the planetary gearbox and the rotor system makes the rotor dynamics problem challenging to solve numerically. Adding a planetary gearbox on high-speed rotating systems can directly affect their global dynamics due to the gyroscopic moments, flexibility, damping, mass and inertia of the planetary gearbox, additional excitation sources from the planetary gearbox, and coupling between the planetary gearbox and global rotor system. For a better understanding of the planetary gearbox effect on the dynamics of rotating systems with these considered effects, more research studies are needed. This is the main motivation of this PhD project.

1.2 Research objectives

The main aim of this research project is to understand the dynamic behaviour of a rotating system with a planetary gearbox and to investigate how a planetary gearbox parameter influences the global dynamics of the rotating system. To meet this aim, six main objectives will be addressed in this research project:

1. Create a six degrees of freedom hybrid dynamic model of the planetary geared rotor system with its damping, stiffness, mass and gyroscopic parameters, and employ the lumped parameter and finite element methods for the dynamic modelling of the planetary gearbox and rotor system, respectively.

2. Develop a rotor dynamics software called “GEAROT” for predicting the dynamic response and analysing the dynamic behaviour of the planetary geared rotor system using the hybrid dynamic model.

3. Identify the vibration modes of the planetary geared rotor systems with and without gyroscopic effects and analyse the impact of the planetary gearbox on the vibration modes of the global rotor system using the modal energy analysis.

4. Investigate the effects of the gearbox parameters on the modal behaviour of the planetary geared rotor systems to determine the influential gearbox parameters on the global dynamics of the rotor system.

5. Design a geared rotor test rig by coupling two shafts with a planetary gearbox to carry out the experimental modal analysis.

6. Validate the numerical computations of the developed hybrid dynamic model against the experimental modal analysis results.

In order to rise to these challenges and answer the research questions, numerical and experimental studies will be shown within the scope of this thesis.

1.3 Thesis outline

This thesis investigates the coupled dynamic behaviour of a planetary geared rotor system with numerical simulations and experiments, showing gearbox parameter effects on the dynamic behaviour of the global rotor system with numerical simulations. It also presents a new method for quantifying the coupling level between the rotor system and planetary gearbox, highlighting the effect of a planetary gearbox on the dynamic behaviour of a rotating system. This thesis consists of seven chapters which include introduction, literature review, dynamic modelling, numerical analyses, experimental studies and conclusion parts.

In the first chapter, the background and main motivation of this thesis are presented, which highlights the importance of the rotating machinery vibration and coupled rotor dynamic problem with the installation of a planetary gearbox. An explanation is also given for why more research is needed to understand the planetary gearbox effect on the dynamics of rotating systems. Following this, research objectives are lined up with six bullet points. Finally, an outline of the thesis is given. This chapter is a brief introduction to the thesis.

In the second chapter, an extensive literature review is given in four main sections, including dynamics of rotating systems, gear dynamics, planetary gear dynamics and geared rotor dynamics research with their brief history. Crucial points in rotating machinery vibration, modelling and solution method of rotor dynamics problem are presented in the dynamics of rotating systems section. Linear and nonlinear gear dynamics research, gear dynamic modelling approaches, gear vibration and planetary gear dynamics research are presented in gear dynamics and planetary gear dynamics sections. Finally, geared rotor dynamics research is discussed in detail.

In the third chapter, a six degrees of freedom hybrid dynamic model of a rotor system with a planetary gearbox is introduced where the dynamic models of the planetary gearbox and rotor system are created with the lumped parameter and finite element methods respectively. In the rotor system, the shafts are modelled with 1-D rotating Timoshenko beam elements and the bearings are assumed to consist of uncoupled linear spring elements. Finally, the equation of motion of the planetary geared rotor system is obtained by combining the dynamic model of the planetary gearbox and rotor system.

In the fourth chapter, the theoretical background of the modal analysis of rotating systems is presented where the quadratic eigenvalue problem due to the damping and gyroscopic effects and the modal energy analysis are provided. The modal analyses are carried out for both helical

and spur planetary geared rotors with and without gyroscopic effects in order to determine their vibration modes and modal behaviour. Planetary gearbox effect on the vibration modes of the global rotor system is then quantified with the modal energy analyses.

In the fifth chapter, the effects of the planetary gearbox parameters on the vibration modes of the planetary geared rotor systems are presented. Sensitivity of natural frequencies and vibration modes to the gearbox parameters are investigated for the gear contact parameters such as gear mesh stiffness, helix angle and pressure angle, gearbox mass and support parameters such as gear material density and support stiffness, and planet gear parameters such as number of planet gears and planet position errors (mistuning).

In the sixth chapter, a spur planetary geared rotor test rig is presented, where free-free modal tests in the lateral directions are carried out to validate the numerical modal analysis results. Lateral modal behaviour of the planetary geared rotor assembly and shafts is shown separately with the experimental modal analysis. Finite element (numerical) modal analysis results of the shafts are validated with their experimental modal analysis results. For the free-free modal tests of the planetary geared rotor assembly, dynamic model of the planetary geared rotor system is updated. Then, the model validation is conducted with the experimental modal analysis results.

In the seventh chapter, the main findings and conclusions are summarised, and recommendations for the future works are presented.

Chapter 2

2 Literature review

2.1 Introduction

This chapter summarises the existing technical knowledge and research concerned with this PhD project. The main objective of this literature survey is to understand the state-of-the-art in the planetary gearbox and rotor dynamics and to introduce important topics related to the research problem which is described in the previous section. With the consideration of the combined engineering problem of the planetary gearbox and rotating system, the literature survey is divided into four main sections including dynamics of rotating systems, gear dynamics, planetary gearbox dynamics and geared rotor dynamics.

2.2 Dynamics of rotating systems

The long history of rotor dynamics commenced with the invention of the wheel and continued with water wheels, windmills and steam engines. Following the invention of the first steam engine, science and technology have hit the top with the development of turbomachinery. Rotor dynamics, as a scientific subject, has been at the centre of these developments in the technology.

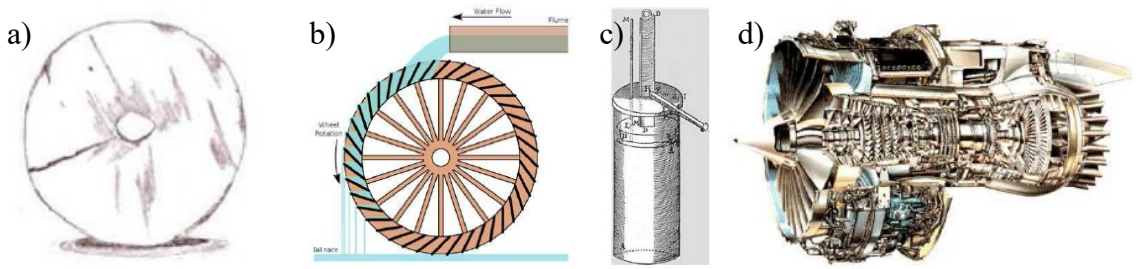

Figure 2.1 : Historical development in rotating systems, a) invention of the wheel, b) the water wheel, c) first steam engine, d) turbofan engine [4].

Today, rotating systems can be seen in a wide range of engineering applications such as jet engines, wind turbines, steam turbines, combustion engines, automotive powertrains, marine propulsion systems and gearboxes.

2.2.1 Vibrations of rotating systems

Rotor dynamics is a special topic of dynamics focusing on the dynamic behaviour of rotating systems in lateral, torsional and axial vibrations [1–4]. The dynamic analysis of a rotating system is substantially different from the classical vibrating systems because the gyroscopic moments acting on the rotating system can affect its eigenvalues and eigenvectors with respect to the rotating speed of the system. Notably, lateral vibrations in a rotor system are more crucial compared with the torsional and axial vibrations due to the gyroscopic effects. Lateral vibration modes are speed-dependent due to the gyroscopic couples, whereas torsional and axial vibration modes are not generally dependent on the rotational speeds [3]. Axial vibrations in a rotor system can be seen in jet engines due to the thrust in the axial direction or helical gears due to the occurrence of axial forces [3]. Furthermore, torsional vibrations can originate from the crankshafts of internal combustion engines, sudden changes in the running condition, or uneven loads on the shaft.

Vibration modes of the rotating systems are different compared with the non-rotating systems. The reason is that the gyroscopic couple results in backward and forward whirling modes in the rotating system where the forward whirling mode and the rotating speed are in the same direction while the backward whirling mode is in the opposite direction to the rotating speed [1–4]. It is worth stating that the backward whirling modes can be excited during a deceleration whereas the forward whirling modes can be excited during an acceleration in a single rotor system. Both forward and backward whirling modes can be excited simultaneously in a counter-rotating rotor system. When looking at the general equation of motion in the matrix form, the gyroscopic matrix has a skew-symmetric property. Therefore, both the skew-symmetry property of the gyroscopic matrix and the spin speed have effects on the whirling modes.

A special tool in rotor dynamics is the natural frequency map (Campbell diagram) [1–4] which shows the changes of natural frequencies with respect to the rotational speed, as shown in Figure 2.2. It should be noted that only the lowest backward and forward modes are shown in Figure 2.2. If the rotor speed matches with the natural frequencies of the system, larger amplitudes will occur due to the resonating structure [13]. This so-called critical speed must be

avoided to prevent catastrophic failures in the rotor system design. The speed dependency of the vibration modes is the most significant property of rotor dynamics.

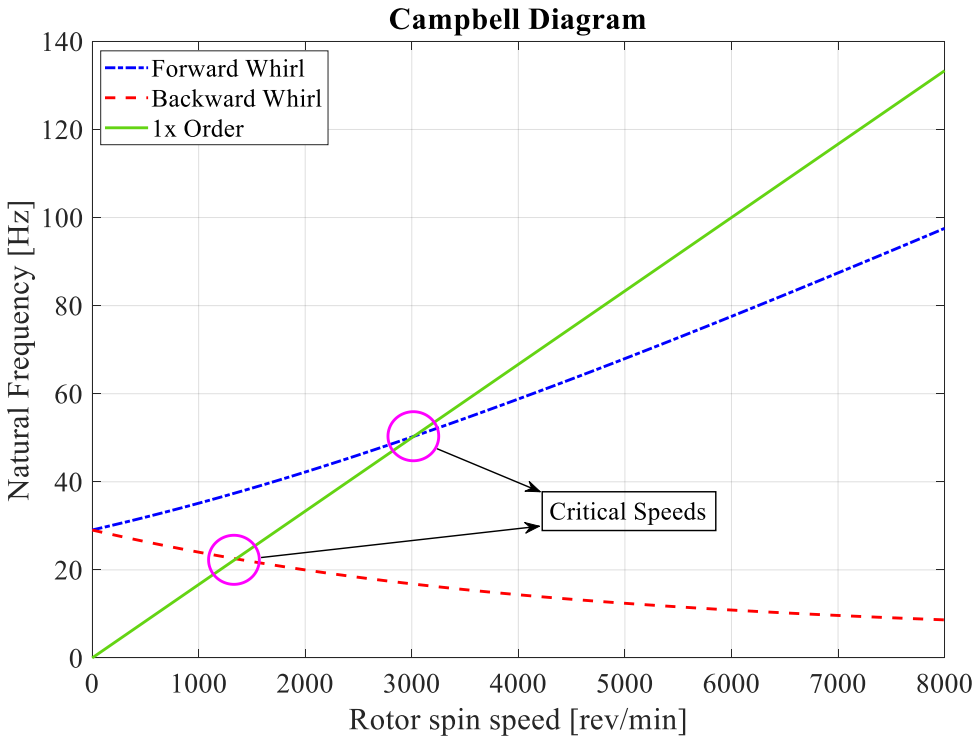

Figure 2.2 : Campbell diagram of a rigid rotor.

Rotor coupling

The coupling effect is an important research topic in rotating systems. Vibration in one direction can cause vibration in another direction due to the coupling phenomenon. Basically, lateral, torsional and axial vibrations can interact with each other in coupled rotor systems [3]. For example, coupled lateral-torsional vibrations is a commonly seen phenomenon in rotating systems where torsional excitations can trigger lateral vibrations. There are some articles in the literature to understand the torsional and lateral coupling effect [14–17]. For instance, Al-Bedoor [14] developed a model for the coupled vibration of unbalanced rotors, and he showed a softening effect of rotor torsional stiffness due to the coupling and a nonlinear interaction between the lateral and torsional vibrations. Then, Patel and Darpe [15] extended this research by investigating coupled lateral-torsional vibrations of rotors with cracks and rub, causing even stronger nonlinearity.

Excitation sources

Imbalances and external forces are the main excitation sources of rotating systems [1,3]. The internal imbalances come from inaccuracies in the manufacture of the system, and they can

create lateral forces at the frequency of rotation. This excitation can lead to an increase in the vibration level of rotating systems in the vicinity of a shaft resonance [3]. The vibrations in rotor dynamic systems are typically divided into two main categories as synchronous or subsynchronous. The synchronous vibrations are caused by imbalances or other synchronous forces, whereas the subsynchronous vibrations can be generated by fluid-induced excitations in the bearings [1–4,18].

2.2.2 Rotor dynamic modelling

A basic rotor system which consists of a single disk on a flexible shaft with bearings was first defined by Föppl in 1895, and it was refined by Jeffcott in 1919 after the damping addition to Föppl`s rotor definition [13,18]. The Jeffcott rotor model is quite simple to understand, and it forms the main backbone of rotor dynamics [13]. In a Jeffcott rotor, a rotating system fundamentally consists of a rotor, bearings and a rigid disk, as seen in Figure 2.3. The rotor can be modelled with a flexible beam and rigid disk, and the bearings may also be described with spring elements including stiffness [1–4].

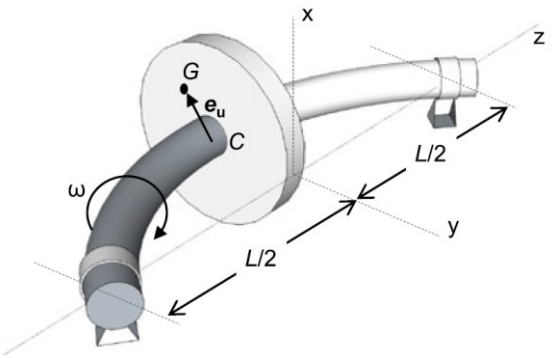

Figure 2.3 : Jeffcott rotor model [18].

In classic rotor dynamics, bearings are often described with stiffness and damping elements which may have speed dependent properties because of the spin softening effect of certain bearing types [3]. Nonlinear behaviour of the bearings can make the rotor dynamics problem even more complicated since an amplitude-dependent bearing stiffness can considerably affect the dynamic behaviour of a rotating system [13,19,20].

Another important modelling parameter in the rotor systems is damping which can exist in both shafts and bearings. Shafts may carry internal damping and bearings may have viscous damping property. It is important to state that the internal damping sometimes may have adverse effects on the rotor system, which can lead to instability [3]. Therefore, a reliable and well-controlled damping mechanism is crucial for a rotor dynamic system design.

Rotating beam theories

There are two main rotating beam theories used in rotor dynamics, which are known as the Timoshenko and Euler-Bernoulli beam theories [2–4]. The whirling deflections and speed-dependent modal properties of shafts can be calculated using both theories in the finite element method. The main differences between the two theories come from the assumptions. In the Euler-Bernoulli beam theory, shear deflections and rotary inertia effects are neglected while these effects are taken into account in Timoshenko beams [21,22]. When doing vibration analysis with an eigenvalue solution, the Timoshenko and Euler-Bernoulli beams give similar natural frequencies at lower frequencies, but they are considerably dissimilar at higher frequencies. The Timoshenko beam gives more accurate results than the Euler-Bernoulli Beam in modal analysis, but its implementation into a finite element solver can be somewhat more complicated.

2.2.3 Dynamic analysis of rotor dynamic systems

The dynamic solution of a simple rotor system such as the Jeffcott rotor is relatively easy. However, more complex systems which consist of a large number of elements represent a significantly bigger challenge. In order to solve the multi-degrees of freedom rotor systems, there are mainly two types of solution methods available, which are the transfer matrix method and the finite element method. In the past, the transfer matrix method [1–5] was a useful tool to solve the multi-degrees of freedom rotor systems. However, recently the finite element method has become much more popular tool to solve the rotor dynamics problems due to the decrease in the computation time with high performance computers [3,4,23]. Therefore, the finite element method will be the focus of this review.

One of the main advantages of the finite element method is the accurate and fast solving of mechanical problems. On the other hand, it can require a huge calculation volume [3,4]. Finite element methods discretise the structure into small elements based on the selected mesh sizes [2–5,18]. For each element, mass, stiffness, damping and gyroscopic matrices are formulated based on their material and geometric properties. A topology matrix then defines the connectivity between each element. As a result, the global matrices are obtained using the finite element assembly procedure. Finally, boundary conditions, such as bearings as stiffness and damping elements and disk elements as mass and inertia elements are added to the global matrices to obtain the full model of the rotor dynamic system.

Eigenvalue solution of rotating systems

Modal parameters such as eigenvalues and eigenvectors can be calculated using the final versions of the global matrices with the help of an eigenvalue solution of the dynamic problem. Eigenvalue solution of a mechanical system with damping or gyroscopic terms is more complicated since the damping and gyroscopic terms introduce the first derivative of the generalized coordinate to the equation of motion. The eigenvalue problem then becomes a quadratic eigenvalue problem, leading to a complex solution of the system [24,25]. The order of the linear differential equation can be reduced to one via a state-space model to solve the quadratic eigenvalue problem [26–30].

In large scale eigenvalue problems, matrices could have special properties; they may be symmetric, skew-symmetric, non-symmetric or Hermitian [31]. For example, the gyroscopic matrix for rotating systems is skew-symmetric, but the addition of damping leads to the loss of this property [32]. Therefore, the eigenvalue problem of the damped or undamped gyroscopic systems often requires special numerical methods for the correct solution, such as eigenvalue shifting techniques [33,34]. Various numerical methods and software tools have been developed to solve large-scale quadratic eigenvalue problems [31,35–37]. There are also existing studies investigating the solution of non-symmetric eigenvalue problems [38]. The Linear Algebra Package (LAPACK) [39], which is one of the most well-known pieces of software, is used to solve eigenvalue problems, including those with non-symmetric matrices. Another important development in the solution of eigenvalue problems has been algorithm reduction techniques, allowing calculation of only certain eigenvalues such as largest or smallest in magnitude [31]. Algorithm reduction is a convenient tool for reducing the computation time.

Eigenvalue problems can be formulated in two forms, (i) the standard eigenvalue problem (SEP) and (ii) the generalized eigenvalue problem (GEP). Inman [40] states that the standard eigenvalue solution is faster than the generalized eigenvalue solution in terms of computational performance. With this, it can be inferred that the standard eigenvalue solution is more advantageous than the generalized one. The global matrices of a dynamic system can sometimes be badly conditioned, which can lead to wrong solutions to the eigenvalue problem. Kannan et al. [41] emphasize the severity of ill-conditioning in the structural finite element analysis, and they state that modelling beam elements with large sections or small lengths can cause these kinds of problems.

2.3 Gear dynamics

Gears are widely known machine elements for power and motion transmission in rotating machines where their main duty is to convert torque and speed between the input and output shafts. Two types of gears which are helical and spur are mainly used in gearboxes, as seen in Figure 2.4. Due to the higher contact ratio advantage of helical gears compared with spur gears, less contact stress and vibration occur in helical gears, and as a result, less gear noise [42].

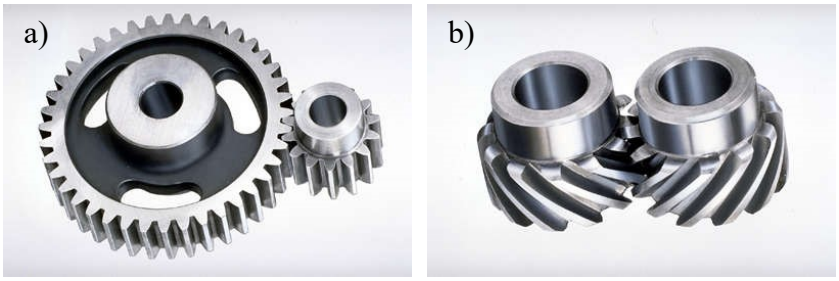

Figure 2.4 : a) spur gear, b) helical gear [Source: Emerson Power Transmission].

The first known gear dynamics research commenced in the 1920s, focusing on the dynamic loads on the gear teeth [9]. The dynamic loads are required to calculate the dynamic factor [43], which is defined as the ratio of maximum dynamic mesh force to maximum static mesh force. After the mid-20th century, for understanding the dynamic behaviour of gears, dynamic models which include spring, mass and damper systems were started to develop with the consideration of gear teeth stiffness and friction damping between the gear teeth [9,10,44,45]. In general, gear dynamics research can be categorised into three groups: (i) gear vibrations, (ii) gear dynamic models and (iii) nonlinear gear dynamics.

2.3.1 Gear vibrations

A large amount of research [9,10] was conducted on the internal dynamics of gear pairs to understand the gear vibration and noise extensively. Two main excitation sources, which are internal and external, can excite the dynamics of the gear systems [10]. External excitations are generally seen at lower frequencies, whereas internal excitations appear at high frequencies [8,46]. Both external and internal excitations can lead to an increase in vibrations as well as noise inside the gear system.

External excitations can occur due to the speed and torque fluctuations of gear shafts. Rotating mass unbalances on gear disks and geometric eccentricities may also become external excitation sources [8]. In practical gear applications, tooth separation or losing tooth contact is an inevitable case. Losing tooth contact within gear backlash (clearance between two gear

teeth) due to the physical relationship between the drag torque and gear inertia torque can result in heavy impacts between the gear teeth. In combination with external excitations such as the torque fluctuations and torsional vibrations on the gear pairs, these impacts can lead to excessive vibrations of the gear disks and the generation of broadband rattle noise [47–49]. Gear impacts are generally defined as (i) no impact, (ii) single side impact and (iii) double side impacts where the mean load on the gears determines the described conditions [8].

Internal excitation mechanisms acting on the gear drive systems are caused by gear parameters such as transmission error, time-varying mesh stiffness, gear or manufacturing errors and gear tooth profile [8–10]. Internal excitations induce deflection of gear teeth under load, leading to gear whine noise (meshing noise). In gear dynamic models, the transmission error, which is defined as the relative displacement between two gears, is assumed to be a periodic displacement excitation at the gear mesh contact [8,42,50]. The period of the displacement excitation is equal to the gear meshing frequency, which is calculated by multiplying the rotating frequency of the gear disk with the corresponding number of gear teeth. Some research was carried out to understand the gear tooth profile effect on the gear dynamics showing that the gear tooth profile has a significant effect on gear vibrations as well as gear noise due to reducing the dynamic loads on gear teeth [10]. The gear vibrations caused by both internal and external excitations can be transmitted outward via the shafts. As a result, it can make the gearbox an additional excitation source for a rotor dynamic system.

2.3.2 Gear dynamic models

The teeth contact between the gear pairs creates a dynamic problem under the operating conditions. Therefore, mathematical modelling of gear dynamic problems have largely been investigated so as to compute gear dynamic forces and estimate modal behaviour and parameters of the gear systems [9,10].

Lumped parameter and finite element methods are commonly used techniques for the dynamic analysis of gear systems. Gear mechanisms can be modelled using a single degree of freedom (SDOF) and multi-degrees of freedom (MDOF) systems [10]. Main model types can thereby be found in the literature, (i) SDOF model with a gear pair, (ii) MDOF model with a single mesh gear pair and (iii) MDOF model with multi-gear pairs [10].

In the lumped parameter method, gear bodies are assumed to be rigid, whereas gear teeth contacts and bearings are accepted as flexible. There are different lumped parameter modelling approaches for the gear pairs in the literature [9,10,44,45]. They can be grouped as the purely

torsional model (PTM), the torsional-transverse model (TTM) and the three-dimensional model (TDM) [7]. The purely torsional model is a one-dimensional model, which only considers torsional gear mesh and bearing stiffnesses [9]. It can provide fairly good results to understand the dynamic behaviour of the spur gears if the lateral vibrations are negligible. Gyroscopic effects at higher operating speeds and rotating unbalanced masses can result in significant lateral vibrations. Therefore, the torsional-transverse model is used for the analysis of high-speed gear systems, which additionally includes the transverse motion, leading to three degrees of freedom [51]. Axial vibrations are inevitable in helical gear pairs due to the occurrence of axial forces, which leads to an extension of torsional-transverse models to the three-dimensional models [45,52]. The three-dimensional model is the most advanced model, including all six degrees of freedom. The PTM and TTM models are suitable for analysing spur gears, but for helical gears, a TDM is required due to the occurrence of axial vibrations in the gears. Recently, the numerical results of the lumped parameter models of gear systems have been validated with the experimental studies [51,52].

In the finite element models, all the elements (gear bodies, contacts and bearings) are assumed to be flexible. Different hybrid modelling approaches such as finite element/contact mechanics model [53], finite element/lumped parameter model [54] and frequency domain finite element approach [55] have been proposed in the literature. Although there are numerous linear and nonlinear vibration analyses done with the analytical models (lumped parameter models), fewer studies have been conducted using the finite element method. For the tooth modes, the lumped parameter models can give fairly good results which are found to be consistent with the results of the finite element models. On the other hand, flexible gear body modes can only be detected with the finite element models. The finite element models also have the capability of detecting dynamic coupling between the gear tooth and gear bodies.

Gear contact dynamics

The contact between the gear teeth can be modelled with stiffness and damping elements. The gear mesh stiffness is higher at the middle of contact and softer at the end [8,10]. The global effect thereby is a stiffening spring behaviour, which can significantly change the frequency behaviour of the gear system. This effect can be modelled with a stiffness value that changes during the contact period, leading to a time-varying mesh stiffness. In numerical analyses, constant or time-dependent mesh stiffness are employed depending on the investigated gear problem. For heavily loaded gears, the constant mesh stiffness approach can be utilized,

because it is assumed that when the gears are heavily loaded, the gear pairs are always in contact [8].

Gear dynamic forces occur between the gear teeth driven by the stiffness and damping forces at gear meshes. The level of the gear dynamic forces depends on the mesh stiffness and damping, the gear mesh displacement vector and gear backlash during the gear contact period. In spur gears, only tangential forces at the gear mesh exist, whereas axial forces occur in helical gears.

2.3.3 Nonlinear gear dynamics

In gear vibration analysis, there are nonlinear factors such as clearance nonlinearity due to loss of teeth contact (gear backlash nonlinearity) and friction between gear teeth [8–10,56–58]. The linear gear dynamics models may not give accurate results at different operating conditions since the gear backlash acts as a nonlinear element. These factors are important to understand the nonlinear vibration characteristics of gear drive systems.

The nonlinear dynamic behaviour of gear systems due to the loss of teeth contact is shown by both numerical and experimental studies [8,10,46,50,59–68]. The loss of teeth contact is mathematically modelled with clearance nonlinearity expression for nonlinear dynamic analyses, which can be excited by the transmission error [8] and multi-frequency excitations [69]. The loss of teeth contact phenomenon is also accepted as a vibro-impact problem, due to the impacts between gear teeth. Two types of vibro-impact models are proposed in the literature as rigid and elastic impact models for the impact analysis [10]. Interactions between time-varying mesh stiffness and clearance nonlinearity have also been investigated in the nonlinear gear dynamic analyses [50,63,65,67,70]. Other nonlinear factors such as friction between gear teeth and nonlinear oil film forces have been less studied in the gear vibration analysis compared with the other factors [10,71–77].

A torsional dynamic model of a gear pair including clearance nonlinearity and time-varying mesh stiffness is shown in Figure 2.5 [8,67] where gear bodies are accepted as rigid, and the gear teeth contact is modelled with stiffness and damping elements. Equations of motion of the gear pair are written as

$$\begin{aligned} I_1\ddot{\theta}_1 + c_m r_1\left(r_1\dot{\theta}_1 - r_2\dot{\theta}_2 - \dot{e}(t)\right) + r_1 k_m(t) q(t) = T_1, \\ I_2\ddot{\theta}_2 - c_m r_2\left(r_1\dot{\theta}_1 - r_2\dot{\theta}_2 - \dot{e}(t)\right) - r_2 k_m(t) q(t) = -T_2, \end{aligned} \quad \textbf{(2.1)}$$

where θ_1 and θ_2 are the angular displacements, r_1 and r_2 are the radii of gears, I_1 and I_2 are the polar mass moment of inertias. Time-varying mesh stiffness and mesh damping, which are the gear teeth contact parameters, are represented by $k_m(t)$ and c_m, respectively. On the right-hand side of Eq. (2.1), T_1 and T_2 represent the net torques acting on the gears. In Eq. (2.1), $e(t)$ represents the external displacement excitation and $q(t)$ below represents nonlinear displacement function written as

$$q(t) = \begin{cases} r_1\theta_1 - r_2\theta_2 - e(t) - b, & r_1\theta_1 - r_2\theta_2 - e(t) > b \\ 0, & |r_1\theta_1 - r_2\theta_2 - e(t)| \le b \\ r_1\theta_1 - r_2\theta_2 - e(t) + b, & r_1\theta_1 - r_2\theta_2 - e(t) < -b \end{cases} \quad \textbf{(2.2)}$$

where $2b$ is the total gear backlash [67].

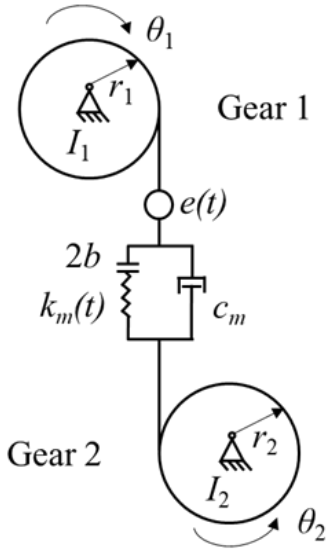

Figure 2.5 : Nonlinear torsional dynamic model of a gear pair.

To analyse the nonlinear characteristics of gear transmission systems, there are two main computation methods which are classified as numerical and analytical methods. Analytical methods can be grouped as piecewise-linear techniques, the harmonic balance method, the perturbation method and the shooting method [10]. The harmonic balance method is thereby the most popular in the analytical methods, and mainly single term or multiple terms are used in this method [7,10]. The disadvantage of using the single term is losing the nonlinearity phenomenon and limited precision [7]. Using multiple terms has importance in the analysis of multi-mesh gear systems [10]. Apart from the nonlinear vibration analysis of a single-stage gear system, research on the nonlinear vibration analyses of multi-stage gear systems was also conducted [78].

2.4 Planetary gearbox dynamics

Planetary gearboxes are widely used mechanical power transmissions in the industry because of their compactness, higher gear ratio and power transmission capacity, and lower noise and vibration advantages [6,7]. They can be seen in a wide range of military, helicopter, marine, automotive, aerospace and wind turbine applications.

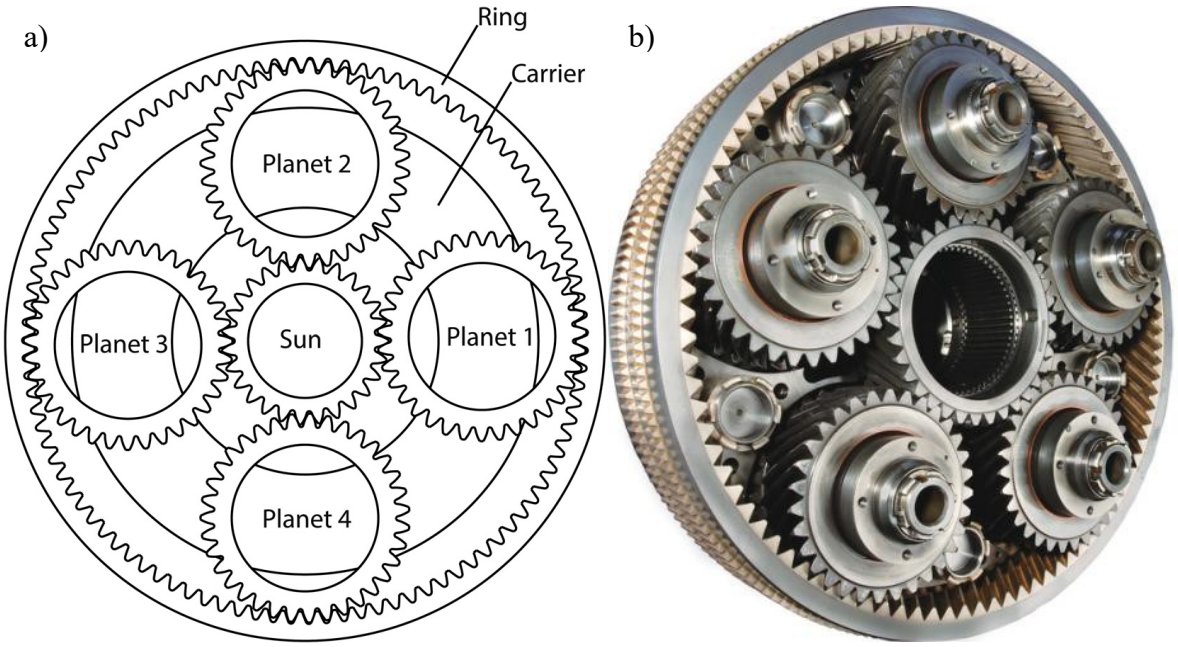

Figure 2.6 : Planetary gearbox, a) schematic [6], b) real application [Source: Pratt & Whitney].

Planet gear mechanisms mainly consist of a ring gear, a carrier, a sun gear and planet gears as seen in Figure 2.6. Motion and power are transmitted from the sun gear to the carrier or ring gear via the planet gears. The input and output shafts connected to the planetary gearbox are coaxially aligned, which makes planetary gearboxes as compact systems. Based on the application fields, planetary gearboxes can comprise of spur, helical or double helical gears. For instance, double-helical planetary gear sets are mostly used to cancel the axial gear mesh forces.

2.4.1 Planetary gear dynamic modelling

Dynamic modelling and linear analysis of planetary gearboxes with different configurations such as single-stage [79–82], two stages [83–85], multiple stages [86–91], compound [92–95] and double-helical [96–99] sets have been carried out extensively. Two main dynamic modelling approaches, flexible and rigid body models, have been employed by researchers.

In flexible body models, ring gears [54,85,100–104] and planet carriers [54,100] are common as flexible elements. A fully coupled dynamic modelling method using virtual equivalent shaft elements has recently been proposed [90,91]. Flexible body models can be classified as two dimensional [101–103], including transverse (lateral) and rotational (torsional) degrees of freedom, and three dimensional [54,90,91,100] models.

In rigid body models, the carrier and all gears (sun, planets, and ring) in the planetary gearbox are assumed to be rigid whereas the bearings and gear contacts are assumed to be flexible. Depending on the number of degrees of freedom, the rigid body dynamic models can be divided into three main groups: (i) purely torsional model, (ii) torsional-transverse model and (iii) three-dimensional model [7]. The purely torsional model has one degree of freedom per node and can be used for the analyses of spur planetary gearboxes if transverse, tilting and axial motions, and gyroscopic effects are negligible [86,88,92,95,105,106]. Expanding the purely torsional model to include transverse motions leads to the three degrees of freedom per node torsional-transverse model [80,83,107,108]. This modelling approach can be employed for high-speed applications of spur planetary gearboxes where gyroscopic effects can lead to motions in transverse directions [82]. Further modifications to the torsional-transverse model have led to the three-dimensional model which includes six degrees of freedom per node (torsional, transverse, tilting, axial), and allows the capture of axial and tilting motions of planetary gearbox members [79,81,84]. The three-dimensional model enables the analysis of helical planetary gear sets in which axial gear mesh forces can occur. Furthermore, dynamic models for double-helical planetary gear sets have been developed using the three-dimensional model approach [96–99,107]. Dynamic analyses of three-dimensional models have also been conducted with gyroscopic effects [81,84,99].

2.4.2 Dynamic behaviour of planetary gears

The modal analysis of a planetary gearbox provides an understanding of the internal motion of the members of the planetary gearbox. Depending on the complexity of the model, different types of mode shapes can be obtained. The purely torsional model can only detect torsional modes, which can either be global modes, or planet modes [80,82,83,107]. The torsional-transverse model seen in Figure 2.7 can provide rotational, translational and planet modes for the spur planetary gearbox whereas the most advanced three-dimensional model approach leads to rotational-axial, translational-tilting and planet modes for the helical gearbox [81,97]. Lower and higher frequency modes are also identified as bearing and tooth modes, respectively, by some studies [6].

To validate the modal behaviour of the dynamic models, some experimental studies have been performed for spur planetary gear sets. Computed rotational, translational and planet modes in the torsional - transverse model were correlated with these experimental studies [108–111]. Furthermore, experimental measurements show that all natural frequencies of planetary gearboxes increase with a higher torque level [112].

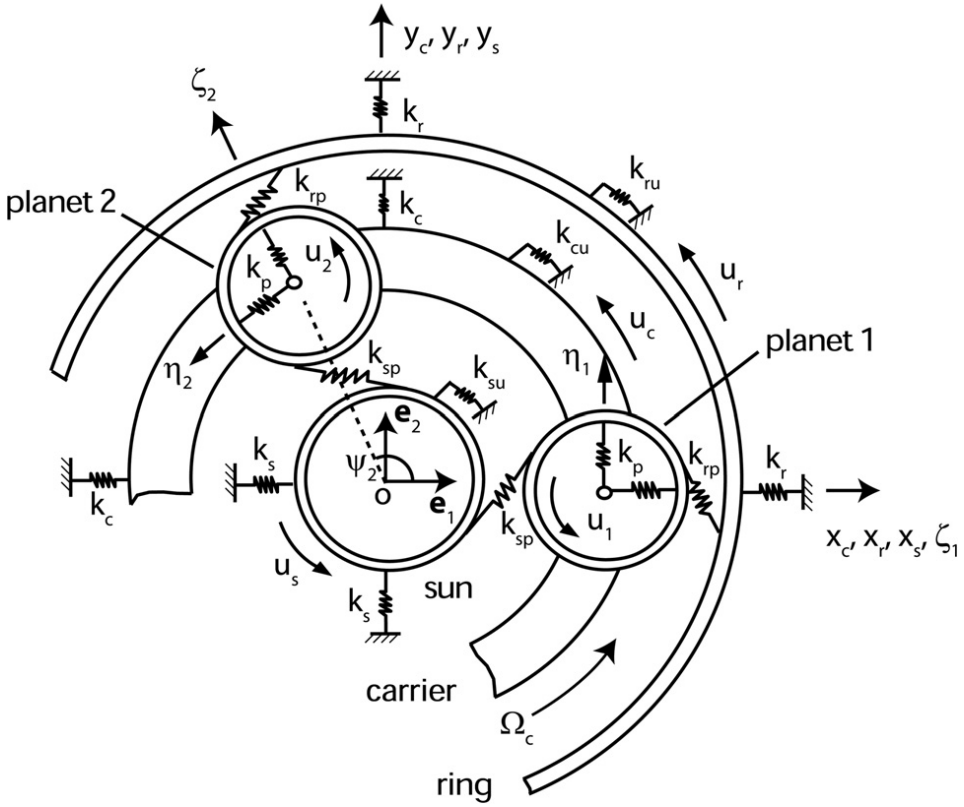

Figure 2.7 : Torsional-transverse lumped parameter model of planetary gearbox [80].

The sensitivity of modal parameters of the planetary gearbox (natural frequencies and mode shapes) with regards to the gearbox input parameters such as gear mesh and bearing stiffness, and gear mass, inertia and speed have also been analysed using these dynamic models [87,91,113,114]. Effects of the gear eccentricities, load and mesh stiffness variation on the dynamic behaviour of planetary gears have been investigated recently [115,116].

In addition to the linear dynamic analysis of planetary gears, a large amount of research has been carried out for the nonlinear vibration analysis of planetary gears [117–130]. Analytical and finite element models [123,124] have been used for the nonlinear vibration analyses of single-stage [118], multiple stages [119] and compound [128] planetary gearboxes. Multiple clearance nonlinearity has also been taken into account by several researchers [117,119,120]. Recently, the harmonic balance method has become popular for the nonlinear vibration analysis of planetary gears [126,128].

2.4.3 Mechanical advantages of planetary gearboxes

Noise, vibration and stress of planetary gearboxes could be reduced significantly with load sharing and mesh phasing mechanisms, which are the important mechanical advantages of planetary gearboxes compared with other types of gearboxes [6,7]. To counterbalance the axial forces in helical gears, thrust bearings are generally used, or double helical gears can be used for the cancellation of axial thrust forces [96]. Double helical gears also provide higher load capacity and lower noise than the others [98].

Load sharing

Load sharing is one of the significant advantages of planetary gearboxes compared with other types of gearboxes such as parallel axis gear transmissions. So far, a good understanding has been achieved for the load sharing behaviour of planetary gearboxes with numerous studies [131–140]. With the load sharing mechanism, each planet gear can share the total loads on the gearbox equally (ideally carrying the same load), leading to reduced gear contact forces for each gear [6]. The torque capability of planetary gearboxes increases with respect to the number of planet gears [7]. For these reasons, load sharing is still an important design parameter of planetary gearboxes. On the other hand, an increase in gear backlashes can affect the load sharing performance negatively [7].

Mesh phasing

Mesh phasing is the phase difference between the gear contacts at different planet gears, which is another advantage of planetary gearboxes [79,141,142]. The mesh phasing is achieved by arranging the location of gear meshes such as sun-planet and ring-planet properly in order to obtain maximum vibration cancellation in total gear meshes [6,7]. This is a useful tool for noise reduction, which has been used in many industrial applications [143]. Unfortunately, the mesh phasing can also have a reverse effect between the rotational and transverse vibrations [7,79]. It is possible to see that rotational vibrations decrease while transverse vibrations increase at different phasing conditions. Therefore, the mesh phasing can be considered as an optimisation problem, and it can be said that there is no exact best phasing condition for a real planetary gear application [7,79].

2.5 Geared rotor dynamics

Gear drive systems are often described as geared rotor systems which consist of shafts, bearings and gears [11,144]. In recent years, the gyroscopic effects on the gear drive system have been started to be taken into consideration by researchers [145–148]. Because gyroscopic effects can change the dynamic behaviour of the system with respect to the rotor spin speed. Geared rotor systems result in more complex rotor dynamic problems since the gears couple the dynamics of the two shafts rotating at different speeds, as well as introducing additional flexibility and inertia into the rotating system. Similar to general rotor systems, three main motions: axial, torsional and lateral, can be seen in geared rotors [11]. There are several numerical techniques available in the literature to analyse geared rotor problems, including lumped parameter and continuous system [9], and finite element methods [11].

2.5.1 Brief history of geared rotor dynamics research

Early geared rotor research focused on the mass imbalance and eccentricity of the gears rather than the effect of the gear mesh dynamics. In the 1970s, uncoupled lateral and torsional models of geared rotors were found to be insufficient to calculate the natural frequencies correctly, and it was found that lateral and torsional coupling due to gear mesh could affect the dynamic behaviour of the system [9,11]. In the 1980s, the coupling between torsional and lateral vibrations in geared rotors was proven by several numerical and experimental studies [9,11]. Both finite element and transfer matrix methods were used to solve complex geared rotor problems [9,11]. It was also suggested that unbalance forces and gear errors might excite the torsional and lateral modes [9]. In the 1990s, bearing stiffness effects were studied, and they were found to be having an important effect on the natural frequencies of the geared rotors [144]. The axial torque effect on the lateral response due to torsional excitation was also studied, and it was to found to be negligible [149]. By the 2000's, Timoshenko beam elements were introduced to the finite element and transfer matrix methods for modelling shafts with their gyroscopic and shearing effects [146,150]. Lateral, torsional and axial vibration coupling in helical gears [151], torsional and lateral coupling effect in herringbone gears [147] and nonlinear contact-impact analysis [152] in geared rotors were also studied in the last decade, highlighting the complexity of the geared rotor problem.

2.5.2 Dynamic behaviour of geared rotors

The dynamic behaviour of geared rotor systems with gyroscopic effects has been studied in great detail with a focus on the coupling effects of the gearbox due to its torsional, axial and lateral stiffness. Lateral-torsional coupling in spur geared rotors and lateral-torsional-axial coupling in helical geared rotors have been shown by many studies [144,146–149,151,153–156]. In addition, dynamic analyses for spiral bevel and face geared rotors were carried out, and their coupled dynamic behaviour was shown [157–159]. Among these studies, the finite element method has become a popular tool for the dynamic analyses [144–149,156,159–161]. Recently, coupling phenomena in geared rotors and their modal behaviour have been shown experimentally [52,162–166].

Torsional models may not be sufficient for the dynamic analysis of geared rotors, because lateral vibrations cannot be ignored in the rotors with relatively longer shafts. Thus, the three DOF torsional-lateral model is widely used in the dynamic analysis of geared rotors. On the other hand, the occurrence of axial forces in helical gears induces coupling between axial, torsional and lateral vibrations in geared rotors [151], leading to the use of six DOF torsional-lateral-axial model for the analysis of helical geared rotors.

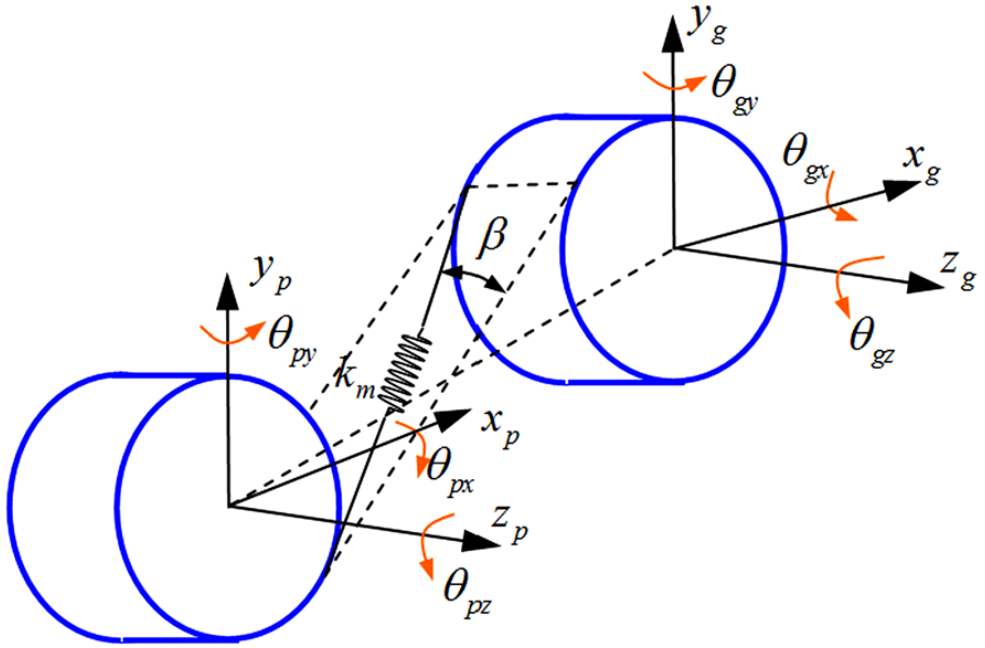

Figure 2.8 : A double-helical geared rotor [146].

In geared rotor systems, coupling originates from gear teeth interactions at gear meshes as seen in Figure 2.8. Here, a linear gear mesh model is presented. The relative displacement vector of the gear mesh pair can be written in general form as [146],

$$\begin{aligned}\delta_m = &\left[\left(x_p - x_g\right) sin\,\emptyset + \left(y_p - y_g\right) cos\,\emptyset + \left(r_p\theta_{pz} + r_g\theta_{gz}\right)\right] cos\,\beta \\ &+ \left[\left(r_p\theta_{py} + r_g\theta_{gy}\right) cos\,\emptyset + \left(r_p\theta_{px} + r_g\theta_{gx}\right) sin\,\emptyset\right. \\ &\left.+ \left(z_g - z_p\right)\right] sin\,\beta - e_{ste}(t),\end{aligned} \tag{2.3}$$

where β is the helix angle, $\emptyset$ is the transverse pressure angle and $e_{ste}(t)$ is the static transmission error. From the Eq. (2.3), it can be easily seen that the gear mesh relative displacement vector results in coupling between lateral, torsional and axial vibrations due to the helix angle β. If spur gears are used in the geared system, the helix angle β becomes zero, leading to a decoupling of the axial vibration. The general equation of motion of a geared rotor can then be expressed as,

$$[\boldsymbol{M}]\ddot{\boldsymbol{q}} + ([\boldsymbol{C}] + \Omega[\boldsymbol{G}])\dot{\boldsymbol{q}} + [\boldsymbol{K}] = \boldsymbol{F}(t), \tag{2.4}$$

where $\boldsymbol{q}$ and Ω represent the generalized coordinates and rotor speeds respectively. $\boldsymbol{M}$, $\boldsymbol{C}$, $\boldsymbol{G}$ and $\boldsymbol{K}$ are the global mass, damping, gyroscopic and stiffness matrices respectively. Here, $\boldsymbol{F}(t)$ represents the internal or external excitations [146]. Internal vibration excitations [73,167–170] can occur because of the transmission error, manufacturing error, tooth profile modifications and time-varying mesh stiffness. In addition, external vibration excitations [148,171–175] can occur because of the rotating imbalance, geometric eccentricities, and torque/speed fluctuations of gears.

Stiffness effects on geared rotors

The stiffnesses of shafts, bearings and gear teeth can directly affect the modal behaviour and dynamic response of geared rotors [146]. Bearings on the geared rotors have a considerable effect on the dynamic forces at the gear contacts and the natural frequencies of the system [144]. It has also been shown that the gear mesh (contact) forces are approximately equal to the forces of stiff bearings in geared rotors [176]. There are also recent studies for the dynamic analyses of geared rotors on rigid bearings [177,178]. The gear mesh stiffness is usually higher than other stiffness components in geared rotor systems; therefore it can be a significant parameter for higher vibration modes [147,179]. Both gear mesh stiffness and gyroscopic effects can change the critical speeds in geared rotors [146]. It is worth stating that lower modes can be controlled with bearing stiffnesses and higher modes can be controlled with mesh stiffnesses.

2.6 Discussion

Introducing a planetary gearbox into a rotating machine can directly affect its global dynamics due to the flexibility, damping and inertia of the planetary gearbox with gyroscopic effects, leading to a coupled dynamic response of the planetary gearbox and rotor. Due to the impact of a planetary gearbox on the dynamic response of the global system, the coupled dynamic behaviour of planetary geared rotor systems has recently become an important research topic.

Although the dynamic behaviour of spur and helical geared rotor systems is well understood today, less research has been carried out to understand the dynamic behaviour of planetary geared rotor systems [180–188]. So far, one-DOF torsional [180–182], three-DOF torsional transverse [183], five-DOF lateral-torsional [184] and six-DOF lateral-torsional-axial [185–188] models of planetary geared rotor systems have been investigated for wind turbine and geared turbofan engine applications. From this research, only two of the six-DOF models have taken gyroscopic effects into account for geared turbofan engine applications [187,188]. Wei et al. [188] considered the forced vibration analysis of a geared turbofan engine due to loss of a blade creating rotating imbalance. Tatar and Schwingshackl [187] used a low fidelity model of the planetary gearbox, including uncoupled gearbox stiffness, to investigate the planetary gearbox impact on the dynamics of the rotor system. However, the modal behaviour of a six-DOF planetary geared rotor system with gyroscopic effects is still not clear and only partially understood. Therefore, more work is needed to provide a full understanding of the dynamic behaviour of such systems.

Chapter 3

3 Dynamic model of planetary geared rotors

3.1 Introduction

In this chapter, a six-degrees of freedom hybrid dynamic model of a planetary geared rotor system is presented by considering gyroscopic effects. For this purpose, a three-dimensional model of an equally spaced planetary gearbox and a rotor system is created by employing the lumped parameter and finite element methods respectively. 1-D rotating Timoshenko beam elements for the shafts and uncoupled linear spring elements for the bearings are used to construct the dynamic model of the rotor system. The planetary gearbox members, which are the ring gear, carrier, planet gears and sun gear, are assumed to be rigid, and the gear teeth contacts (gear meshes) and bearing elements are assumed to be flexible. It is important to point out that the planetary gearbox is introduced to couple the shafts in the rotor system.

A basic planetary geared rotor system consists of input and output shafts, several bearings and a planetary gearbox as shown in Figure 3.1. The input and output shafts rotate at different speeds, which are coupled by the planetary gearbox and supported via the bearing elements at each end. The planetary gearbox is also grounded via its bearings.

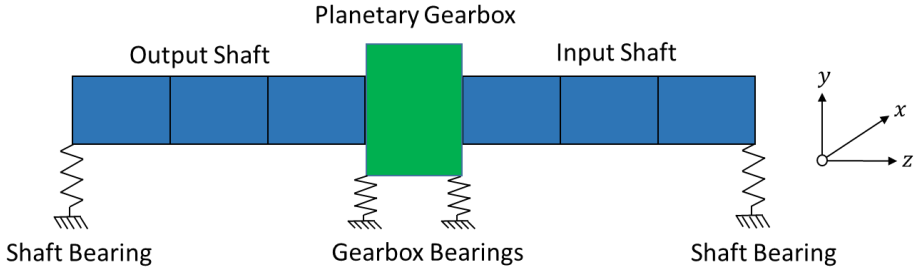

Figure 3.1 : Planetary geared rotor system.

Coordinate system

Throughout this thesis, the stationary coordinate system is employed for the dynamic model, and the generalized coordinates are written as

$$\boldsymbol{q} = \left[x, y, z, \theta_x, \theta_y, \theta_z\right], \tag{3.1}$$

where the generalized coordinates include transverse(x, y), axial(z), tilting $\left(\theta_x, \theta_y\right)$ and torsional (θ_z) motions.

3.2 Rotor-Bearing System

3.2.1 Shafts

Longer rotating shafts can be modelled as flexible beams where their mass, stiffness and gyroscopic matrices can be obtained using the finite element method [3]. The shafts are discretised into small beam elements so as to obtain element mass, stiffness and gyroscopic matrices in the finite element method. Then, the global matrices are obtained using the element matrices in the finite element assembly procedure where the connectivity between beam elements is defined via a topology matrix.

Modelling assumptions

Due to the high number of modes included in this study, 1-D rotating Timoshenko beam elements are employed to capture potential shear deflection and rotational inertia terms [3]. Each beam element has two nodes with twelve degrees of freedom, including transverse, tilting, axial and torsional directions. The geometry of the beam element with its local coordinates can be seen in Figure 3.2.

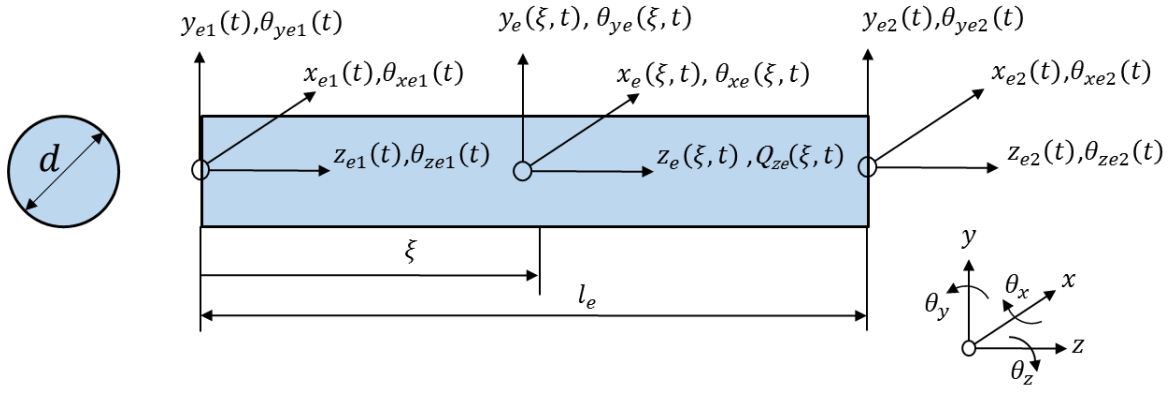

Figure 3.2 : The shaft finite element.

Finite element formulations

The local coordinates, $\boldsymbol{q}_e(t)$, and shape functions, $\boldsymbol{N}_e(\xi)$, for the Timoshenko beam element can be expressed as [3]

$$\begin{aligned}\boldsymbol{q}_e(t) = \big[&x_{e1}(t), y_{e1}(t), z_{e1}(t), \theta_{xe1}(t), \theta_{ye1}(t), \theta_{ze1}(t),\\ &x_{e2}(t), y_{e2}(t), z_{e2}(t), \theta_{xe2}(t), \theta_{ye2}(t), \theta_{ze2}(t)\big],\end{aligned} \tag{3.2}$$

$$\begin{aligned}\boldsymbol{N}_e(\xi) = [&N_{e1}(\xi), N_{e2}(\xi), N_{e3}(\xi), N_{e4}(\xi), N_{e5}(\xi), N_{e6}(\xi),\\ &N_{e7}(\xi), N_{e8}(\xi), N_{e9}(\xi), N_{e10}(\xi), N_{e11}(\xi), N_{e12}(\xi)].\end{aligned} \tag{3.3}$$

The deflections, $\boldsymbol{q}_e(\xi, t)$, throughout the beam element can then be approximated by multiplying the shape functions and local coordinates with the Hadamard product as

$$\boldsymbol{q}_e(\xi, t) = \boldsymbol{N}_e(\xi) \circ \boldsymbol{q}_e(t), \tag{3.4}$$

$$\begin{aligned}\boldsymbol{q}_e(\xi, t) = \big[&x_{e1}(\xi, t), y_{e1}(\xi, t), z_{e1}(\xi, t), \theta_{xe1}(\xi, t), \theta_{ye1}(\xi, t), \theta_{ze1}(\xi, t),\\ &x_{e2}(\xi, t), y_{e2}(\xi, t), z_{e2}(\xi, t), \theta_{xe2}(\xi, t), \theta_{ye2}(\xi, t), \theta_{ze2}(\xi, t)\big].\end{aligned} \tag{3.5}$$

Then, the kinetic, T_s, and potential, V_s, energies of an individual Timoshenko beam element become [3,4,146,149]

$$\begin{aligned}T_s = \frac{1}{2}\int_0^{l_e} \rho_e \Big\{&A_e\left(\dot{x}_e{}^2 + \dot{y}_e{}^2 + \dot{z}_e{}^2\right) + I_e\left(\dot{\theta}_{xe}{}^2 + \dot{\theta}_{ye}{}^2\right)\\ &+ J_e\left[\left(\Omega_e + \dot{\theta}_{ze}\right)^2 + \left(\Omega_e + \dot{\theta}_{ze}\right)\left(\theta_{ye}\dot{\theta}_{xe} - \theta_{xe}\dot{\theta}_{ye}\right)\right]\Big\} d\xi,\end{aligned} \tag{3.6}$$

$$\begin{aligned}V_s = \frac{1}{2}\int_0^{l_e} \Big\{&E_e I_e\left(\theta_{xe}'{}^2 + \theta_{ye}'{}^2\right) + G_e J_e\left(\theta_{ze}'\right)^2\\ &+ \kappa_e G_e A_e\left[\left(x_e' - \theta_{ye}\right)^2 + \left(y_e' + \theta_{xe}\right)^2\right] + E_e A_e (z_e')^2\Big\} d\xi,\end{aligned} \tag{3.7}$$

where the dot $\dot{}$ and prime $'$ denote differentiation with respect to time (t) and natural coordinates (ξ), respectively. The kinetic energy includes the transverse, axial, tilting and torsional motions with gyroscopic terms. The potential energy includes the axial, torsional, bending and shear deflections where the shear constant, κ_e, for a solid shaft is [3]

$$\kappa_e = \frac{6(1+\nu_e)}{(7+6\nu_e)}, \tag{3.8}$$

where ν_e is Poisson`s ratio which is written as

$$\nu_e = \frac{E_e}{2G_e} - 1. \tag{3.9}$$

Following the energy equations, the finite element formulations for the mass, gyroscopic and stiffness element matrices are obtained by applying the Lagrange`s equations of the second kind (see Appendix A).

Finite element matrices

The full mathematical derivation of the stiffness, mass, gyroscopic matrices and shape functions of the system can be found in reference [3], and the 12 DOF finite element matrices are also given explicitly in reference [146]. Here, the stiffness, mass and gyroscopic element matrices for a cyclically symmetric beam are listed. The stiffness element matrix of the Timoshenko beam element is written as

$$\mathbf{K}_{el} = \mathbf{K}_{lat} + \mathbf{K}_{ax} + \mathbf{K}_{tor}, \tag{3.10}$$

where the stiffness element matrix ($\mathbf{K}_{el}$) consists of three parts which represent lateral ($\mathbf{K}_{lat}$), axial ($\mathbf{K}_{ax}$) and torsional ($\mathbf{K}_{tor}$) stiffness matrices of the Timoshenko beam element. The lateral stiffness element matrix, $\mathbf{K}_{lat}$ is written as

$$\mathbf{K}_{lat} = \mathbb{C}_{lat}\begin{bmatrix} 12 & 0 & 0 & 0 & 6l_e & 0 & -12 & 0 & 0 & 0 & 6l_e & 0 \\ 0 & 12 & 0 & -6l_e & 0 & 0 & 0 & -12 & 0 & -6l_e & 0 & 0 \\ 0 & 0 & 0 & 0 & 0 & 0 & 0 & 0 & 0 & 0 & 0 & 0 \\ 0 & -6l_e & 0 & k_1 & 0 & 0 & 0 & 6l_e & 0 & k_2 & 0 & 0 \\ 6l_e & 0 & 0 & 0 & k_1 & 0 & -6l_e & 0 & 0 & 0 & k_2 & 0 \\ 0 & 0 & 0 & 0 & 0 & 0 & 0 & 0 & 0 & 0 & 0 & 0 \\ -12 & 0 & 0 & 0 & -6l_e & 0 & 12 & 0 & 0 & 0 & -6l_e & 0 \\ 0 & -12 & 0 & 6l_e & 0 & 0 & 0 & 12 & 0 & 6l_e & 0 & 0 \\ 0 & 0 & 0 & 0 & 0 & 0 & 0 & 0 & 0 & 0 & 0 & 0 \\ 0 & -6l_e & 0 & k_2 & 0 & 0 & 0 & 6l_e & 0 & k_1 & 0 & 0 \\ 6l_e & 0 & 0 & 0 & k_2 & 0 & -6l_e & 0 & 0 & 0 & k_1 & 0 \\ 0 & 0 & 0 & 0 & 0 & 0 & 0 & 0 & 0 & 0 & 0 & 0 \end{bmatrix}, \tag{3.11}$$

where k_1 and k_2 are expressed as

$$k_1 = (4 + \Phi_e){l_e}^2,$$
$$k_2 = (2 - \Phi_e){l_e}^2, \tag{3.12}$$

and the constant, $\mathbb{C}_{lat}$ is

$$\mathbb{C}_{lat} = \frac{E_e I_e}{(1 + \Phi_e){l_e}^3}. \tag{3.13}$$

Here, the constant Φ_e is defined as

$$\Phi_e = \frac{12 E_e I_e}{\kappa_e G_e A_e {l_e}^2}. \tag{3.14}$$

The axial stiffness element matrix, $\mathbf{K}_{ax}$ is written as

$$\mathbf{K}_{ax} = \begin{bmatrix} 0 & 0 & 0 & 0 & 0 & 0 & 0 & 0 & 0 & 0 & 0 & 0 \\ 0 & 0 & 0 & 0 & 0 & 0 & 0 & 0 & 0 & 0 & 0 & 0 \\ 0 & 0 & \frac{E_e A_e}{l_e} & 0 & 0 & 0 & 0 & 0 & -\frac{E_e A_e}{l_e} & 0 & 0 & 0 \\ 0 & 0 & 0 & 0 & 0 & 0 & 0 & 0 & 0 & 0 & 0 & 0 \\ 0 & 0 & 0 & 0 & 0 & 0 & 0 & 0 & 0 & 0 & 0 & 0 \\ 0 & 0 & 0 & 0 & 0 & 0 & 0 & 0 & 0 & 0 & 0 & 0 \\ 0 & 0 & 0 & 0 & 0 & 0 & 0 & 0 & 0 & 0 & 0 & 0 \\ 0 & 0 & 0 & 0 & 0 & 0 & 0 & 0 & 0 & 0 & 0 & 0 \\ 0 & 0 & -\frac{E_e A_e}{l_e} & 0 & 0 & 0 & 0 & 0 & \frac{E_e A_e}{l_e} & 0 & 0 & 0 \\ 0 & 0 & 0 & 0 & 0 & 0 & 0 & 0 & 0 & 0 & 0 & 0 \\ 0 & 0 & 0 & 0 & 0 & 0 & 0 & 0 & 0 & 0 & 0 & 0 \\ 0 & 0 & 0 & 0 & 0 & 0 & 0 & 0 & 0 & 0 & 0 & 0 \end{bmatrix}. \tag{3.15}$$

Following, the torsional stiffness element matrix, $\mathbf{K}_{tor}$ is written as

$$\mathbf{K}_{tor} = \begin{bmatrix} 0 & 0 & 0 & 0 & 0 & 0 & 0 & 0 & 0 & 0 & 0 & 0 \\ 0 & 0 & 0 & 0 & 0 & 0 & 0 & 0 & 0 & 0 & 0 & 0 \\ 0 & 0 & 0 & 0 & 0 & 0 & 0 & 0 & 0 & 0 & 0 & 0 \\ 0 & 0 & 0 & 0 & 0 & 0 & 0 & 0 & 0 & 0 & 0 & 0 \\ 0 & 0 & 0 & 0 & 0 & 0 & 0 & 0 & 0 & 0 & 0 & 0 \\ 0 & 0 & 0 & 0 & 0 & \frac{G_e J_e}{l_e} & 0 & 0 & 0 & 0 & 0 & -\frac{G_e J_e}{l_e} \\ 0 & 0 & 0 & 0 & 0 & 0 & 0 & 0 & 0 & 0 & 0 & 0 \\ 0 & 0 & 0 & 0 & 0 & 0 & 0 & 0 & 0 & 0 & 0 & 0 \\ 0 & 0 & 0 & 0 & 0 & 0 & 0 & 0 & 0 & 0 & 0 & 0 \\ 0 & 0 & 0 & 0 & 0 & 0 & 0 & 0 & 0 & 0 & 0 & 0 \\ 0 & 0 & 0 & 0 & 0 & 0 & 0 & 0 & 0 & 0 & 0 & 0 \\ 0 & 0 & 0 & 0 & 0 & -\frac{G_e J_e}{l_e} & 0 & 0 & 0 & 0 & 0 & \frac{G_e J_e}{l_e} \end{bmatrix}. \tag{3.16}$$

The mass matrix of the Timoshenko beam element is expressed as

$$\mathbf{M}_{el} = \mathbf{M}_{lat} + \mathbf{M}_{ax} + \mathbf{M}_{tor}, \tag{3.17}$$

where the mass matrix ($\mathbf{M}_{el}$) consists of three parts which are lateral ($\mathbf{M}_{lat}$), axial ($\mathbf{M}_{ax}$) and torsional ($\mathbf{M}_{tor}$) components of the mass matrix of the Timoshenko beam element. Lateral component of the mass matrix also includes translational ($\mathbf{M}_{tr}$) and rotational ($\mathbf{M}_{rot}$) mass matrices, which is written as

$$\mathbf{M}_{lat} = \mathbf{M}_{tr} + \mathbf{M}_{rot}. \tag{3.18}$$

Translational mass matrix, $\mathbf{M}_{tr}$ is expressed as

$$\mathbf{M}_{tr} = \mathbb{C}_{tr}\begin{bmatrix} m_1 & 0 & 0 & 0 & m_2 & 0 & m_3 & 0 & 0 & 0 & m_4 & 0 \\ 0 & m_1 & 0 & -m_2 & 0 & 0 & 0 & m_3 & 0 & -m_4 & 0 & 0 \\ 0 & 0 & 0 & 0 & 0 & 0 & 0 & 0 & 0 & 0 & 0 & 0 \\ 0 & -m_2 & 0 & m_5 & 0 & 0 & 0 & m_4 & 0 & m_6 & 0 & 0 \\ m_2 & 0 & 0 & 0 & m_5 & 0 & -m_4 & 0 & 0 & 0 & m_6 & 0 \\ 0 & 0 & 0 & 0 & 0 & 0 & 0 & 0 & 0 & 0 & 0 & 0 \\ m_3 & 0 & 0 & 0 & -m_4 & 0 & m_1 & 0 & 0 & 0 & -m_2 & 0 \\ 0 & m_3 & 0 & m_4 & 0 & 0 & 0 & m_1 & 0 & m_2 & 0 & 0 \\ 0 & 0 & 0 & 0 & 0 & 0 & 0 & 0 & 0 & 0 & 0 & 0 \\ 0 & -m_4 & 0 & m_6 & 0 & 0 & 0 & m_2 & 0 & m_5 & 0 & 0 \\ m_4 & 0 & 0 & 0 & m_6 & 0 & -m_2 & 0 & 0 & 0 & m_5 & 0 \\ 0 & 0 & 0 & 0 & 0 & 0 & 0 & 0 & 0 & 0 & 0 & 0 \end{bmatrix}, \tag{3.19}$$

and rotational mass matrix, $\mathbf{M}_{rot}$ is also expressed as

$$\mathbf{M}_{rot} = \mathbb{C}_{rot}\begin{bmatrix} m_7 & 0 & 0 & 0 & m_8 & 0 & -m_7 & 0 & 0 & 0 & m_8 & 0 \\ 0 & m_7 & 0 & -m_8 & 0 & 0 & 0 & -m_7 & 0 & -m_8 & 0 & 0 \\ 0 & 0 & 0 & 0 & 0 & 0 & 0 & 0 & 0 & 0 & 0 & 0 \\ 0 & -m_8 & 0 & m_9 & 0 & 0 & 0 & m_8 & 0 & m_{10} & 0 & 0 \\ m_8 & 0 & 0 & 0 & m_9 & 0 & -m_8 & 0 & 0 & 0 & m_{10} & 0 \\ 0 & 0 & 0 & 0 & 0 & 0 & 0 & 0 & 0 & 0 & 0 & 0 \\ -m_7 & 0 & 0 & 0 & -m_8 & 0 & m_7 & 0 & 0 & 0 & -m_8 & 0 \\ 0 & -m_7 & 0 & m_8 & 0 & 0 & 0 & m_7 & 0 & m_8 & 0 & 0 \\ 0 & 0 & 0 & 0 & 0 & 0 & 0 & 0 & 0 & 0 & 0 & 0 \\ 0 & -m_8 & 0 & m_{10} & 0 & 0 & 0 & m_8 & 0 & m_9 & 0 & 0 \\ m_8 & 0 & 0 & 0 & m_{10} & 0 & -m_8 & 0 & 0 & 0 & m_9 & 0 \\ 0 & 0 & 0 & 0 & 0 & 0 & 0 & 0 & 0 & 0 & 0 & 0 \end{bmatrix}, \tag{3.20}$$

where $m_1, m_2, m_3, m_4, m_5, m_6, m_7, m_8, m_9, m_{10}$ are given by:

$$
\begin{aligned}
m_1 &= 312 + 588\Phi_e + 280{\Phi_e}^2,\\
m_2 &= \left(44 + 77\Phi_e + 35{\Phi_e}^2\right)l_e,\\
m_3 &= 108 + 252\Phi_e + 140{\Phi_e}^2,\\
m_4 &= -\left(26 + 63\Phi_e + 35{\Phi_e}^2\right)l_e,\\
m_5 &= \left(8 + 14\Phi_e + 7{\Phi_e}^2\right){l_e}^2,\\
m_6 &= -\left(6 + 14\Phi_e + 7{\Phi_e}^2\right){l_e}^2,\\
m_7 &= 36,\\
m_8 &= (3 - 15\Phi_e)l_e,\\
m_9 &= \left(4 + 5\Phi_e + 10{\Phi_e}^2\right){l_e}^2,\\
m_{10} &= \left(-1 - 5\Phi_e + 5{\Phi_e}^2\right){l_e}^2.
\end{aligned}
\tag{3.21}
$$

and the constants, $\mathbb{C}_{tr}$ and $\mathbb{C}_{rot}$ are expressed as

$$\mathbb{C}_{tr} = \frac{\rho_e A_e l_e}{840(1+\Phi_e)^2}, \tag{3.22}$$

$$\mathbb{C}_{rot} = \frac{\rho_e I_e}{30 l_e (1+\Phi_e)^2}. \tag{3.23}$$

The axial ($\mathbf{M}_{ax}$) and torsional ($\mathbf{M}_{tor}$) components of the mass matrix of the beam element are written as

$$
\mathbf{M}_{ax} = \begin{bmatrix}
0 & 0 & 0 & 0 & 0 & 0 & 0 & 0 & 0 & 0 & 0 & 0\\
0 & 0 & 0 & 0 & 0 & 0 & 0 & 0 & 0 & 0 & 0 & 0\\
0 & 0 & \frac{\rho_e A_e l_e}{3} & 0 & 0 & 0 & 0 & 0 & \frac{\rho_e A_e l_e}{6} & 0 & 0 & 0\\
0 & 0 & 0 & 0 & 0 & 0 & 0 & 0 & 0 & 0 & 0 & 0\\
0 & 0 & 0 & 0 & 0 & 0 & 0 & 0 & 0 & 0 & 0 & 0\\
0 & 0 & 0 & 0 & 0 & 0 & 0 & 0 & 0 & 0 & 0 & 0\\
0 & 0 & 0 & 0 & 0 & 0 & 0 & 0 & 0 & 0 & 0 & 0\\
0 & 0 & 0 & 0 & 0 & 0 & 0 & 0 & 0 & 0 & 0 & 0\\
0 & 0 & \frac{\rho_e A_e l_e}{6} & 0 & 0 & 0 & 0 & 0 & \frac{\rho_e A_e l_e}{3} & 0 & 0 & 0\\
0 & 0 & 0 & 0 & 0 & 0 & 0 & 0 & 0 & 0 & 0 & 0\\
0 & 0 & 0 & 0 & 0 & 0 & 0 & 0 & 0 & 0 & 0 & 0\\
0 & 0 & 0 & 0 & 0 & 0 & 0 & 0 & 0 & 0 & 0 & 0
\end{bmatrix},
\tag{3.24}
$$

$$\mathbf{M}_{tor} = \begin{bmatrix} 0 & 0 & 0 & 0 & 0 & 0 & 0 & 0 & 0 & 0 & 0 & 0 \\ 0 & 0 & 0 & 0 & 0 & 0 & 0 & 0 & 0 & 0 & 0 & 0 \\ 0 & 0 & 0 & 0 & 0 & 0 & 0 & 0 & 0 & 0 & 0 & 0 \\ 0 & 0 & 0 & 0 & 0 & 0 & 0 & 0 & 0 & 0 & 0 & 0 \\ 0 & 0 & 0 & 0 & 0 & 0 & 0 & 0 & 0 & 0 & 0 & 0 \\ 0 & 0 & 0 & 0 & 0 & \frac{\rho_e A_e l_e d^2}{24} & 0 & 0 & 0 & 0 & 0 & \frac{\rho_e A_e l_e d^2}{48} \\ 0 & 0 & 0 & 0 & 0 & 0 & 0 & 0 & 0 & 0 & 0 & 0 \\ 0 & 0 & 0 & 0 & 0 & 0 & 0 & 0 & 0 & 0 & 0 & 0 \\ 0 & 0 & 0 & 0 & 0 & 0 & 0 & 0 & 0 & 0 & 0 & 0 \\ 0 & 0 & 0 & 0 & 0 & 0 & 0 & 0 & 0 & 0 & 0 & 0 \\ 0 & 0 & 0 & 0 & 0 & 0 & 0 & 0 & 0 & 0 & 0 & 0 \\ 0 & 0 & 0 & 0 & 0 & \frac{\rho_e A_e l_e d^2}{48} & 0 & 0 & 0 & 0 & 0 & \frac{\rho_e A_e l_e d^2}{24} \end{bmatrix}, \tag{3.25}$$

respectively.

Finally, the gyroscopic matrix of the beam element is written as

$$\mathbf{G}_{el} = \mathbb{C}_{el} \begin{bmatrix} 0 & -m_7 & 0 & m_8 & 0 & 0 & 0 & m_7 & 0 & m_8 & 0 & 0 \\ m_7 & 0 & 0 & 0 & m_8 & 0 & -m_7 & 0 & 0 & 0 & m_8 & 0 \\ 0 & 0 & 0 & 0 & 0 & 0 & 0 & 0 & 0 & 0 & 0 & 0 \\ -m_8 & 0 & 0 & 0 & -m_9 & 0 & m_8 & 0 & 0 & 0 & -m_{10} & 0 \\ 0 & -m_8 & 0 & m_9 & 0 & 0 & 0 & m_8 & 0 & m_{10} & 0 & 0 \\ 0 & 0 & 0 & 0 & 0 & 0 & 0 & 0 & 0 & 0 & 0 & 0 \\ 0 & m_7 & 0 & -m_8 & 0 & 0 & 0 & -m_7 & 0 & -m_8 & 0 & 0 \\ -m_7 & 0 & 0 & 0 & -m_8 & 0 & m_7 & 0 & 0 & 0 & -m_8 & 0 \\ 0 & 0 & 0 & 0 & 0 & 0 & 0 & 0 & 0 & 0 & 0 & 0 \\ -m_8 & 0 & 0 & 0 & -m_{10} & 0 & m_8 & 0 & 0 & 0 & -m_9 & 0 \\ 0 & -m_8 & 0 & m_{10} & 0 & 0 & 0 & m_8 & 0 & m_9 & 0 & 0 \\ 0 & 0 & 0 & 0 & 0 & 0 & 0 & 0 & 0 & 0 & 0 & 0 \end{bmatrix}, \tag{3.26}$$

where the constant, $\mathbb{C}_{el}$ is expressed as

$$\mathbb{C}_{el} = \frac{-\rho_e I_e}{15 l_e (1+\Phi_e)^2}. \tag{3.27}$$

Damping can also be added to the shaft model via proportional damping [189] as

$$\mathbf{C_s} = \alpha_1 \mathbf{M_s} + \alpha_2 \mathbf{K_s}. \tag{3.28}$$

Finally, the global mass ($\mathbf{M}_s$), stiffness ($\mathbf{K}_s$), damping ($\mathbf{C}_s$) and gyroscopic ($\mathbf{G}_s$) matrices of the shafts are obtained using the finite element matrices.

3.2.2 Bearings

Bearings are used to support rotating systems, which can be either rigid or flexible, depending on the application. Bearing element models are available in the literature, ranging from the simple linear models to advanced nonlinear dynamic models [3]. Floating bearings are also utilized in rotating systems so as to compensate misalignments by allowing to float radially, which can be seen in some applications such as planetary geared rotors [190].

Modelling assumptions

In the present model, the bearing elements are assumed to be flexible and consist of linear translational and rotational spring elements. This thesis focuses on the understanding of the effect of a planetary gearbox on the dynamics of the rotor system. Therefore, basic bearing elements with no coupling terms are considered sufficient for this study.

Matrix formulations

The stiffness matrix of the bearing elements, $\mathbf{K}_b$:

$$\mathbf{K}_b = \begin{bmatrix} k_x & 0 & 0 & 0 & 0 & 0 \\ 0 & k_y & 0 & 0 & 0 & 0 \\ 0 & 0 & k_z & 0 & 0 & 0 \\ 0 & 0 & 0 & k_{Q_x} & 0 & 0 \\ 0 & 0 & 0 & 0 & k_{Q_y} & 0 \\ 0 & 0 & 0 & 0 & 0 & k_{Q_z} \end{bmatrix}, \tag{3.29}$$

and the damping matrix of the bearing elements, $\mathbf{C}_b$:

$$\mathbf{C}_b = \begin{bmatrix} c_x & 0 & 0 & 0 & 0 & 0 \\ 0 & c_y & 0 & 0 & 0 & 0 \\ 0 & 0 & c_z & 0 & 0 & 0 \\ 0 & 0 & 0 & c_{Q_x} & 0 & 0 \\ 0 & 0 & 0 & 0 & c_{Q_y} & 0 \\ 0 & 0 & 0 & 0 & 0 & c_{Q_z} \end{bmatrix}, \tag{3.30}$$

are written as seen in Eq. (3.29) and Eq. (3.30) respectively [3]. When looking into these equations, the stiffness and damping matrices are in diagonal form, which means that the bearings consist of uncoupled stiffness and damping elements. Torsional stiffness, k_{Q_z}, and damping, c_{Q_z}, of the bearing elements will be assumed to be zero, allowing the shaft to rotate freely without any resistance.

3.3 Planetary Gearbox

3.3.1 Modelling assumptions

A basic single-stage planetary gearbox consists of a ring gear, a carrier, a sun gear and N planet gears. A six-degrees of freedom linear lumped parameter of a planetary gearbox is employed for the dynamic modelling from references [79,96]. In this model, all the members of the planetary gearbox, which are the sun, ring and planet gears and the carrier, are assumed to be rigid disks. The gear teeth contacts and bearing elements are assumed to be flexible. Linear time-varying mesh stiffness and clearance nonlinearity due to loss of teeth contact are neglected. All the planet gears have the same property, and they are equally spaced. It should be noted that the gearbox housing is neglected in this lumped parameter model [79,96].

As seen schematically in Figure 3.3, the gear teeth contacts are represented with linear springs, which are between the sun gear and planet gears (k_{sp}), and between the ring gear and the planet gears (k_{rp}). These gear teeth contacts are also known as gear mesh stiffnesses, which are assumed to be constant in the model due to the linear spring elements [79,96]. All the planetary gearbox members have six-DOF bearing elements, represented by linear springs (k_r, k_c, k_s, k_p) defined in Eq. (3.29).

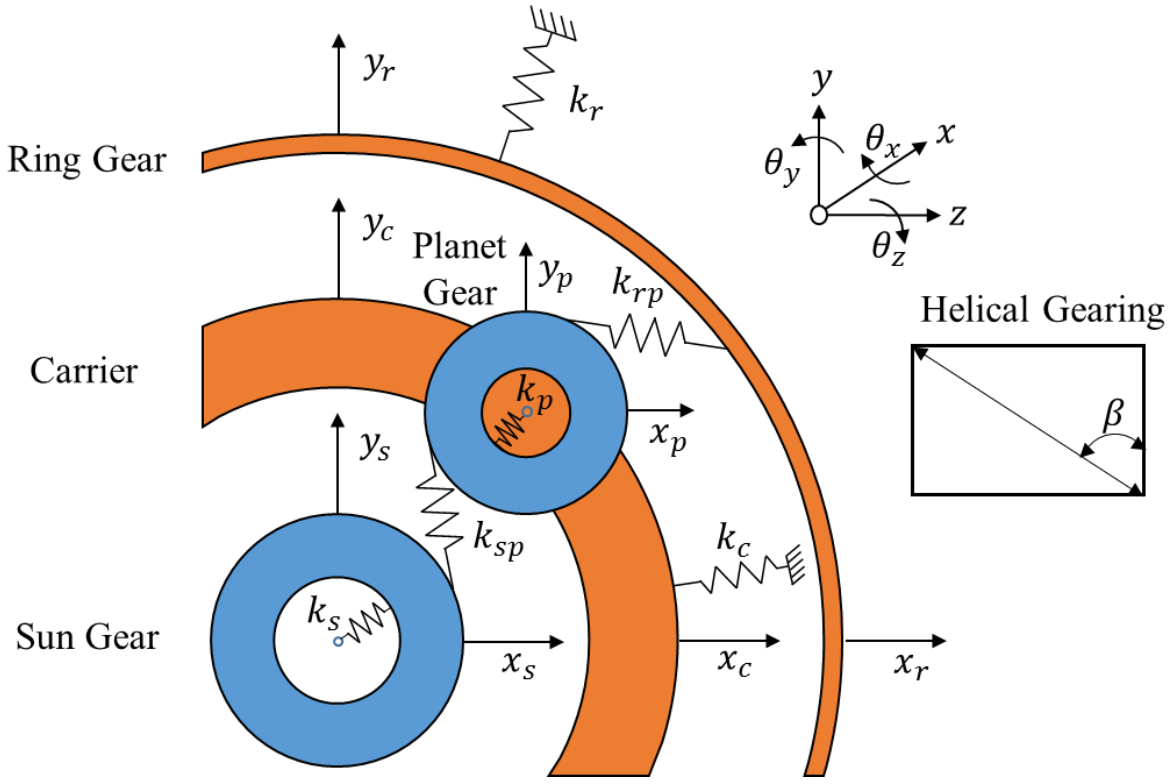

Figure 3.3 : Dynamic model of a planetary gearbox.

3.3.2 Energy equations

The equation of motion of the planetary gearbox is obtained using Lagrange's equations. For this purpose, the total kinetic and potential energies of the system must be obtained. With the small rotation assumption in the θ_{xh} and θ_{yh} tilting directions, the kinetic energies of the central members (ring gear, sun gear and carrier) and planet gears can be written as

$$T_h = \frac{1}{2}\sum_{h=1}^{3}\Big(m_h\left(\dot{x}_h{}^2 + \dot{y}_h{}^2 + \dot{z}_h{}^2\right) + I_{dh}\left(\dot{\theta}_{xh}{}^2 + \dot{\theta}_{yh}{}^2\right) + I_{ph}\left(\Omega_h{}^2 - 2\Omega_h\dot{\theta}_{yh}\theta_{xh} + \dot{\theta}_{zh}{}^2\right)\Big), \tag{3.31}$$

$$T_p = \frac{1}{2}\sum_{i=1}^{N}\Big(m_{pi}\left(\dot{x}_{pi}{}^2 + \dot{y}_{pi}{}^2 + \dot{z}_{pi}{}^2\right) + I_{dpi}\left(\dot{\theta}_{xpi}{}^2 + \dot{\theta}_{ypi}{}^2\right) + I_{ppi}\left(\Omega_{pi}{}^2 - 2\Omega_{pi}\dot{\theta}_{ypi}\theta_{xpi} + \dot{\theta}_{zpi}{}^2\right)\Big), \tag{3.32}$$

respectively [3]. Here, h is the central member index for the ring gear, carrier and sun gear. The kinetic energies include all motions in three dimensions with the gyroscopic terms, similar to the kinetic energy of the Timoshenko beam elements, defined in Eq. (3.6). The gyroscopic terms in the planetary gearbox originate from the $\dot{\theta}_y\theta_x$ multiplication. The strain energies of the bearings for the central members and planet gears can be written respectively as [190]

$$V_h = \frac{1}{2}\sum_{h=1}^{3}\Big(k_{xh}x_h{}^2 + k_{yh}y_h{}^2 + k_{zh}z_h{}^2 + k_{\theta_{xh}}\theta_{xh}{}^2 + k_{\theta_{yh}}\theta_{yh}{}^2 + k_{\theta_{zh}}\theta_{zh}{}^2\Big), \tag{3.33}$$

$$\begin{aligned} V_p = \frac{1}{2}\sum_{i=1}^{N}\Big(&k_{xp}\left(x_c - x_{pi} - r_c\theta_{zc}\,sin\,\alpha_{pi}\right)^2 \\ &+ k_{yp}\left(y_c - y_{pi} + r_c\theta_{zc}\,cos\,\alpha_{pi}\right)^2 \\ &+ k_{zp}\left(z_c - z_{pi} + r_c\theta_{xc}\,sin\,\alpha_{pi} - r_c\theta_{yc}\,cos\,\alpha_{pi}\right)^2 \\ &+ k_{\theta_{xp}}\left(\theta_{xc} - \theta_{xpi}\right)^2 + k_{\theta_{yp}}\left(\theta_{yc} - \theta_{ypi}\right)^2\Big), \end{aligned} \tag{3.34}$$

where α_{pi} is the angular position of each planet, which can be defined for the non-rotating carrier configuration as

$$\alpha_{pi+1} = \alpha_{pi} + \frac{2\pi}{N}. \tag{3.35}$$

Here, α_{p1} represents the first planet gear`s angular position, which is assumed to be zero. The torsional bearing stiffnesses of the rotating members in the planetary gearbox are assumed to be zero based on the planetary gearbox configurations. For instance, torsional bearing stiffnesses of the ring, sun and planet gears are set as zero in the rotating ring-fixed carrier configuration since the gears rotate and the carrier does not rotate in this configuration. Another potential energy component given by the gear mesh strain energy due to the gear teeth deflections must also be included in the model [190] as

$$V_m = \sum_{i=1}^{N} \left(\frac{1}{2} k_{sp} {\delta_{spi}}^2 + \frac{1}{2} k_{rp} {\delta_{rpi}}^2 \right), \tag{3.36}$$

where δ_{spi} and δ_{rpi} represent the relative displacement between the sun-planet and ring-planet gear meshes respectively. These relative displacements depend on the geometry of the gear meshes and can be expressed as

$$\begin{aligned} \delta_{spi} = {} & \left[\left(x_s - x_{pi}\right) \sin\psi_{spi} + \left(y_s - y_{pi}\right) \cos\psi_{spi} + \left(r_s\theta_{zs} + r_p\theta_{zpi}\right) \right] \cos\beta \\ & + \left[\left(r_s\theta_{xs} + r_p\theta_{xpi}\right) \sin\psi_{spi} + \left(r_s\theta_{ys} + r_p\theta_{ypi}\right) \cos\psi_{spi} \right. \\ & \left. + \left(z_{pi} - z_s\right) \right] \sin\beta, \end{aligned} \tag{3.37}$$

$$\begin{aligned} \delta_{rpi} = {} & \left[\left(x_{pi} - x_r\right) \sin\psi_{rpi} + \left(y_r - y_{pi}\right) \cos\psi_{rpi} \right. \\ & \left. + \left(r_r\theta_{zr} - r_p\theta_{zpi}\right) \right] \cos\beta \\ & + \left[\left(r_r\theta_{xr} - r_p\theta_{xpi}\right) \sin\psi_{rpi} + \left(r_p\theta_{ypi} - r_r\theta_{yr}\right) \cos\psi_{rpi} \right. \\ & \left. + \left(z_r - z_{pi}\right) \right] \sin\beta, \end{aligned} \tag{3.38}$$

where β is the gear helix angle. A spur gear configuration for the planetary gearbox can be obtained by setting the helix angle, β, to zero. In Eq. (3.37) and Eq. (3.38), ψ is the angle between the plane of action and the vertical y axis, which is defined for a counter-clockwise motion of the sun gear as [96,190]

$$\psi_{spi} = \phi_{sp} - \alpha_{pi}, \tag{3.39}$$

$$\psi_{rpi} = \phi_{rp} + \alpha_{pi}, \tag{3.40}$$

for the sun-planet and ring-planet gear meshes, respectively. Here, ϕ_{sp} and ϕ_{rp} are the transverse pressure angles of the sun-planet and the ring-planet gear meshes, respectively [96,190]. The total kinetic and potential energies of the planetary gearbox can then be expressed as

$$T = T_h + T_p, \tag{3.41}$$

$$V = V_h + V_p + V_m. \tag{3.42}$$

Finally, the planetary gearbox equation of motion can be derived using the Lagrange`s equations of the second kind (see Appendix A) as

$$\mathbf{M}_{\boldsymbol{g}}\ddot{\boldsymbol{q}}_{\boldsymbol{g}}(t) + \left[\mathbf{C}_g + \mathbf{G}_g\left(\Omega_h, \Omega_{\mathrm{pi}}\right)\right]\dot{\boldsymbol{q}}_{\boldsymbol{g}}(t) + \mathbf{K}_g\boldsymbol{q}_{\boldsymbol{g}}(t) = 0, \tag{3.43}$$

which leads to the mass, $\mathbf{M}_{\boldsymbol{g}}$, stiffness, $\mathbf{K}_g$, gyroscopic, $\mathbf{G}_g$ matrices of the planetary gearbox. Proportional damping defined in Eq. (3.28) may also be employed for the damping of the planetary gearbox, $\mathbf{C}_g$. It must be noted that $\boldsymbol{q}_g(t)$ in Eq. (3.43) represents the generalized coordinates for the planetary gearbox. The full derivation of mass, stiffness and gyroscopic matrices can be seen in references [79,96,190].

The mass matrix of the planetary gearbox is in block diagonal form, and it can be expressed as

$$\mathbf{M}_{\boldsymbol{g}} = \begin{bmatrix} [\mathbf{M}_r] & 0 & 0 & \cdots & \cdots & 0 \\ 0 & [\mathbf{M}_c] & 0 & & & 0 \\ 0 & 0 & [\mathbf{M}_{pi}] & & & 0 \\ \vdots & & & \ddots & & \vdots \\ \vdots & & & & \ddots & \vdots \\ 0 & 0 & 0 & \cdots & \cdots & [\mathbf{M}_s] \end{bmatrix}, \tag{3.44}$$

where $\mathbf{M}_r$, $\mathbf{M}_c$, $\mathbf{M}_{pi}$, $\mathbf{M}_s$ represent the mass matrices of the ring gear, carrier, planet gears and sun gear, respectively, and they are expressed as

$$\mathbf{M}_j = \begin{bmatrix} m_j & 0 & 0 & 0 & 0 & 0 \\ 0 & m_j & 0 & 0 & 0 & 0 \\ 0 & 0 & m_j & 0 & 0 & 0 \\ 0 & 0 & 0 & I_{dj} & 0 & 0 \\ 0 & 0 & 0 & 0 & I_{dj} & 0 \\ 0 & 0 & 0 & 0 & 0 & I_{pj} \end{bmatrix}. \tag{3.45}$$

Here, j is the planetary gearbox member index ($j = r, c, pi, s$) for the ring gear, carrier, planet gears and sun gear, respectively.

The gyroscopic matrix of the planetary gearbox is expressed as

$$\mathbf{G_g} = \begin{bmatrix} [\mathbf{G}_r] & 0 & 0 & \cdots & \cdots & 0 \\ 0 & [\mathbf{G}_c] & 0 & & & 0 \\ 0 & 0 & [\mathbf{G}_{pi}] & & & 0 \\ \vdots & & & \ddots & & \vdots \\ \vdots & & & & \ddots & \vdots \\ 0 & 0 & 0 & \cdots & \cdots & [\mathbf{G}_s] \end{bmatrix} \tag{3.46}$$

where $\mathbf{G}_r$, $\mathbf{G}_c$, $\mathbf{G}_{pi}$, $\mathbf{G}_s$ represent gyroscopic matrices of the ring gear, carrier, planet gears and sun gear respectively, which are expressed as

$$\mathbf{G_j} = \begin{bmatrix} 0 & 0 & 0 & 0 & 0 & 0 \\ 0 & 0 & 0 & 0 & 0 & 0 \\ 0 & 0 & 0 & 0 & 0 & 0 \\ 0 & 0 & 0 & 0 & I_{pj} & 0 \\ 0 & 0 & 0 & -I_{pj} & 0 & 0 \\ 0 & 0 & 0 & 0 & 0 & 0 \end{bmatrix} \tag{3.47}$$

As can be seen from the mass, $\mathbf{M_g}$ and gyroscopic, $\mathbf{G_g}$ matrices of the planetary gearbox, they are uncoupled in lateral, axial and torsional directions. On the other hand, the stiffness matrix of the planetary gearbox, $\mathbf{K}_g$ is coupled in all directions due to the relative displacement between gear meshes and helix angle as seen in Eq. (3.37) and Eq. (3.38). Figure 3.4, which represents the stiffness matrix of the planetary gearbox, also shows its coupled structure.

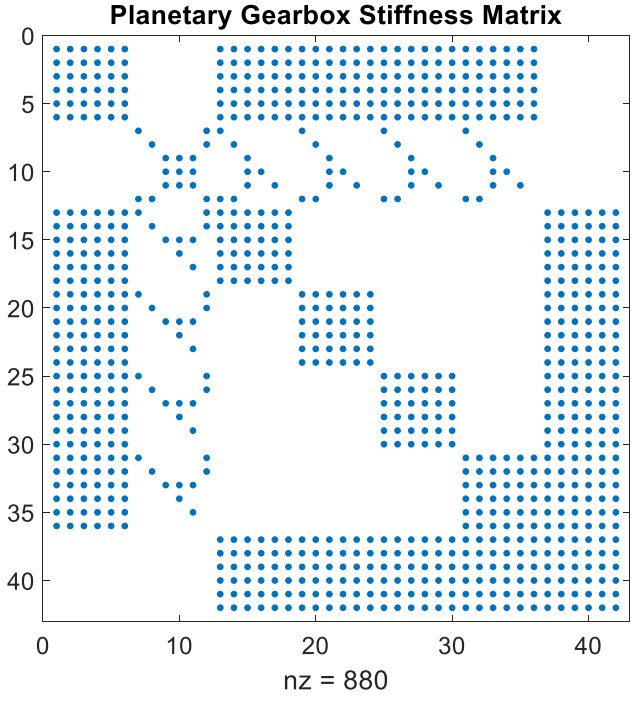

Figure 3.4 : Stiffness matrix of the planetary gearbox.

3.4 Assembly of planetary geared rotors

The planetary geared rotor system created consists of input and output shafts with their bearings and a planetary gearbox with the bearings of planetary gearbox members. The details of the planetary geared rotor system are seen schematically in Figure 3.5 where the planet gears are connected to the ring and sun gears via gear meshes, and the planetary gearbox itself is grounded via the bearings of the carrier, ring gear and sun gear. The input and output shafts are also supported with the bearings at the edges.

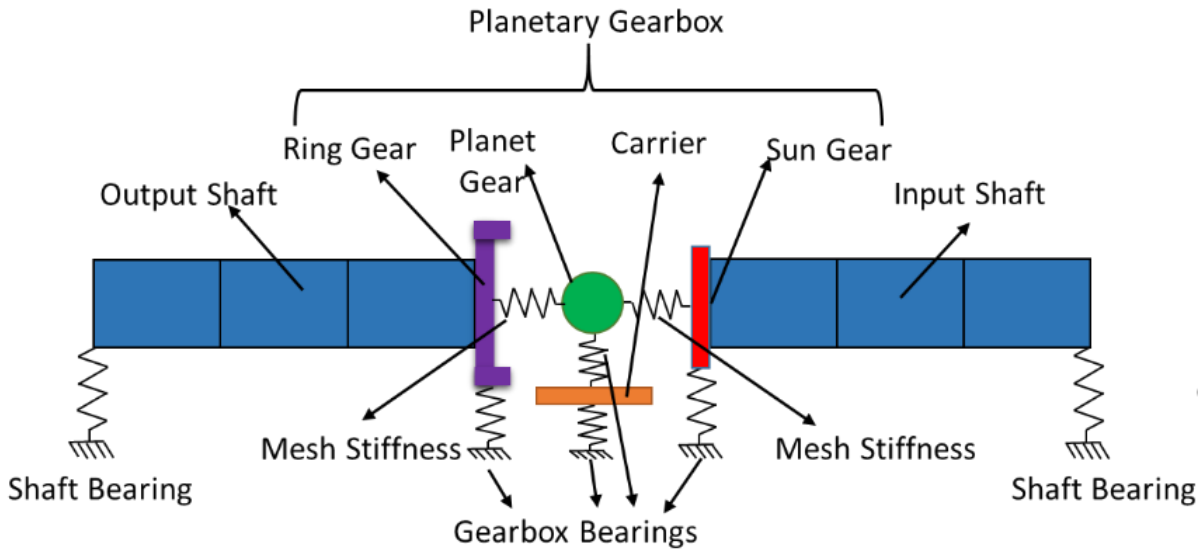

Figure 3.5 : Detail of the planetary geared rotor system.

The general equation of motion of a planetary geared rotor system with n degrees of freedom system can be obtained after the assembly of the shafts, bearings and planetary gearbox matrices. The global mass, $\mathbf{M}$, gyroscopic, $\mathbf{G}$, stiffness, $\mathbf{K}$, and damping matrices, $\mathbf{C}$, are obtained using the standard assembly methods for the rotor dynamic analysis. These matrices are defined as

$$[\mathbf{M}] = \mathbf{M}(\mathbf{M}_s, \mathbf{M}_g), \tag{3.48}$$

$$[\mathbf{G}] = \mathbf{G}(\mathbf{G}_s, \mathbf{G}_g), \tag{3.49}$$

$$[\mathbf{K}] = \mathbf{K}(\mathbf{K}_s, \mathbf{K}_b, \mathbf{K}_g), \tag{3.50}$$

$$[\mathbf{C}] = \mathbf{C}(\mathbf{C}_s, \mathbf{C}_b, \mathbf{C}_g). \tag{3.51}$$

As seen from the Eqs. (3.48, 3.49, 3.50, 3.51), the global mass and gyroscopic matrices are obtained directly from the shafts and planetary gearbox. On the other hand, global stiffness and damping matrices include bearings in addition to the shaft and planetary gearbox.

Figure 3.6 shows the general distribution of entries in the global matrices where mass and stiffness matrices are symmetric while the gyroscopic matrix is skew-symmetric. The planetary gearbox contribution in the matrices is highlighted by the red frames where the mass matrix of the planetary gearbox is in block diagonal form, and the gyroscopic matrix of the planetary gearbox is skew-symmetric. The stiffness matrix of the planetary gearbox makes the dynamic problem coupled since coupling terms arise.

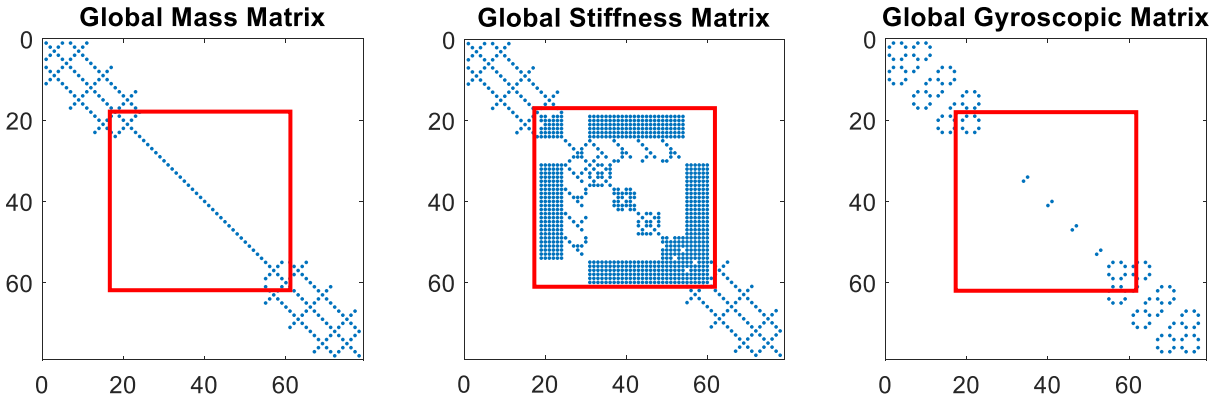

Figure 3.6 : Global mass, stiffness, gyroscopic matrices with 78 DOFs.

Finally, the system equation of the planetary geared rotor system for free responses can be written as

$$\mathbf{M}\ddot{\boldsymbol{q}}(t) + \left[\mathbf{C} + \mathbf{G}\left(\Omega_h, \Omega_{\mathrm{pi}}\right)\right]\dot{\boldsymbol{q}}(t) + \mathbf{K}\boldsymbol{q}(t) = 0. \tag{3.52}$$

In this model, the input and output shafts are rigidly connected to the input and output members of the planetary gearbox. For the rotating ring-fixed carrier gear configuration, the input and output members of the planetary gearbox thereby become the sun and ring gears, respectively. In the case of the rotating carrier-fixed ring configuration, the carrier becomes the output member whilst the sun gear remains the input member. Speed ratios of the planetary gearbox members can be obtained for the different configurations from the reference [191]. The model presented in this chapter allows analysing a rotating ring-fixed carrier configuration of the planetary gearbox. However, it is not sufficient to analyse a configuration with a rotating carrier since the spacing angles are currently constant, and the centripetal acceleration of the planets is not included in the formulation.

3.5 Concluding remarks

A six-degrees of freedom hybrid dynamic model of a planetary geared rotor system is created using the lumped parameter and finite element methods for the modelling of the planetary gearbox and rotor system respectively. All the elements are assumed to be flexible in the rotor-bearing system where 1-D rotating Timoshenko beam elements are used for the shaft modelling and uncoupled flexible spring elements are used for the bearing modelling. Members of the planetary gearbox, which are the ring, planet and sun gears and carrier, are assumed to be rigid disks, and the gear contacts are considered as flexible in the lumped parameter model of the planetary gearbox. Energy equations are given for the rotor-bearing system and planetary gearbox. Finally, the system equation of motions is obtained by applying Lagrange`s equations of the second kind. The dynamic model generated can be employed for the rotor dynamic analysis of planetary geared rotor systems.

Chapter 4

4 Modal behaviour of planetary geared rotors

4.1 Introduction

In this chapter, coupled dynamic behaviour of equally spaced spur and helical planetary geared rotor systems and the planetary gearbox impact on the modal behaviour of the global system are investigated for both static and rotating (including gyroscopic effects) cases using the previously introduced dynamic model in Chapter 3. The modal analysis of rotating systems requires different solution techniques compared with the non-rotating systems because gyroscopic forces on the rotating systems change the natural frequencies and mode shapes. The eigenvalue problem of rotating systems becomes quadratic due to the gyroscopic matrix in the system equation of motion of rotating systems. To solve the quadratic eigenvalue problem, it can be converted into the first order via the state space method. In the first part, the generalized and standard eigenvalue solutions of the quadratic eigenvalue problem are explained. In the second part, vibration modes of the helical and spur planetary geared rotors and the gearbox itself are identified using the standard eigenvalue solution. Here, the main difference between the mode shapes of the helical and spur planetary geared rotors are discussed by considering the helix angle effect in gear teeth. To analyse the dynamic coupling between the planetary gearbox and rotor system, modal energy analysis is employed. With this, the modal energy percentage of the planetary gearbox for each global mode can be computed in the planetary geared rotor system. In the final part, the high-speed dynamic behaviour of the helical planetary geared rotor due to the gyroscopic effects is investigated. For this purpose, the mode shapes of the low and high-speed cases with and without the planetary gearbox are compared to see the direct impact of planetary gearbox gyroscopic terms on the global rotor modes at higher speeds.

4.2 Quadratic eigenvalue problem of rotating systems

The natural frequencies and mode shapes of the previously introduced geared rotor system in Chapter 3 can be obtained with a free-free modal analysis by solving the eigenvalue problem. The modal analysis of a rotating system is slightly different from a static one since gyroscopic moments acting on the rotating systems affect their modal parameters in terms of natural frequencies and mode shapes. It is important to point out that gyroscopic effects cause the modal parameters to vary with the rotor speed. Similar to the damping terms, the gyroscopic terms introduce a term involving the first derivative of the generalized coordinate to the equation of motion. Therefore, the rotor dynamics problem becomes a quadratic eigenvalue problem [24]. In order to obtain the eigenvalues and eigenvectors, the quadratic eigenvalue problem can be expressed using the state space representation, which yields a first order eigenvalue problem [192,193]. However, this also doubles the sizes of the matrices in the eigenvalue problem, leading to an increase in computational time.

There are two forms of eigenvalue problems, known as standard and generalized eigenvalue problem. There is one input matrix in the standard eigenvalue problem, whereas there are two input matrices in the generalized eigenvalue problem. In MATLAB, the generalized and standard eigenvalue problems can be solved using the `eig` or `eigs` functions. The `eig` function computes all the eigenvalues whereas the `eigs` function computes a subset of eigenvalues such as the smallest or largest eigenvalues, using algorithmic reduction techniques. MATLAB uses LAPACK [39] routines to calculate the eigenvalues; and the eigenvalue solution algorithm is determined based on whether the input matrices are real or complex, symmetric or non-symmetric, Hermitian or non-hermitian; or positive definite [194,195].

4.2.1 Generalized eigenvalue problem

The generalized eigenvalue problem of gyroscopic systems [3] can be derived by first expressing the equations of motion from Eq. (3.52) in state space form as shown below:

$$\begin{bmatrix} \mathbf{C} + \Omega\mathbf{G}\left(\Omega_h, \Omega_{\mathrm{pi}}\right) & \mathbf{M} \\ \mathbf{M} & 0 \end{bmatrix} \begin{Bmatrix} \dot{\boldsymbol{q}} \\ \ddot{\boldsymbol{q}} \end{Bmatrix} + \begin{bmatrix} \mathbf{K} & 0 \\ 0 & -\mathbf{M} \end{bmatrix} \begin{Bmatrix} \boldsymbol{q} \\ \dot{\boldsymbol{q}} \end{Bmatrix} = \begin{Bmatrix} 0 \\ 0 \end{Bmatrix}. \tag{4.1}$$

Then, this equation can be rewritten using the state vectors $\boldsymbol{x} = \begin{Bmatrix} \boldsymbol{q} \\ \dot{\boldsymbol{q}} \end{Bmatrix}$ and $\dot{\boldsymbol{x}} = \begin{Bmatrix} \dot{\boldsymbol{q}} \\ \ddot{\boldsymbol{q}} \end{Bmatrix}$ as

$$[\mathbf{A}]_{2n \times 2n}\{\dot{\boldsymbol{x}}\}_{2n \times 1} + [\mathbf{B}]_{2n \times 2n}\{\boldsymbol{x}\}_{2n \times 1} = 0. \tag{4.2}$$

The size of the eigenvalue problem is now $2n$ as can be seen from the matrix equations. Therefore, $2n$ eigenvalues and eigenvectors are obtained with the eigenvalue solution. Half of the eigenvalues and eigenvectors are the complex conjugates of the other half. After solving the standard eigenvalue problem, the eigenvalue and eigenvector matrices are given by:

$$\begin{aligned} &[\lambda]_{2n \times 2n}, \\ &[\phi]_{2n \times 2n}, \end{aligned} \tag{4.3}$$

respectively. It should be noted that these matrices consist of complex conjugate pairs. Finally, the mode shapes are extracted from the eigenvector matrix $[\phi]$, and the undamped natural frequencies are obtained using the eigenvalues $[\lambda]$ as [40]

$$\omega_i = \sqrt{Re(\lambda_i)^2 + Im(\lambda_i)^2}. \tag{4.4}$$

In order to evaluate the accuracy of the generalized eigenvalue solution, a parity check can also be done with a residual matrix calculation as defined below

$$residual = B \times \phi + A \times \phi \times \lambda. \tag{4.5}$$

The residual matrix calculation is a useful tool to quantify the numerical errors.

4.2.2 Standard eigenvalue problem

The system equation of motion of the planetary geared rotor system defined in Eq. (3.52) can be reformulated to construct the state-space representation via the inverse matrix operation as [40]

$$\ddot{\boldsymbol{q}}(t) + \mathbf{M}^{-1}\left[\mathbf{C} + \mathbf{G}\left(\Omega_h, \Omega_{\mathrm{pi}}\right)\right]\dot{\boldsymbol{q}}(t) + (\mathbf{M}^{-1}\mathbf{K})\boldsymbol{q}(t) = 0. \tag{4.6}$$

With the state vectors $\boldsymbol{x} = \begin{Bmatrix} \boldsymbol{q} \\ \dot{\boldsymbol{q}} \end{Bmatrix}$ and $\dot{\boldsymbol{x}} = \begin{Bmatrix} \dot{\boldsymbol{q}} \\ \ddot{\boldsymbol{q}} \end{Bmatrix}$, the standard eigenvalue problem in matrix form is expressed as

$$\begin{Bmatrix} \dot{\boldsymbol{q}} \\ \ddot{\boldsymbol{q}} \end{Bmatrix} = \begin{bmatrix} \mathbf{0} & \boldsymbol{I} \\ -\mathbf{M}^{-1}\mathbf{K} & -\mathbf{M}^{-1}\left[\mathbf{C} + \mathbf{G}\left(\Omega_h, \Omega_{\mathrm{pi}}\right)\right] \end{bmatrix} \begin{Bmatrix} \boldsymbol{q} \\ \dot{\boldsymbol{q}} \end{Bmatrix}, \tag{4.7}$$

where $\boldsymbol{I}$ represents the identity matrix. The matrix equation for the standard eigenvalue problem can then be rewritten as

$$\{\dot{\boldsymbol{x}}\}_{2n\times 1} = [\mathbf{A}]_{2n\times 2n}\{\boldsymbol{x}\}_{2n\times 1}. \tag{4.8}$$

where **A** is called state matrix. As with the generalized eigenvalue problem, the size of the standard eigenvalue problem is $2n$ and half of them are the complex conjugates of the other half, but only one matrix needs to be computed for Eq. (4.8) instead of two for Eq. (4.2). The eigenvalue $[\lambda]$ and eigenvector $[\phi]$ matrices are obtained with the solution of the standard eigenvalue problem. Similar to the parity check of the generalized eigenvalue solution, a residual matrix formula can be defined for the standard eigenvalue solution as

$$residual = A \times \phi - \phi \times \lambda. \tag{4.9}$$

Throughout the numerical analyses in this thesis, the standard eigenvalue solution is going to be used rather than the generalized one to compute the eigenvalues and eigenvectors because of its computational performance [40].

4.3 Mode identification

Mode shapes in rotor systems can either be uncoupled with no interaction between the lateral, axial and torsional vibration of the system, or coupled where these modes can interact. A simple cyclically symmetric rotor system can be considered as uncoupled [3], but the presence of a gearbox in the system can lead to lateral, torsional and axial mode interaction [151]. To quantify the impact of a planetary gearbox on the coupling behaviour of the global modes of the geared rotor system, a modal energy approach is used where the modal energy of the gearbox for each mode is compared to the total modal energy in the system.

Modal energy analysis

The total modal energies of the rotor system and the planetary gearbox are computed by summing their kinetic and potential energies. The kinetic, T_r, potential, V_r, and total, L_r, energies of the rotor system are written as

$$T_r(i) = \frac{1}{2}[\dot{\boldsymbol{q}}_r(i)]^T[\mathbf{M}][\dot{\boldsymbol{q}}_r(i)], \tag{4.10}$$

$$V_r(i) = \frac{1}{2}[\boldsymbol{q}_r(i)]^T[\mathbf{K}][\boldsymbol{q}_r(i)], \tag{4.11}$$

$$L_r(i) = T_r(i) + V_r(i), \tag{4.12}$$

in terms of discrete time. Similarly, the kinetic, potential and total energies of the planetary gearbox in the rotor system can be written, respectively, as

$$T_r^g(i) = \frac{1}{2}[\dot{\boldsymbol{q}}_r(i)]^T[\mathbf{M}_g][\dot{\boldsymbol{q}}_r(i)], \tag{4.13}$$

$$V_r^g(i) = \frac{1}{2}[\boldsymbol{q}_r(i)]^T[\mathbf{K}_g][\boldsymbol{q}_r(i)], \tag{4.14}$$

$$L_r^g(i) = T_r^g(i) + V_r^g(i). \tag{4.15}$$

In Eqs. (4.10), (4.11), (4.13) and (4.14), $\boldsymbol{q}_r$ is the motion vector in translational and rotational directions for each mode, defined as

$$\boldsymbol{q}_r = [q_{r1}, q_{r2}, q_{r3}, q_{r4}, q_{r5}, q_{r6}, \dots\dots\dots\dots\dots\dots\dots\dots\dots\dots, q_{rk}], \tag{4.16}$$

where k represents the total number of degrees of freedom of the system and r is the mode number. q_{rk} is defined as a function of time as [196]

$$q_{rk}(i) = \phi_{rk} \sin\left(\frac{2\pi t(i)}{\tau_r} + \varphi_{rk}\right), \tag{4.17}$$

where $t(i)$ is the discrete time for the simulation. ϕ_{rk} and φ_{rk} represent the individual elements of the r^{th} eigenvector and its corresponding phase angle respectively. In Eq. (4.17), τ_r is the vibration period of the r^{th} mode [196]. The discrete time is also defined as

$$t(i) = [0{:}\,\Delta t{:}\,t_s], \tag{4.18}$$

where Δt is time step, i is the index for the number of time data points and t_s is the vibration simulation time. By using the total energies from Eqs. (4.12) and (4.15), the mean values of the total energies of the global rotor system and the gearbox can be computed as

$$L_r = \frac{1}{n}\sum_{i=1}^{n} L_r(i), \tag{4.19}$$

$$L_r^g = \frac{1}{n}\sum_{i=1}^{n} L_r^g(i). \tag{4.20}$$

The modal energy percentage of the gearbox then becomes

$$\varepsilon = \frac{L_r^g}{L_r} \times 100, \tag{4.21}$$

which allows an estimate of the gearbox contribution to the overall dynamic response of the system. It should be noted that damping will be neglected in the following numerical analyses, since it does not affect the presented results significantly and the modal energy defined in Eq. (4.21) can only be computed for undamped cases (conservative systems).

Rotor dynamics analysis software

There are currently three rotor dynamics software suites based on the finite element method, written in MATLAB. They were developed by Bucher [197], Genta [198] and Friswell et al. [199], called "RotFE", "DynRot" and "Rotordynamics", respectively. These software programs use four degrees of freedom, considering just lateral vibrations. Among these programs, Bucher [197] uses the generalized eigenvalue problem in his RotFE code whereas Friswell et al. [199] use the standard eigenvalue problem in their rotor dynamics software. During this PhD project, a novel six degrees of freedom finite element/lumped parameter based rotor dynamics software, called "GEAROT", has been developed for the dynamic and modal analyses of geared rotor systems in MATLAB. The dynamic model defined in Chapter 3 and modal analysis theory defined in this chapter are used in "GEAROT" where just rotor system analysis can also be done without a gearbox. High or low order geared rotor models can be chosen depending on the analysis purpose. The main output of the analysis of the geared rotor system is the mode characterisation, modal energy analysis, obtaining the frequency response functions and Campbell diagrams. The flow chart of "GEAROT" is shown in Figure 4.1.

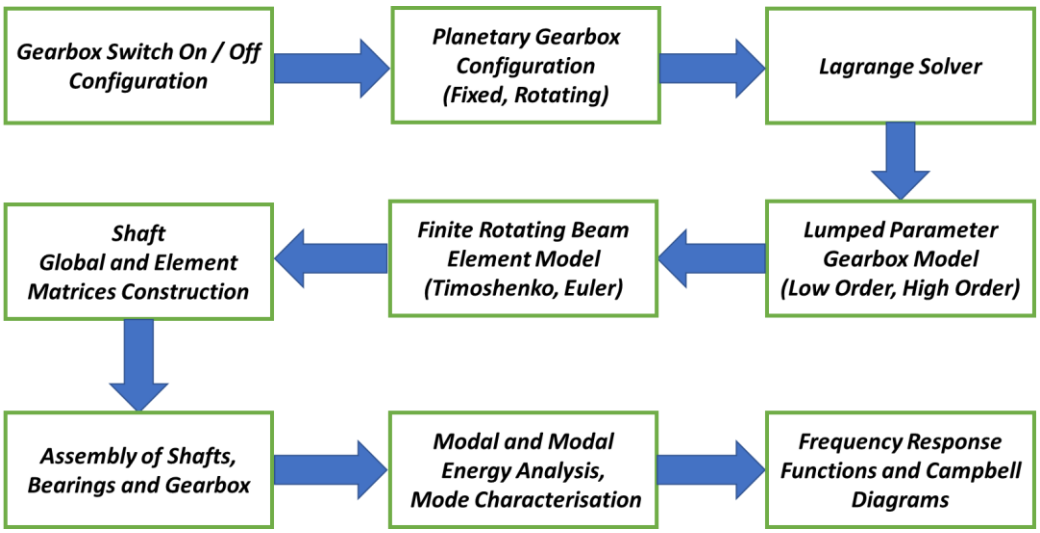

Figure 4.1 : GEAROT software flow chart.

4.3.1 Helical planetary geared rotor

Modal analysis of the helical planetary gearbox on its own, and also the corresponding geared rotor system were conducted. Initially, an undamped non-rotating (static) case with the model parameters given in Table 4.1 was considered.

Table 4.1 : Parameters of the planetary geared rotor system.

Parameter	Output Shaft	Input Shaft	Carrier	Ring	Planets	Sun
Length [m]	2	2	0.02	0.1	0.1	0.1
Outer Diameter [m]	0.2	0.2	0.63	0.7	0.2	0.23
Inner Diameter [m]			0.23	0.63	0.18	0.2
Material density [kg/m^3]	7800	7800	7800	7800	7800	7800
Young`s modulus [GPa]	211	211				
Shear modulus [GPa]	81.2	81.2				
Proportional damping α_1 constant	0	0	0	0	0	0
Proportional damping α_2 constant	0	0	0	0	0	0
Bearing radial stiffness [N/m]	10^9	10^9	10^9	10^9	10^9	10^9
Bearing axial stiffness [N/m]	10^9	10^9	10^9	10^9	10^9	10^9
Bearing tilting stiffness [N.m/rad]	10^7	10^7	10^7	10^7	10^7	10^7
Bearing torsional stiffness [N.m/rad]	0	0	10^{11}	0	0	0
Bearing radial damping [N/(m/s)]	0	0	0	0	0	0
Bearing axial damping [N/(m/s)]	0	0	0	0	0	0
Bearing tilting damping [N.m/(rad/s)]	0	0	0	0	0	0
Bearing torsional damping [N.m/(rad/s)]	0	0	0	0	0	0
Helix angle β [deg]				30	30	30
Transverse pressure angle ϕ [deg]				22.5	22.5	22.5
Mesh Stiffness [N/m]				10^8	10^8	10^8
Number of planets					4	
Number of beam elements	18	18				

The shafts from Figure 3.1 were modelled with 36 finite Timoshenko beam elements, and the planetary gearbox was modelled with seven rigid masses which represent the ring gear, carrier, sun gear and four planet gears. Modal analysis results are given for the first thirty modes as seen in Table 4.2 where natural frequencies and mode types of the planetary gearbox and the planetary geared rotor system are listed. It should be noted that the first mode of the planetary geared rotor and the gearbox on its own are rotational rigid body modes due to the free rotation of the shafts and gears in the rotational θ_Z direction. In addition, the modal energy percentage of the planetary gearbox for each global mode was also computed using the Eq. (4.21), and it is shown in Table 4.2.

Table 4.2 : Modes of the helical planetary geared rotor and just the gearbox.

	Helical Planetary Geared Rotor			Helical Planetary Gearbox	
Mode #	Gearbox Modal Energy %	Natural Frequency [Hz]	Mode Type	Natural Frequency [Hz]	Mode Type
1	27	0	Torsional (Rigid Body)	0	Rotational (Rigid Body)
2	10	114	Lateral	299	Translational - Tilting
3	10	114	Lateral	299	Translational - Tilting
4	10	115	Lateral	324	Translational - Tilting
5	10	115	Lateral	324	Translational - Tilting
6	60	220	Torsional - Axial	524	Rotational - Axial
7	29	301	Torsional - Axial	633	Rotational - Axial
8	27	318	Torsional - Axial	642	Translational - Tilting
9	94	322	Lateral	642	Translational - Tilting
10	94	322	Lateral	711	Translational - Tilting
11	17	333	Lateral	711	Translational - Tilting
12	17	333	Lateral	735	Rotational - Axial
13	15	346	Lateral	908	Planet
14	15	346	Lateral	1018	Translational - Tilting
15	20	466	Torsional - Axial	1018	Translational - Tilting
16	62	508	Lateral	1227	Rotational - Axial
17	62	508	Lateral	1895	Translational - Tilting
18	97	595	Torsional - Axial	1895	Translational - Tilting
19	23	601	Lateral	1905	Rotational - Axial
20	23	601	Lateral	2263	Translational - Tilting
21	32	649	Lateral	2263	Translational - Tilting
22	32	649	Lateral	2332	Planet
23	84	710	Lateral	2367	Rotational - Axial
24	84	710	Lateral	2428	Planet
25	18	782	Torsional - Axial	2437	Translational - Tilting
26	28	873	Lateral	2437	Translational - Tilting
27	28	873	Lateral	2464	Planet
28	100	908	Gearbox	2484	Rotational - Axial
29	18	943	Lateral	2869	Translational - Tilting
30	18	943	Lateral	2869	Translational - Tilting

Three main mode families can be identified from the modal analysis of the helical planetary gearbox, consisting of (i) rotational-axial, (ii) translational-tilting and (iii) planet modes. This definition is in accordance with Eritenel and Parker [81], where for the planet modes, the central members (ring, carrier and sun) do not move in any direction while the planets can freely move in all directions. In the case of the rotational-axial mode, the central members only move in rotational and axial directions while the planets move in all directions. Likewise, if the mode is translational-tilting, the central members only move in the translational and tilting

directions, and the planets move in all directions. These coupling effects in the planetary gearbox will have a significant impact on the geared rotor system, since it can lead to coupling terms in the equation of motion, and consequently lead to coupling between the two rotors that are connected via the planetary gearbox. This mode identification is valid for applications with more than one planet because one planet leads to coupled translational-tilting-rotational-axial modes.

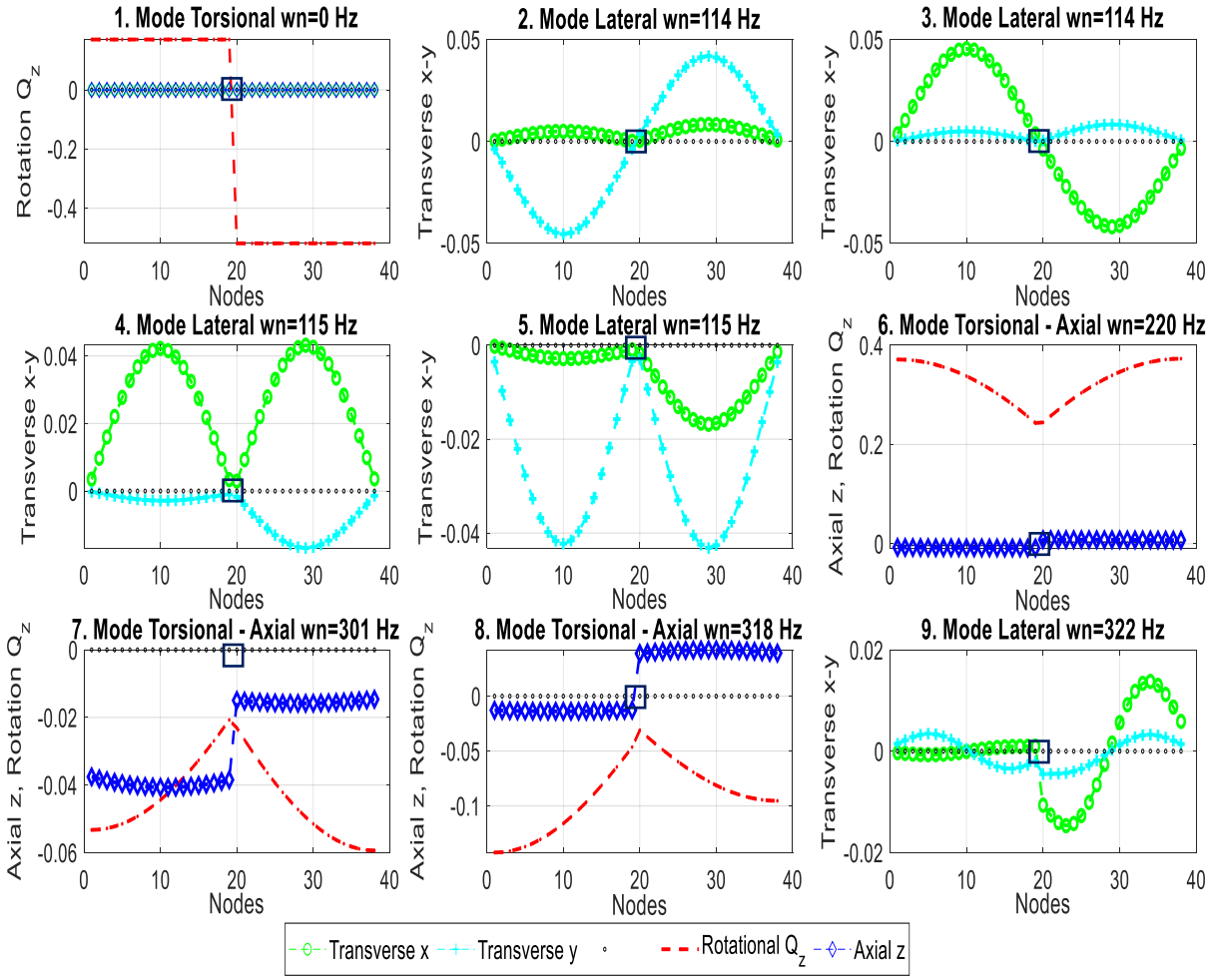

Figure 4.2 : Mode shapes of the helical planetary geared rotor system.

As listed in Table 4.2, the mode shapes of the helical planetary geared rotor systems can be classified as (i) torsional-axial, (ii) lateral (bending) and (iii) gearbox modes. Figure 4.2 shows the first nine mode shapes of the rotor system in which the gearbox location is also pointed with the rectangles. As stated, the first mode is a pure torsional rigid body mode, where the two shafts rotate around their axes as rigid bodies, and the gearbox determines the speed ratio. The following lateral modes of the shafts come in orthogonal pairs, and they are coupled due to the translational and tilting motion of the gearbox. Due to the helical configuration of the gearbox, axial motion of the rotor can lead to a torsional motion and vice versa, which in turn leads to a

torsional-axial mode coupling, as can be seen in Figure 4.2 for modes 6, 7 and 8. In the coupled torsional-axial modes, mode shape decoupling in the axial direction can also be seen between the two shafts due to the relatively high shaft stiffness compared to the planetary gearbox. The final set of observed modes shapes for the planetary geared rotor system are the isolated gearbox modes, which are associated with the planet modes of the gearbox itself. As discussed previously for the gearbox planet modes, the central members do not move, and consequently no vibration transmission from the planets to the shafts can occur. Since these modes are independent of the rotor system, the resonance frequencies are identical to the gearbox only computation. Figure 4.2 also shows that there is an asymmetric motion in the two shafts despite the fact that the planetary gearbox is located between the identical two shafts. This phenomenon occurs due to the different mass and inertia properties of the input and output members of the planetary gearbox itself.

In order to better understand the gearbox contribution to the overall mode shape of the rotor system, the gearbox modal energy values from Table 4.2 can be considered. The planetary gearbox modal energy in the global system is 100% for each gearbox mode. These modes coincide with the planet modes of the gearbox itself. For example, the 13th mode of the planetary gearbox is a planet mode at 908 Hz, and also seen as the 28th mode of the planetary geared rotor system as a gearbox mode. There is no deflection on the shaft in any direction for these particular gearbox modes. There are also some other global modes in which gearbox has higher modal energies. For instance, the gearbox has higher modal energies for the 9th, 10th, 18th, 23rd and 24th global modes where the modal energy percentages are 94%, 94%, 97%, 84% and 84% respectively. The 9th and 10th modes are lateral modes at 322 Hz, and they are very close to the 4th and 5th mode (transverse-tilting) of the gearbox at 324 Hz. Similarly, the 23rd and 24th modes of the global rotor system are the lateral mode at 710 Hz, which is very close to the gearbox transverse-tilting mode at 711 Hz. These results show that some global torsional-axial and lateral modes are highly coupled with some of the rotational-axial and transverse-tilting modes of the planetary gearbox respectively.

The distributions of the total and gearbox modal energies during a vibration cycle are shown in Figure 4.3 for the first nine modes. Not surprisingly, the total modal energy of the global rotor system is constant during the vibration period (transfer of energy from potential to kinetic and back, no losses in the undamped system) while the modal energy of the gearbox is fluctuating except for the 1st mode, which is a rigid body torsional mode. This makes perfect sense since the modal analysis was carried out for the global rotor system, and the modal energy

of the global rotor system should be constant. However, the planetary gearbox is a part of the global rotor system, and the modal analysis of the system was not carried out using the mass and stiffness matrices of the gearbox. Therefore, the modal energy of the planetary gearbox fluctuates during the vibration cycle. To capture this fluctuation, the time domain approach is used. Then, the mean value of the modal energy of the planetary gearbox was computed for each global mode by averaging the fluctuating modal energy, using the Eqs. (4.19) and (4.20).

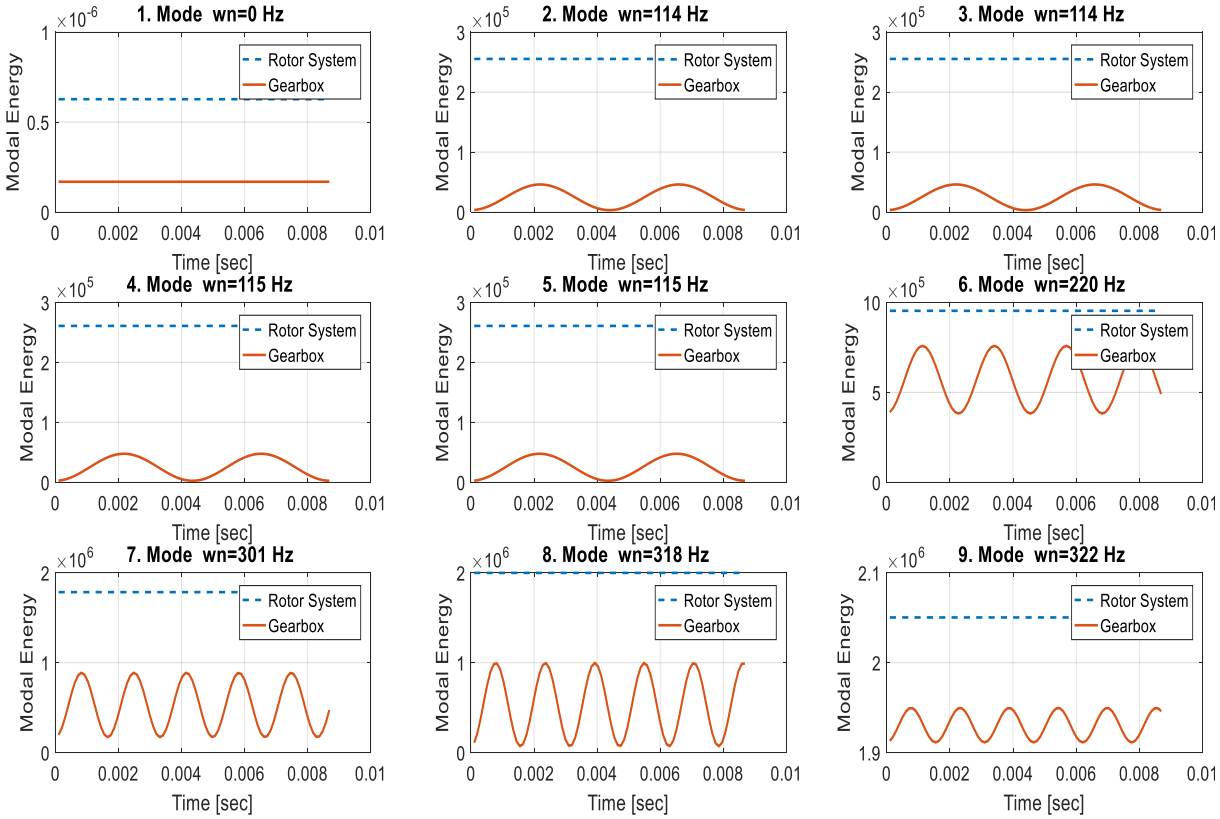

Figure 4.3 : Modal energy of the helical planetary geared rotor system over time.

4.3.2 Spur planetary geared rotor

Modal analyses of the spur planetary geared rotor system and the planetary gearbox were carried out by setting the helix angle of all gears zero. The system and gearbox parameters from Table 4.1 and the assumptions from Section 4.3.1 were used for the analysis. The results in Table 4.3 show that modes of the shafts for the spur planetary geared rotor system are identified as torsional, axial, lateral and gearbox modes for the first thirty modes. Moreover, modes of the spur planetary gearbox are also identified as rotational, axial, translation, tilting and planet modes. The modes which are rotational-axial and translational-tilting in the helical planetary gearbox becomes uncoupled in the spur planetary gearbox as rotational, axial, translational and tilting. Therefore, there is no coupling between the torsional, axial and lateral modes of the shafts.

Table 4.3 : Modes of the spur planetary geared rotor and just the gearbox.

	Spur Planetary Geared Rotor			Spur Planetary Gearbox	
Mode #	Gearbox Modal Energy %	Natural Frequency [Hz]	Mode Type	Natural Frequency [Hz]	Mode Type
1	27	0	Torsional (Rigid Body)	0	Rotational (Rigid Body)
2	10	113	Lateral	281	Tilting
3	10	113	Lateral	281	Tilting
4	8	114	Lateral	340	Tilting
5	8	114	Lateral	340	Tilting
6	57	256	Torsional	638	Axial
7	29	298	Axial	640	Translational
8	25	311	Axial	640	Translational
9	16	333	Lateral	666	Axial
10	16	333	Lateral	692	Rotational
11	100	340	Gearbox	738	Translational
12	100	340	Gearbox	738	Translational
13	10	345	Lateral	1077	Planet
14	10	345	Lateral	1081	Translational
15	21	473	Torsional	1081	Translational
16	62	509	Lateral	1462	Rotational
17	62	509	Lateral	1790	Axial
18	24	601	Lateral	1971	Translational
19	24	601	Lateral	1971	Translational
20	100	638	Gearbox	2197	Tilting
21	24	655	Lateral	2197	Tilting
22	24	655	Lateral	2332	Planet
23	89	727	Lateral	2376	Planet
24	89	727	Lateral	2385	Rotational
25	17	789	Torsional	2461	Translational
26	28	880	Lateral	2461	Translational
27	28	880	Lateral	2524	Planet
28	13	948	Lateral	2550	Rotational
29	13	948	Lateral	2835	Axial
30	100	1077	Gearbox	2898	Tilting

As seen in Figure 4.4, the first mode is once more the torsional rigid body mode. The other modes are torsional, axial and lateral modes. The 7^{th} and 8^{th} axial modes show that the input and output shafts have independent dynamic behaviour since there is no deflection in the input shaft for the 7^{th} axial mode and the output shaft for the 8^{th} mode. The reason for this phenomenon is that the axial component of the gear mesh stiffness is zero due to the zero-helix angle in the spur gear configuration. As a result, there cannot be vibration transmission between the output and input shafts in these independent axial modes. In other words, no axial response

occurs in one shaft due to axial excitation from the other shaft. The asymmetric motion described for the helical planetary geared rotor is also seen for the spur planetary geared rotor in Figure 4.4.

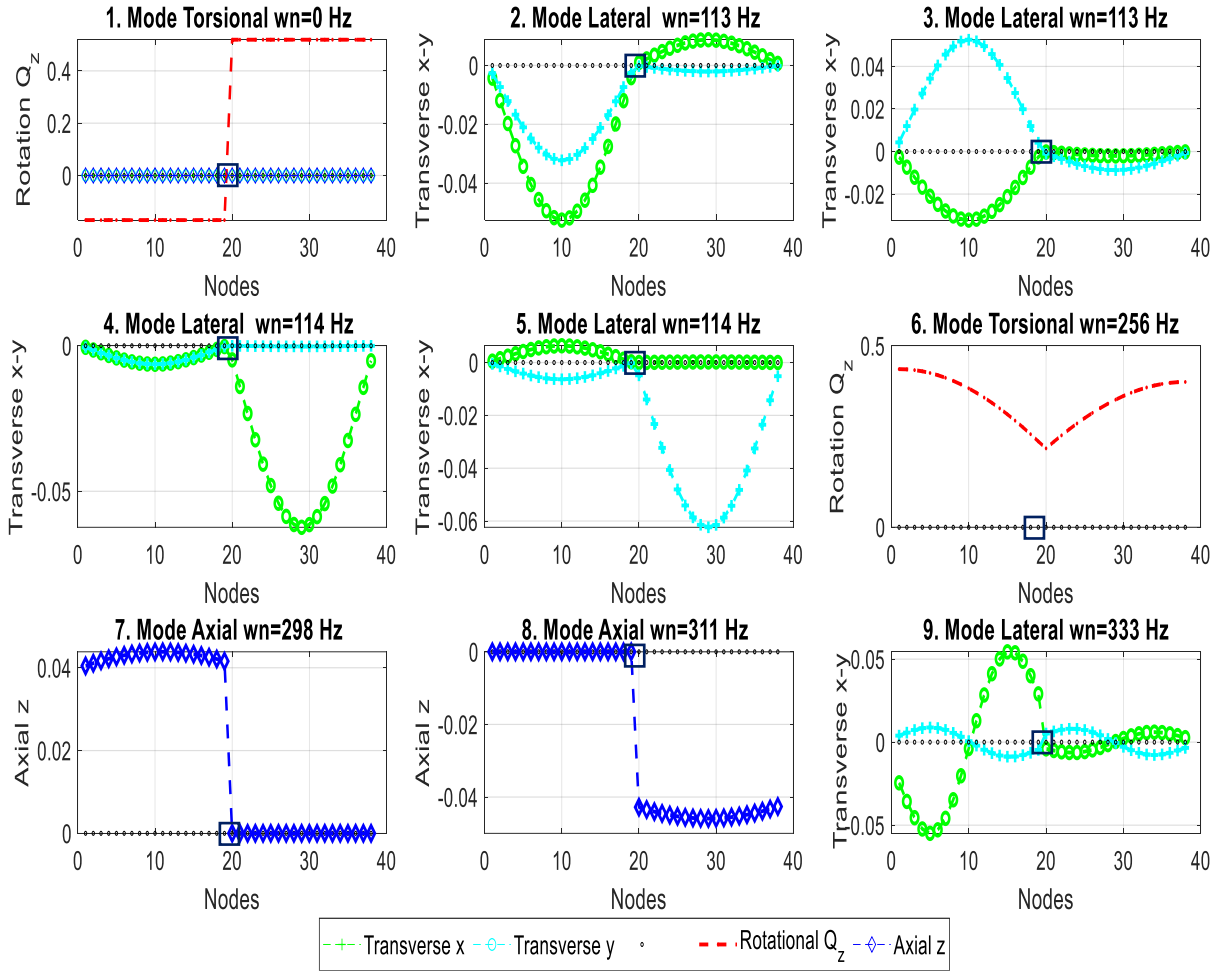

Figure 4.4 : Mode shapes of the spur planetary geared rotor system.

In some modes, modal energies of the planetary gearbox were also computed as 100%, which are the 11th, 12th, 20th, 30th gearbox modes, respectively. These modes are associated with the 4th, 5th, 6th and 13th modes of the planetary gearbox, and they were observed at precisely the same frequency for the global modes. Among these modes, the 4th, 5th and 6th modes are identified as carrier-planet, which means the carrier and planets can move freely and the 13th mode is identified as a planet mode, meaning that only the planets can move freely. Since the ring and sun gears do not move for these modes, no rotation or displacement occurs on the shafts. As a result, these modes are isolated from the shafts. The gearbox modal energies in Table 4.3 further highlight that even in the spur gear case some significant modal energy can be stored in the gearbox for some of the modes, highlighting the importance of the gearbox for the overall dynamic behaviour of the rotor system.

During a vibration period, the gearbox modal energy in the spur planetary geared rotor system can also be seen for the first nine modes in Figure 4.5.

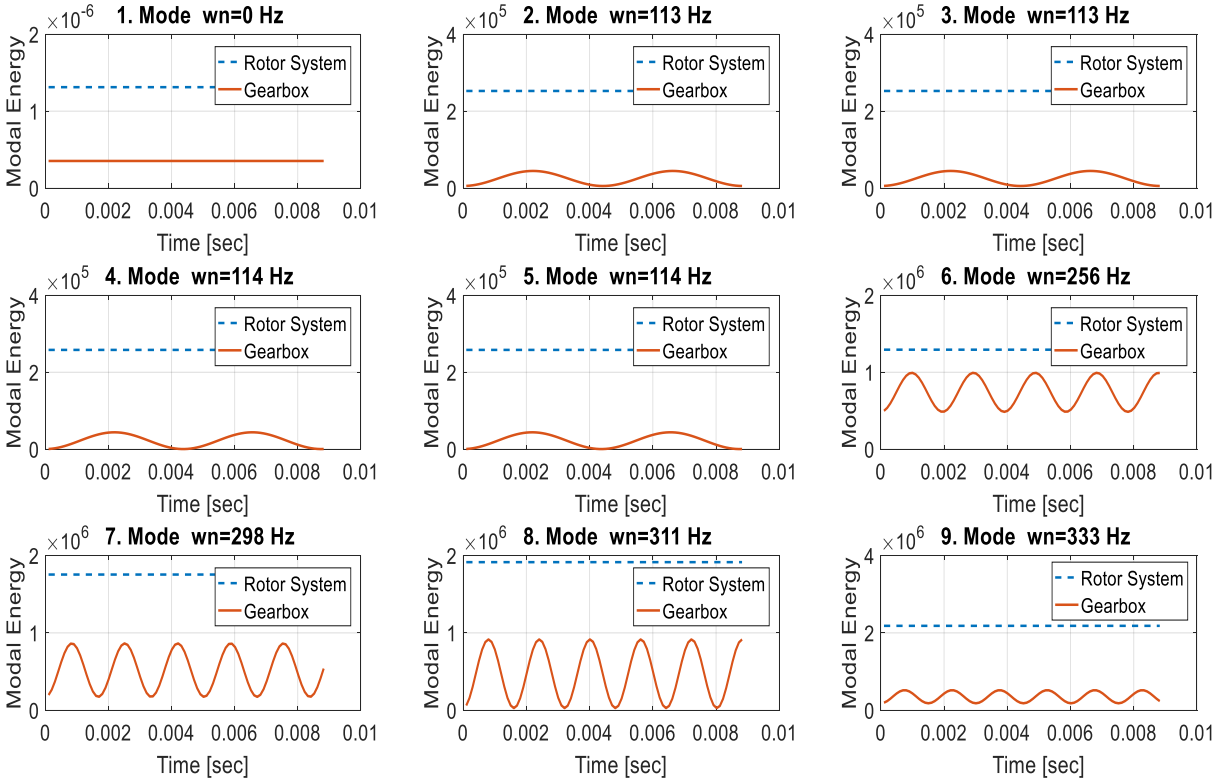

Figure 4.5 : Modal energy of the spur planetary geared rotor system over time.

Figure 4.6 summarises the results of the modal energy analysis given in Table 4.2 and 4.3 for the helical and the spur gear configurations.

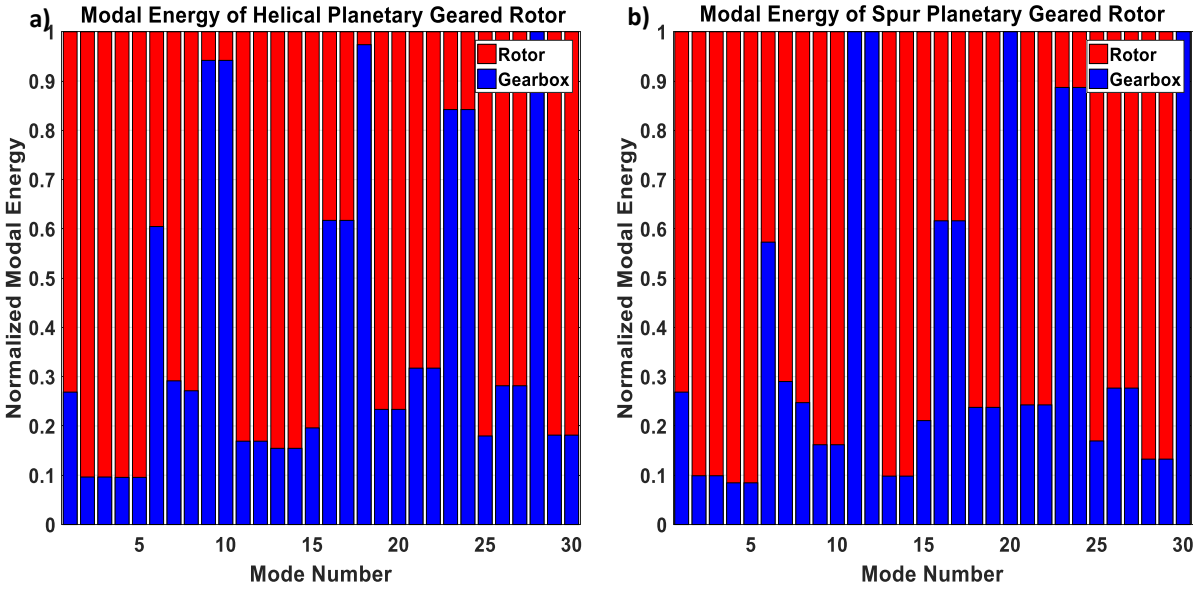

Figure 4.6 : Modal energy of the rotor system, a) helical planetary gearbox, b) spur planetary gearbox.

4.4 High-speed modal behaviour

Planetary geared rotors can work at higher operating speeds, and therefore gyroscopic moments can significantly affect their dynamic behaviour. To investigate the high-speed dynamic behaviour of the helical planetary geared rotor system, modal analysis was carried out at 8000 rpm input speed. Lateral forward and backward whirling, coupled torsional-axial and torsional rigid body mode shapes were plotted for the first twelve modes, as seen in Figure 4.7. The speed ratio between the two shafts was determined as 3.04 based on the gear geometry given in Table 4.1. As a result, the input shaft rotates faster than the output shaft in this system.

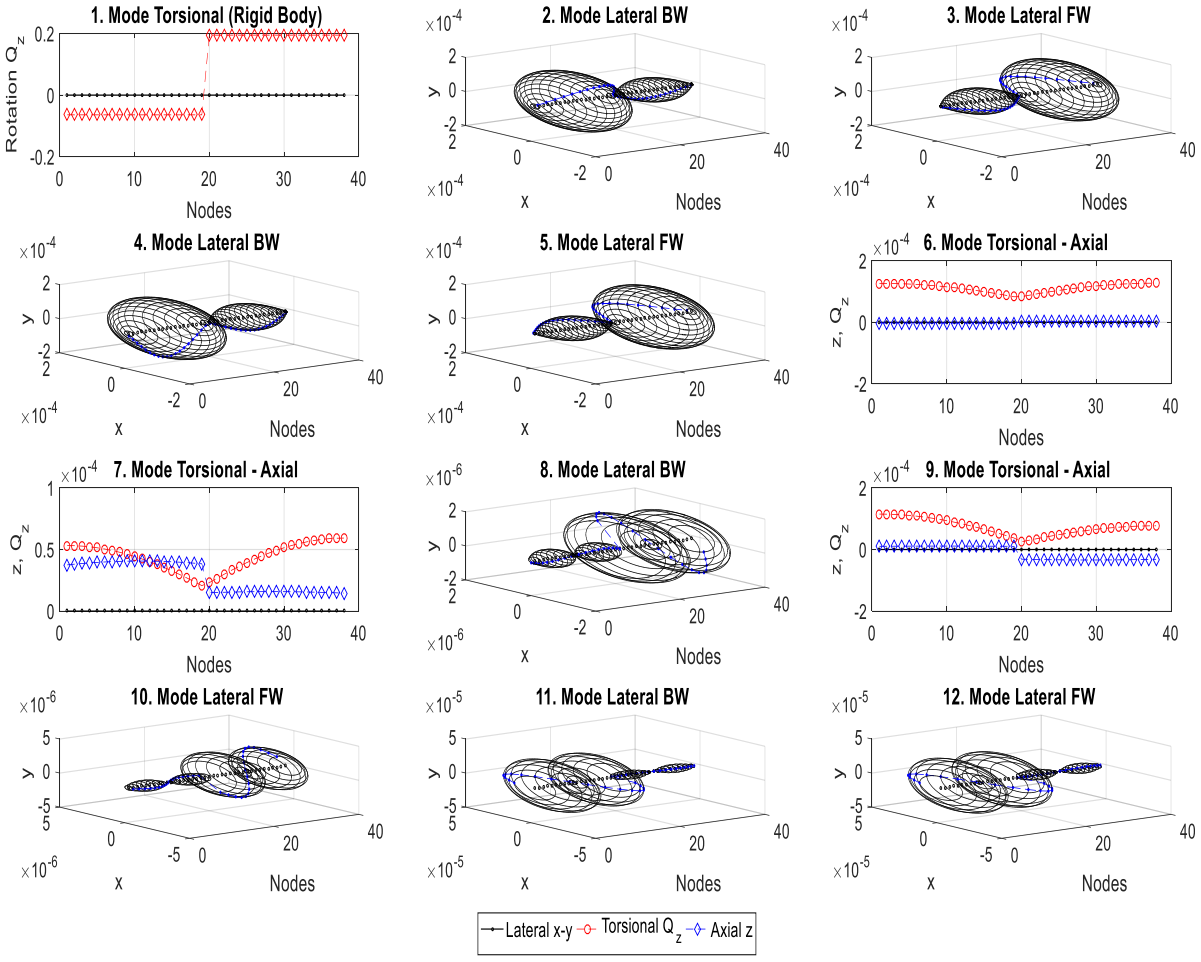

Figure 4.7 : Mode shapes of the helical planetary geared rotor system at 8000 rpm.

In contrast to the previous investigation, which focused on a static case, the orthogonal modes now combine to give lateral backward (BW) and forward (FW) whirling modes, while the coupled torsional-axial and torsional rigid body modes remain the same. The natural frequencies of the lateral backward and forward whirling modes are dependent on the shaft speeds due to the gyroscopic effect. On the other hand, there is no gyroscopic term in the axial

and torsional components of the gyroscopic matrix, which leads to speed independent coupled torsional-axial modes.

Table 4.4 : Low and high speed dynamic behaviour of the planetary geared rotor system.

	100 rpm			8000 rpm		
Mode #	Natural Frequency [Hz]	Mode Type	Frequency Shift %	Natural Frequency [Hz]	Mode Type	Frequency Shift %
1	0.0	Torsional	0.000	0.0	Torsional	0.000
2	113.8	Lateral BW	0.001	113.4	Lateral BW	0.281
3	113.8	Lateral FW	0.000	113.5	Lateral FW	0.222
4	115.0	Lateral BW	0.001	115.2	Lateral BW	0.182
5	115.0	Lateral FW	0.001	115.3	Lateral FW	0.292
6	219.8	Torsional - Axial	0.000	219.8	Torsional - Axial	0.000
7	300.7	Torsional - Axial	0.000	300.7	Torsional - Axial	0.000
8	318.2	Torsional - Axial	0.000	317.8	Lateral BW	1.406
9	322.2	Lateral BW	0.017	318.2	Torsional - Axial	0.000
10	322.3	Lateral FW	0.017	326.6	Lateral FW	1.327
11	332.6	Lateral BW	0.003	331.8	Lateral BW	0.244
12	332.6	Lateral FW	0.003	333.3	Lateral FW	0.210

The speed-dependent property of the lateral modes leads to a frequency split in the Campbell diagrams in Figure 4.8 where the natural frequencies of the lateral modes change with respect to the shaft speed whilst the torsional-axial modes are not affected by the shaft speeds. The forward whirling mode thereby experiences an increase in frequency, while the backward whirling mode sees a decrease in frequency.

Gyroscopic moments can originate from the shafts and the rigid disk elements inside the planetary gearbox (gears and carrier). To understand the impact of the planetary gearbox gyroscopic moments on the frequency response, Campbell diagrams were generated with and without gearbox gyroscopic effects for two different frequency ranges in Figure 4.8. For instance, a significant gearbox gyroscopic effect is seen for the 9^{th} and 10^{th} lateral BW and FW modes (numbering from the static case). When plotting the Campbell diagram without the gearbox gyroscopic effect, the natural frequency change becomes very small for these modes. A small frequency change can still be observed due to the gyroscopic effects from the shafts. The frequency shifts between the static case and 8000 rpm for these modes are 1.41% and 1.33% respectively, as seen in Table 4.4. On the other hand, the gearbox gyroscopic effect is just visible for the 2^{nd}, 3^{rd}, 4^{th}, 5^{th}, 11^{th}, 12^{th} lateral modes. The frequency shifts between the

static case and 8000 rpm are 0.28%, 0.22%, 0.18%, 0.29%, 0.24%, 0.21% for these modes, as seen in Table 4.4. The highest gearbox gyroscopic effect within the first twelve modes is observed for the 9th and 10th mode (in the static case) and the gearbox has a higher modal energy of about 94% for these modes. However, the gearbox has lower modal energy at a value of 10% for the 2nd, 3rd, 4th and 5th modes and 17% for the 11th and 12th modes. It can be concluded that the planetary gearbox gyroscopic effect is much more dominant in some modes where the planetary gearbox has higher modal energy.

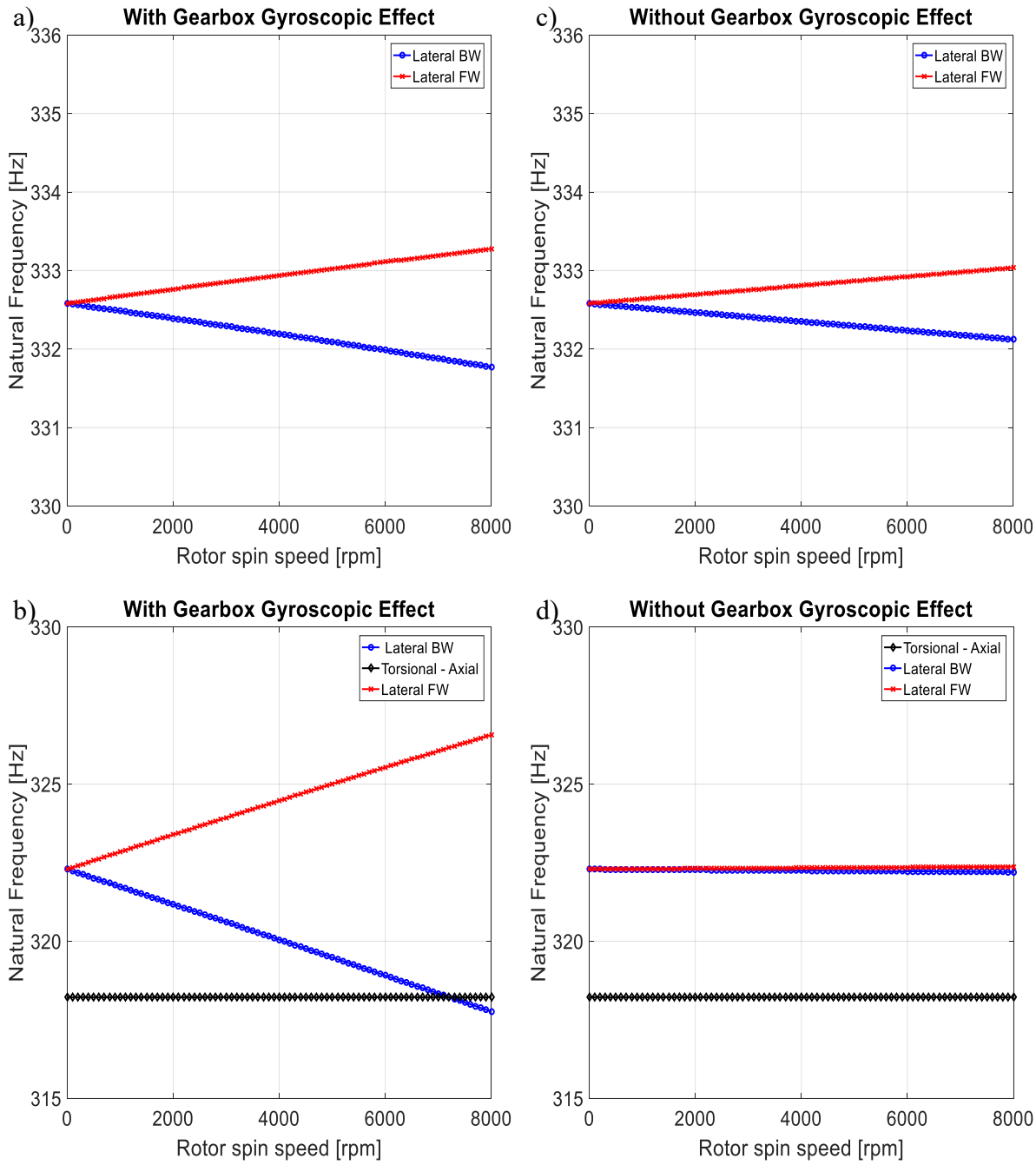

Figure 4.8 : Campbell diagram, a) and b) with gearbox gyroscopic effect, c) and d) without gearbox gyroscopic effect for two different frequency ranges.

Table 4.4 also provides data for low speed (100 rpm) modal analysis, where the natural frequencies, mode types and frequency shifts can be compared to the high-speed case (8000 rpm). It is clear that there is a natural frequency shift between the low and high speeds. To better understand the impact of the gyroscopic effects on the mode shapes, the Modal Assurance Criteria (MAC) is used to compare the eigenvectors at low and high speeds. The MAC formula is [26]

$$MAC(L,H) = \frac{\left|\{\phi_L\}_r^T\{\phi_H\}_q\right|^2}{(\{\phi_L\}_r^T\{\phi_L\}_r)\left(\{\phi_H\}_q^T\{\phi_H\}_q\right)}, \tag{4.22}$$

where ϕ_L and ϕ_H are the low and high-speed eigenvectors, respectively, and r and q represent the corresponding mode number. The resulting MAC matrices with and without gyroscopic effects in the gearbox are shown in Figures 4.9a and b, respectively.

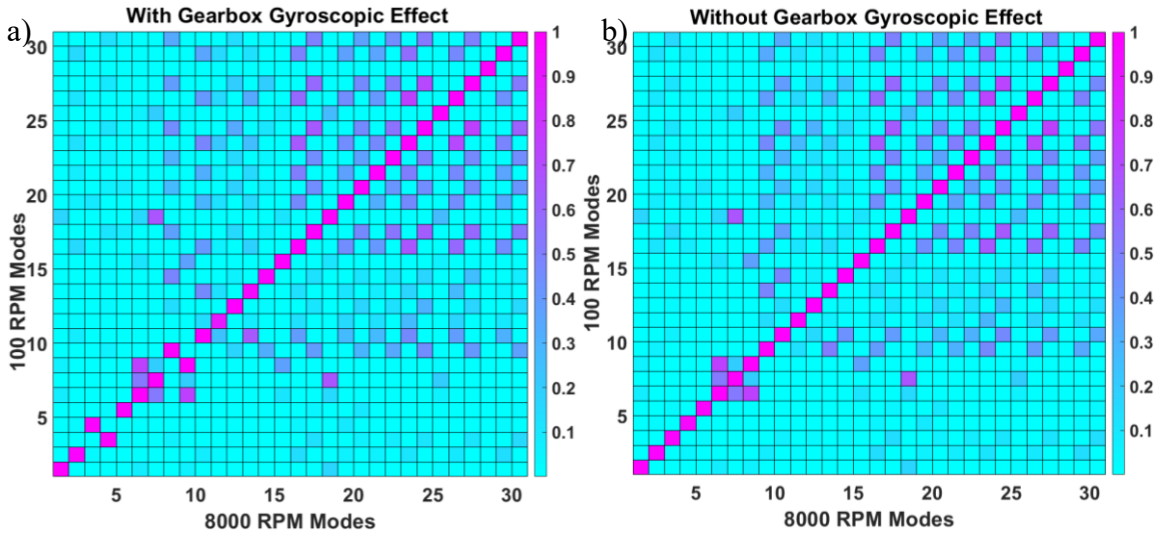

Figure 4.9 : MAC matrices for low (100 rpm) and high (8000 rpm) speeds, a) with planetary gearbox gyroscopic effect, b) without planetary gearbox gyroscopic effect.

The MAC matrix in Figure 4.9a shows that modes eight and nine reverse their order due to the crossing in Campbell diagram (veering), while the other modes do not seem to be affected by the shaft speed. A further reduction in speed dependence can be observed when the gyroscopic effects of the gearbox are neglected, leading to a nearly 100% MAC diagonal in Figure 4.9b. The MAC is not 100% in Figure 4.9b because there is a small gyroscopic effect from the two shafts. In summary, it can be said that the rotor dynamic behaviour is only mildly affected by the rotational speed, and for modes with a high gearbox contribution stronger splitting of the frequencies may lead to unexpected mode veering regions.

4.5 Discussion

The main focus of this investigation is to understand the impact of an equally spaced planetary gearbox on the global dynamic behaviour of a rotor system. Mode shapes of the helical planetary geared rotors are identified as coupled torsional-axial, lateral and gearbox modes whereas mode shapes with the spur planetary gearbox become torsional, axial, lateral and gearbox. The main difference between the spur and helical planetary geared rotors is the presence of coupling between torsional and axial modes in the latter due to the helix angle. The helix angle effect can be clearly seen in the composition of the global stiffness matrix of the planetary geared rotors in Figure 4.10. Here, it is clear that zero helix angle makes the gear mesh stiffness zero in the axial directions. Therefore, the input and output shafts have independent dynamic behaviours from each other in the axial modes, and the axial vibrations cannot transmit between them. Moreover, making the helix angle zero cancels the coupling term between the axial and torsional directions, resulting in uncoupled torsional, axial and lateral modes. In the case of helical gears, axial thrust forces can create unexpected torsional excitations on the shaft, which can be of great significance for geared turbofan engines where planetary gearboxes are commonly used.

A further feature of the modes for both spur and helical planetary geared rotors is the asymmetric motion in the two shafts, although the planetary gearbox is located at the middle of the system and the shafts have identical properties. This breaking of the symmetry can be attributed to the different mass and inertia properties of the input and output members of the planetary gearbox itself, which are directly attached to the two shafts.

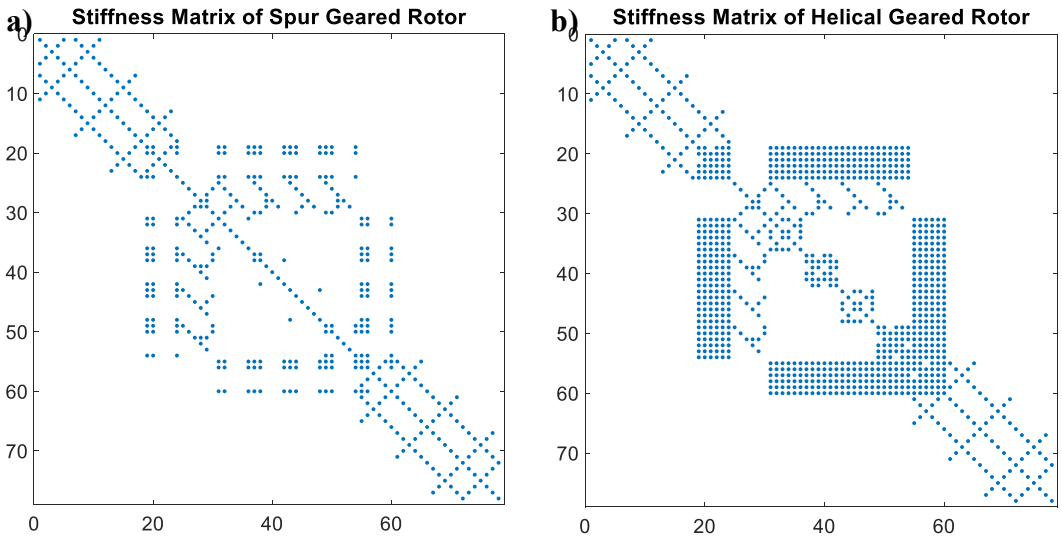

Figure 4.10 : Helix angle effect on the global stiffness matrix, a) spur, b) helical.

To better understand the contribution of the planetary gearbox to the global modes of the system, the modal energy of the gearbox compared to the total modal energy of the system has been computed. Tables 4.2 and 4.3 summarise the results of this analysis for the helical and the spur gear configurations. It shows that there are some global modes in which no motion of the shaft is observed, and all the energy is stored in the gearbox. These modes can be directly related to the internal modes of the planetary gearbox where the planets or planets and carrier move in the case of the helical or spur planetary gearbox respectively, while the central members do not move, leading to a decoupling of the planetary gearbox and the shafts. They are classified as gearbox modes in the global rotor system. In contrast to these internal gearbox modes, the other modes in which the planetary gearbox has higher modal energy are highly coupled with the shafts. For these modes, the natural frequencies of the rotor system and planetary gearbox are very close to each other.

An additional effect that needs to be considered when studying the dynamics of a geared rotor system is the gyroscopic effect originating from the planetary gearbox. This can lead to a mode veering phenomenon in the MAC comparison between low (100 rpm) and high (8000 rpm) speeds. In addition, they can significantly influence the natural frequencies of the backward and forward lateral modes of the planetary geared rotor system, particularly for the modes with higher gearbox modal energy.

4.6 Concluding remarks

The dynamic behaviour of two shaft rotor systems with equally spaced spur and helical planetary gearboxes were investigated in detail by considering the gyroscopic effects and neglecting damping. Modal analysis of the geared rotor system was conducted to study the impact of the planetary gearbox on the modal behaviour of the shafts. On the basis of mode shapes of the shafts, mode identification of the rotor system was carried out for the static case and the rotating case (including gyroscopic effects). The effect of the planetary gearbox on each global rotor mode was then quantified for the static case by the modal energy analysis. The effect of the planetary gearbox gyroscopic terms on the global rotor modes was also investigated.

The modal analysis of the planetary geared rotor system highlights the strong modal coupling introduced by the planetary gearbox. Modes of the helical planetary geared rotors are identified as coupled torsional-axial, lateral and gearbox modes whereas spur planetary geared rotors have uncoupled modes, which are classified as axial, torsional, lateral modes and gearbox

modes. The gear helix angle is the main coupling parameter in planetary geared rotor systems, which makes torsional and axial modes coupled. It is also found that axial vibrations of the input and output shafts are uncoupled from each other in spur planetary geared rotors. In helical planetary geared rotors, coupled torsional-axial modes can also result in mode shape decoupling (discontinuity) in the axial direction between the input and output shafts of the planetary gearbox due to the lower axial stiffness of the planetary gearbox compared to the shaft stiffness. Gearbox modes are fully isolated from the shafts because no dynamic interaction between the shafts and gearbox occurs for these modes. Moreover, no displacement and rotation occur on the shafts for the gearbox modes. Therefore, the modal energy of the planetary gearbox for the gearbox modes is 100%. The natural frequencies of the gearbox modes, computed with a global rotor modal analysis, are directly associated with the planet modes, computed with an independent modal analysis of the planetary gearbox. Apart from the gearbox modes, the planetary gearbox has higher modal energy in some other modes where the coupling level between the gearbox and shafts is much higher. At these modes, natural frequencies of the planetary geared rotor system and the planetary gearbox are close to each other. This clearly shows that gearbox is dominant when there is a high coupling between the global rotor system and gearbox. As a result of the dominancy of the planetary gearbox, the natural frequencies computed from the independent modal analysis of the gearbox and the global rotor system become closer to each other.

For the high-speed dynamic behaviour, the global backward and forward lateral modes in which the planetary gearbox has higher modal energy can experience significant gyroscopic effects due to the gearbox members. This can lead to significant changes in the natural frequencies of the global system. When compared to the gyroscopic effects originating from the shafts, the gyroscopic effects of the planetary gearbox can result in a mode veering phenomenon.

Chapter 5

5 Planetary gearbox parameter effects on the vibration modes of geared rotor systems

5.1 Introduction

In this chapter, an extensive parameter study is presented to investigate planetary gearbox parameter effects on the vibration modes of planetary geared rotor systems. The parameter study is divided into three sections as gear contact parameters, planetary gearbox mass and support parameters, and planet gear parameters. The dynamic model of the planetary geared rotor system, introduced in Chapter 3, is used. Its baseline parameters are selected from Table 4.1 throughout this chapter. In the first section, gear mesh stiffness, pressure angle and helix angle are selected as gear contact parameters and their effects on the vibration modes of the helical and spur planetary geared rotors are analysed. In the second section, gear material density and planetary gearbox support stiffness effects on the helical and spur planetary geared rotor vibration modes are investigated. In the third section, the number of planet gears that effect the vibration modes of the helical planetary geared rotor, and mistuning (positioning error of planet gears) effects on the vibration modes of both helical and spur planetary geared rotors are investigated. The sensitivity of the natural frequencies of planetary geared rotors is analysed by plotting the natural frequency maps and computing the frequency shifts between the two extreme cases. Mode shapes of the planetary geared rotors for the two extreme cases are compared using the modal assurance criteria. Sensitive vibration modes are also tried to be identified with the frequency shifts and mode shape comparisons. In the final section, a brief discussion for the gearbox parameters effects on the vibration modes is given to understand the influential gearbox parameters; and concluding remarks are presented.

5.2 Gear contact parameter effects

5.2.1 Mesh stiffness

Gear mesh stiffness is identified as the contact stiffness between gear teeth. It is one of the important stiffness parameters in gearboxes and geared rotor systems. In this parameter study, gear mesh stiffness is assumed to be constant for each case, which is a valid assumption for heavily-loaded gears [8]. In reality, gear mesh stiffness fluctuates during a contact period [8,10], which is explained in detail in Chapter 2, section 2.3.2. Numerous linear and nonlinear dynamic analyses have been undertaken for understanding the time-varying mesh stiffness effect on the dynamic behaviour of gear pair. On the other hand, there are only a few parameter studies that have investigated the constant gear mesh stiffness effect on the dynamic behaviour of planetary gearboxes and geared rotor systems. One parameter study was conducted for investigating the mesh stiffness effect on critical speeds of a double-helical gear transmission system by Chen et al. [146], highlighting the importance of the frequency veering phenomenon. Rao et al. [149] also showed a gear mesh stiffness region which affects the natural frequencies in geared rotors. However, they did not give a sufficient explanation for the mesh stiffness effect on modal behaviour. Apart from the geared rotors, Parker et al. did a sensitivity analysis of planetary gearbox vibration modes to the gear mesh stiffness. Despite these gear mesh stiffness parameter studies for gearboxes and geared rotors, no parameter study has been done, investigating the gear mesh stiffness effects on the vibration modes of planetary geared rotor systems. For this purpose, a gear mesh stiffness parameter study was carried out to investigate its effect on the modal behaviour of spur and helical planetary geared rotor systems.

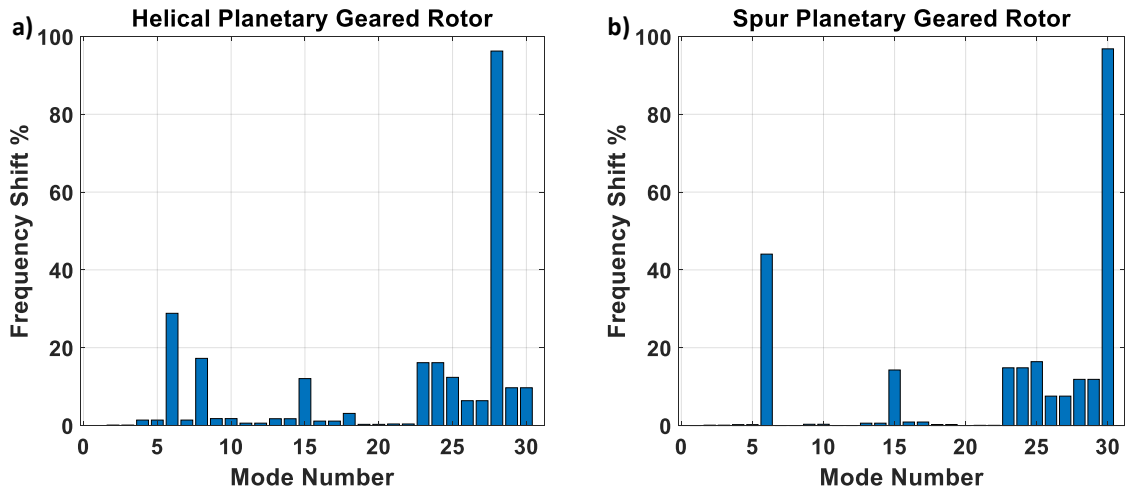

Figure 5.1 : Frequency shifts of planetary geared rotor vibration modes due to gear mesh stiffness, a) helical, b) spur.

Table 5.1 : Vibration modes of the helical and spur planetary geared rotors for various gear mesh stiffness.

Helical Planetary Geared Rotor					Spur Planetary Geared Rotor			
	$k_m = 10^8$ [N/m] (Baseline)	$k_m = 10^9$ [N/m]			$k_m = 10^8$ [N/m] (Baseline)	$k_m = 10^9$ [N/m]		
Mode #	Nat. Freq. [Hz]	Nat. Freq. [Hz]	Mode Type	Freq. Shift %	Nat. Freq. [Hz]	Nat. Freq. [Hz]	Mode Type	Freq. Shift %
1	0	0	Torsional	0	0	0	Torsional	0
2	114	114	Lateral	0	113	113	Lateral	0
3	114	114	Lateral	0	113	113	Lateral	0
4	115	117	Lateral	1	114	115	Lateral	0
5	115	117	Lateral	1	114	115	Lateral	0
6	220	283	Torsional - Axial	29	256	369	Torsional	44
7	301	305	Torsional - Axial	1	298	298	Axial	0
8	318	373	Torsional - Axial	17	311	311	Axial	0
9	322	328	Lateral	2	333	334	Lateral	0
10	322	328	Lateral	2	333	334	Lateral	0
11	333	335	Lateral	1	340	340	Gearbox	0
12	333	335	Lateral	1	340	340	Gearbox	0
13	346	352	Lateral	2	345	347	Lateral	1
14	346	352	Lateral	2	345	347	Lateral	1
15	466	522	Torsional - Axial	12	473	540	Torsional	14
16	508	514	Lateral	1	509	514	Lateral	1
17	508	514	Lateral	1	509	514	Lateral	1
18	595	614	Torsional - Axial	3	601	602	Lateral	0
19	601	602	Lateral	0	601	602	Lateral	0
20	601	602	Lateral	0	638	638	Gearbox	0
21	649	651	Lateral	0	655	655	Lateral	0
22	649	651	Lateral	0	655	655	Lateral	0
23	710	825	Lateral	16	727	834	Lateral	15
24	710	825	Lateral	16	727	834	Lateral	15
25	782	879	Torsional - Axial	12	789	918	Torsional	16
26	873	929	Lateral	6	880	946	Lateral	8
27	873	929	Lateral	6	880	946	Lateral	8
28	908	1783	Gearbox	96	948	1061	Lateral	12
29	943	1035	Lateral	10	948	1061	Lateral	12
30	943	1035	Lateral	10	1077	2119	Gearbox	97

Gear mesh stiffness ranges between 10^8 N/m and 10^9 N/m, up to 10 times, was selected for the parameter study. The first 30 modes and frequency shifts between 10^8 N/m and 10^9 N/m gear

mesh stiffness values were computed for both helical and spur planetary geared rotors as shown in Table 5.1 where the corresponding mode types can also be seen. It should be noted that $k_m = 10^8$ [N/m] is the baseline gear mesh stiffness value as given in Table 4.1 previously.

The gear mesh stiffness effect on the natural frequencies is shown for the significant modes in Figure 5.2. Overall, the natural frequencies increase with respect to the mesh stiffness. There is no significant change in the natural frequencies up to the 6th mode, therefore the first five modes were not plotted. To understand the reason for vibration mode sensitivity, the modes which have more than 10 % frequency shift were investigated further.

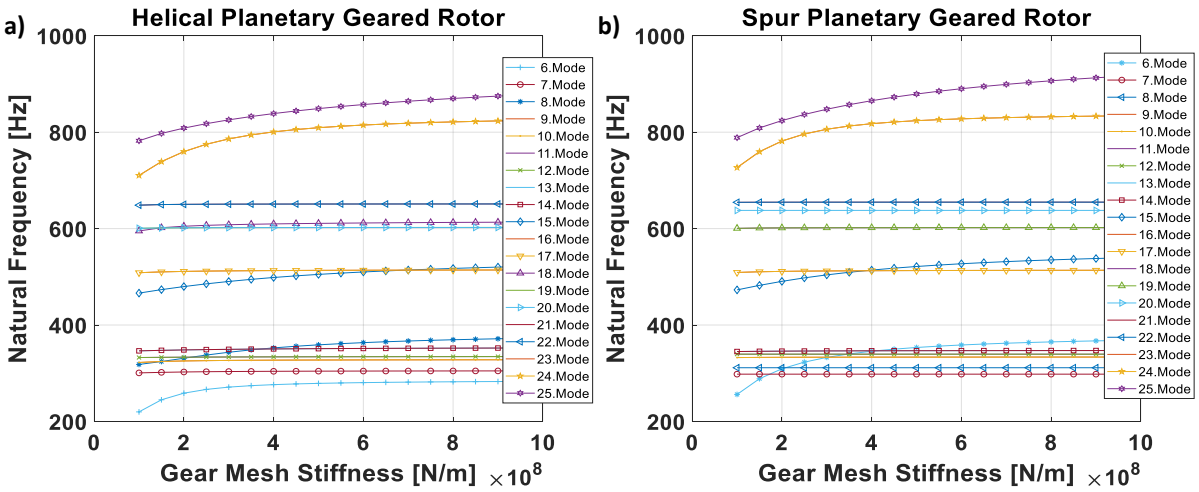

Figure 5.2 : Visualisation of sensitivity of planetary geared rotor vibration modes to gear mesh stiffness, a) helical, b) spur.

For the helical planetary geared rotor, higher frequency shifts were computed as 29 %, 17 %, 12 % and 12 % at the 6th, 8th, 15th and 25th torsional-axial modes respectively. Similarly, the frequency shifts were computed as 16 % for the 23rd and 24th lateral modes and 96 % for the 28th gearbox mode. In general, the torsional-axial modes in the helical planetary geared rotors are much more sensitive to the gear mesh stiffness change compared to the lateral modes. The so-called gearbox modes are directly affected by gear mesh stiffness change as clearly seen at the gearbox mode (28th mode). For the spur planetary geared rotor, higher frequency shifts were computed as 44 %, 14 % and 16 % at the 6th, 15th and 25th torsional modes, respectively. Moreover, the frequency shifts at the 23rd, 24th, 28th and 29th lateral modes were computed as 15 %, 15 %, 12 % and 12 %, respectively, and 97 % for the 30th mode (gearbox mode). All the torsional modes within the first 30 modes are found to be much more sensitive to the gear mesh stiffness change in the spur planetary geared rotor. The axial modes of the spur planetary geared rotor are not sensitive to the gear mesh stiffness change since there is no axial component of the gear mesh stiffness in spur gears.

When comparing the helical and spur planetary geared rotor modes, there are some torsional-axial modes in the helical planetary geared rotor, which are more sensitive to the gear mesh stiffness change due to the fact that the torsional vibrations are more dominant than the axial one at these modes. It can be directly inferred from the torsional and axial modes of the spur planetary geared rotor given in Table 5.1.

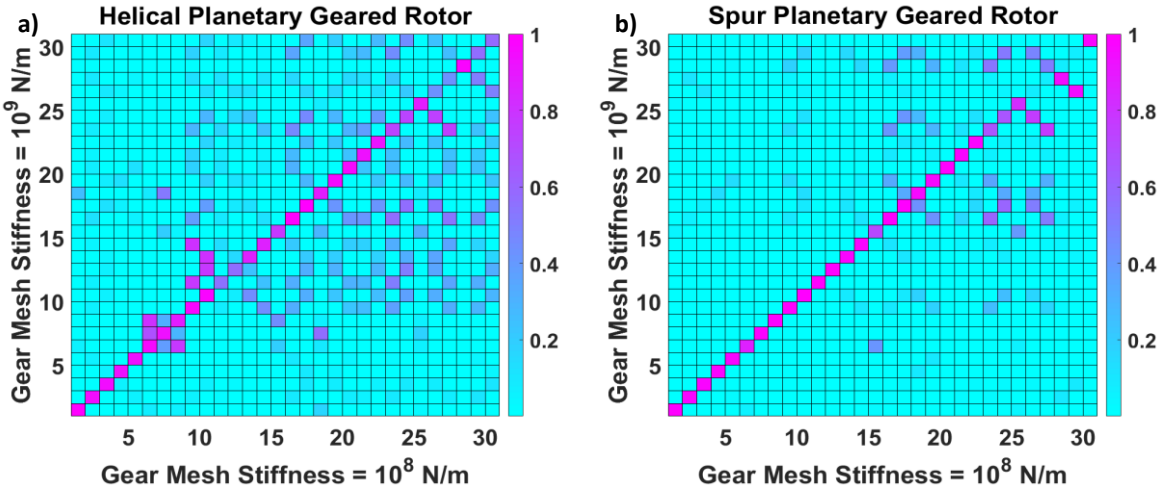

Figure 5.3 : MAC for 10^8 and 10^9 N/m gear mesh stiffness, a) helical, b) spur.

MAC matrices between 10^8 N/m and 10^9 N/m gear mesh stiffness values were created in Figure 5.3 so as to see the difference between the mode shapes of the helical and spur planetary geared rotors for these stiffness values. For the helical planetary geared rotor, it is clearly seen that there is a good mode shape agreement up to the 26th mode and at the 28th mode. For the spur planetary geared rotor, a good mode shape agreement up to the 30th mode is also seen except the 26th, 27th, 28th and 29th modes due to the mode veering phenomenon at these modes, leading to unmatching cases in the MAC plot. Briefly, reduced MAC agreement is seen at the higher modes for both helical and spur planetary geared rotors, which indicates that a change in gear mesh stiffness mostly affects the higher global modes of a planetary geared rotor system.

5.2.2 Pressure angle

Gear pressure angle is defined as the angle between the gear wheel tangent and the tooth face. In this section, a gear pressure angle parameter study is presented to investigate its effect on the vibration modes of the helical and spur planetary geared rotors. Gear pressure angle range from 10° to 30° degrees was determined for the parameter study based on its values in real gearing applications [191,200]. Similar to the gear mesh stiffness parameter study, the first 30 modes were computed, and the frequency shifts between 10° and 30° degrees were plotted for the helical and spur planetary geared rotors as seen in Figure 5.4.

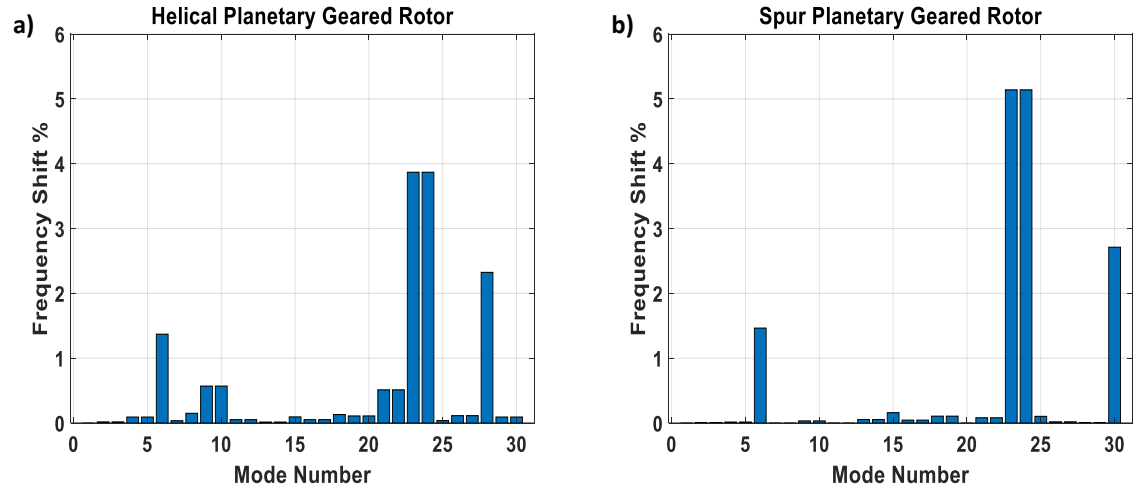

Figure 5.4 : Frequency shifts of planetary geared rotor vibration modes due to gear pressure angle, a) helical, b) spur.

In addition, the gear pressure angle effect on the natural frequencies of the planetary geared rotors was plotted for the significant modes as shown in Figure 5.5. In general, there is no significant change in the natural frequencies as seen in both Figure 5.4 and 5.5. The modes having more than 1 % frequency shifting were investigated. For the helical planetary geared rotors, the significant frequency shifts were noted as 1.4 % at the 6th torsional-axial mode, 3.9 % at the 23rd and 24th lateral modes and 2.3 % at the 28th gearbox mode. The natural frequencies of the torsional-axial modes nearly remain constant except the 6th torsional-axial mode, which gradually increases with respect to the increase in pressure angle. Similarly, the frequency shifts for the spur planetary geared rotor were computed as 1.5 % at the 6th torsional mode, 5.1 % at the 23rd and 24th lateral modes and 2.7 % at the 28th gearbox mode. Here, the natural frequencies of the torsional modes slightly increase with respect to the pressure angle.

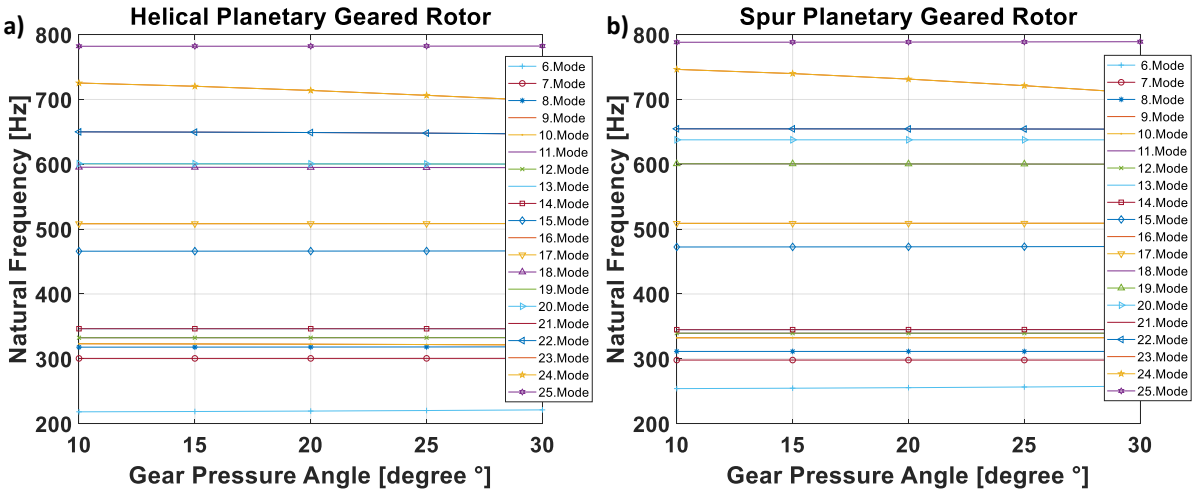

Figure 5.5 : Visualisation of sensitivity planetary geared rotor vibration modes to gear pressure angle, a) helical, b) spur.

However, natural frequencies of the lateral modes have a decreasing tendency with respect to the pressure angle. The natural frequencies can increase or decrease, depending on the vibration mode. When looking at both vibration modes of helical and spur planetary geared rotors, no significant natural frequency shift was observed with respect to the gear pressure angle.

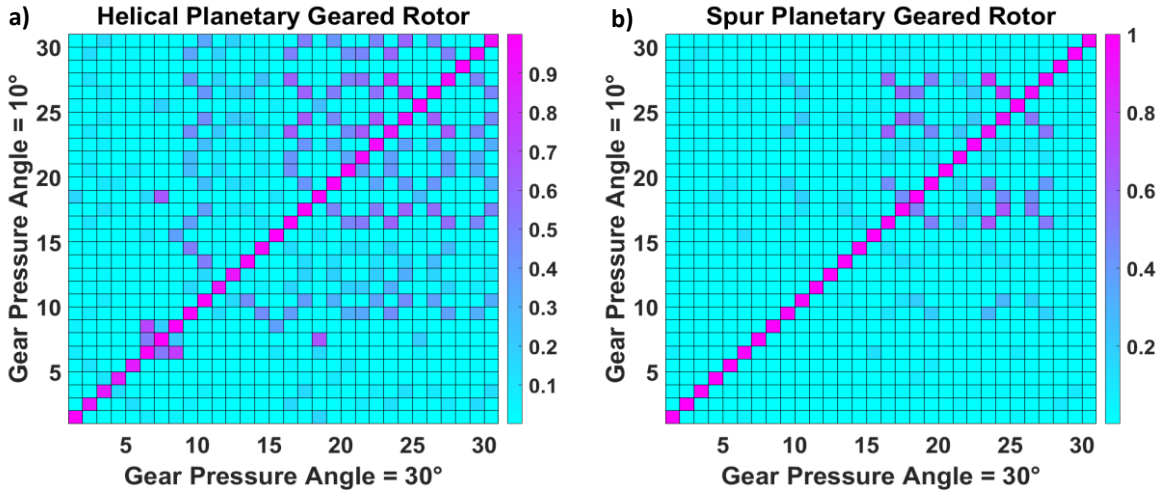

Figure 5.6 : MAC for gear pressure angle, a) helical, b) spur.

A MAC between 10° and 30° degrees of gear pressure angles was also created as seen in Figure 5.6 to see the difference between the mode shapes of the helical and spur planetary geared rotors for these pressure angle values. Overall, there is a good mode shape agreement at all modes of the helical and spur planetary geared rotors, highlighting that no significant effect of the gear pressure angle on the modal behaviour of planetary geared rotors.

5.2.3 Helix angle

The gear helix angle is defined as the angle between the helical gear axis and the helix line. It is one of the main coupling parameters in geared rotor systems, leading to lateral-torsional-axial coupling in single-stage geared rotors and torsional-axial coupling in planetary geared rotors. This section presents a parameter study of the gear helix angle in order to understand its effect on the modal behaviour of helical planetary geared rotors. Although there is one helix angle parameter study carried out on geared rotors to investigate its effect on the forced response [161], the helix angle effect on the modal behaviour of planetary geared rotors is still a pending research question. In this parameter study, gear helix angle was assumed to be varying from 10° to 30° with the consideration of helix angle values in single helical planetary gearbox applications [191,200]. The first 30 modes and their corresponding frequency shifts were computed for the helix angles varying from 10° to 30° degrees, which are given in Table 5.2. The highest frequency shifts were noted as 14.4 % at the 6th mode (torsional-axial), 6.5 %

at the 18th mode (torsional-axial), 4.7 % at the 9th and 10th modes (lateral) and 16.3 % at the 28th mode (gearbox). In general, the torsional-axial modes seem to be more sensitive to the helix angle than the lateral modes for the first 30 global modes.

Table 5.2 : Vibration modes of the helical planetary geared rotor for various gear helix angle.

Helical Planetary Geared Rotor				
Mode #	Nat. Freq. [Hz] β = 10°	Nat. Freq. [Hz] β = 30°	Mode Type	Frequency Shift %
1	0	0	Torsional (Rigid Body)	0.0
2	113	114	Lateral	0.5
3	113	114	Lateral	0.5
4	114	115	Lateral	0.5
5	114	115	Lateral	0.5
6	251	220	Torsional - Axial	14.4
7	299	301	Torsional - Axial	0.6
8	312	318	Torsional - Axial	1.9
9	338	322	Lateral	4.7
10	338	322	Lateral	4.7
11	333	333	Lateral	0.1
12	333	333	Lateral	0.1
13	346	346	Lateral	0.2
14	346	346	Lateral	0.2
15	472	466	Torsional - Axial	1.3
16	509	508	Lateral	0.1
17	509	508	Lateral	0.1
18	634	595	Torsional - Axial	6.5
19	601	601	Lateral	0.0
20	601	601	Lateral	0.0
21	654	649	Lateral	0.8
22	654	649	Lateral	0.8
23	725	710	Lateral	2.0
24	725	710	Lateral	2.0
25	788	782	Torsional - Axial	0.7
26	879	873	Lateral	0.7
27	879	873	Lateral	0.7
28	1057	908	Gearbox	16.3
29	948	943	Lateral	0.5
30	948	943	Lateral	0.5

Natural frequency sensitivity to the gear helix angle was plotted for the significant modes as shown in Figure 5.7. When looking at both Table 5.2 and Figure 5.7, natural frequencies of the torsional-axial modes and lateral modes may increase or decrease with respect to gear helix angle. If the torsional vibrations are more dominant than the axial vibrations in the torsional-axial modes, natural frequencies of the global rotor system decrease with respect to gear helix

angle. In contrast, the torsional-axial modes in which their axial vibrations are much more dominant than their torsional vibrations increase with respect to the helix angle. It makes perfect sense since increasing the helix angle reduces the torsional stiffness at the gear contacts, whereas the axial stiffness increases with an increase in helix angle. Similarly, there is a reverse effect between the transverse and tilting motions in the lateral modes when looking into the equation of motion of planetary gearbox in the dynamic models [96]. Therefore, the natural frequencies of the lateral modes can increase or decrease with respect to gear helix angle based on the dominancy of the transverse or tilting vibrations on each other.

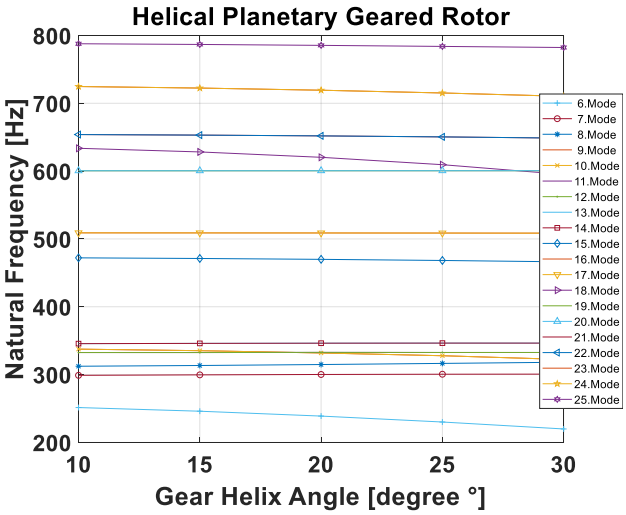

Figure 5.7 : Visualisation of sensitivity planetary geared rotor vibration modes to gear helix angle.

Mode shape comparison between 10° and 30° degrees of gear helix angles was also made by using the modal assurance criteria as seen in Figure 5.8. It can be concluded that there is a reasonable mode shape agreement in most of the first 30 modes.

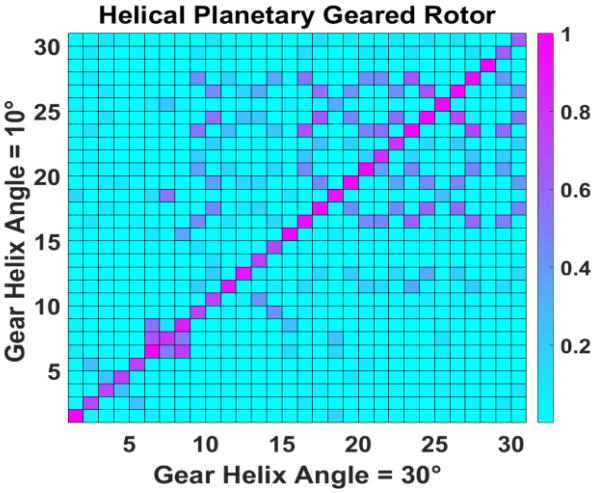

Figure 5.8 : MAC for gear helix angle.

5.3 Planetary gearbox mass and support parameter effects

5.3.1 Material density

Natural frequencies of planetary gearboxes can be controlled easily by changing their mass and inertia parameters. There are some studies carried out in the literature to investigate mass and inertia parameter effects on the modal behaviour of planetary gearboxes [113,114]. However, there is no study, investigating gearbox mass and inertia effects on the modal behaviour of planetary geared rotor systems. In order to eliminate this research gap from the literature, a parameter study for gear material density of the spur and helical planetary geared rotors is presented in this section. It should be noted that the mass and inertia of gearboxes directly change with respect to gear material density.

Aluminium, iron and steel are the commonly used gear materials in gearboxes [191,200]. Steel has the highest density value as 7800 kg/m^3, and aluminium has the lowest density value as 2700 kg/m^3 among the stated materials above. For this reason, gear material density range from 2700 kg/m^3 to 7800 kg/m^3 was determined for the parameter study. After the modal analysis was carried out, the frequency shifts between the two extreme cases, which are 2700 kg/m^3 and 7800 kg/m^3, were computed for the first 30 modes as shown in Figure 5.9.

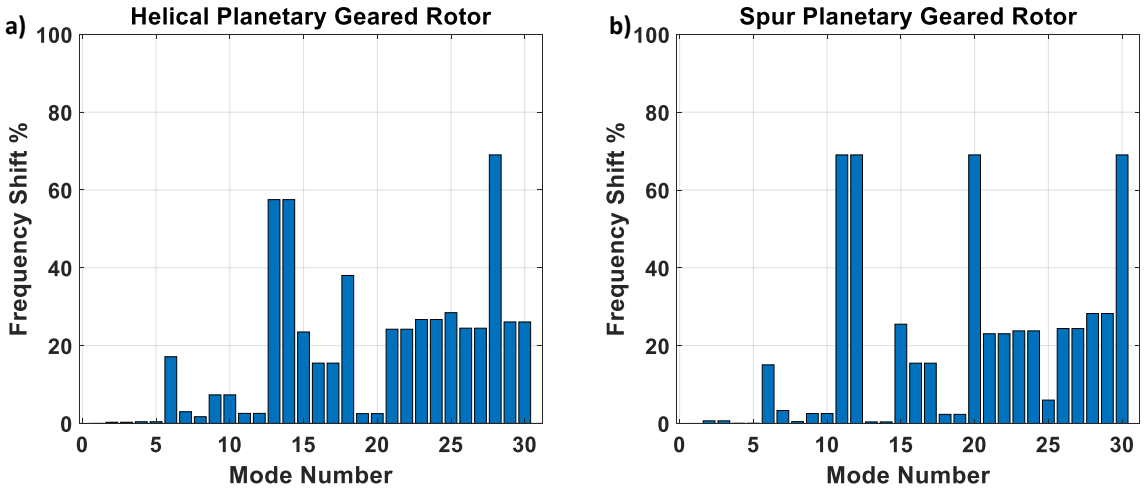

Figure 5.9 : Frequency shifts of planetary geared rotor vibration modes due to change of gear material density, a) helical, b) spur.

The gear material density value, 7800 kg/m^3 is the baseline parameter for the vibration modes of both helical and spur planetary geared rotors. The corresponding vibration modes for the baseline parameter are presented in Table 5.1. The gear material density effect on the natural frequencies is shown in Figure 5.10 for the significant modes between the 6th and 25th modes since there is no significant change in the natural frequencies up to the 6th mode. The modes

having more than 20 % frequency shift were investigated comprehensively for a better understanding of vibration mode sensitivity.

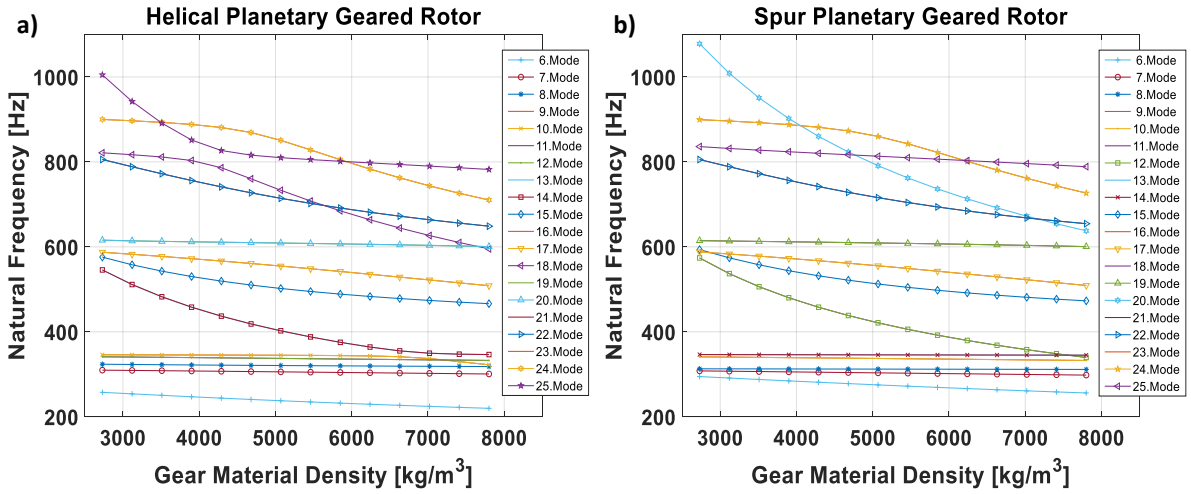

Figure 5.10 : Visualisation of sensitivity planetary geared rotor vibration modes to gear material density, a) helical, b) spur.

In the helical planetary geared rotor, the important frequency shifts are seen at the 13th and 14th lateral modes as 58 %, and at the 15th, 18th and 25th torsional-axial modes as 24, 38, 28 %, respectively. Moreover, the lateral modes between the 21st and 30th modes show remarkable frequency shifts ranging from 24 to 27 %. The most significant change is also observed at the 28th gearbox mode as 69 %. In the spur planetary geared rotor, the highest frequency shifts are seen at the 11th, 12th, 20th and 30th gearbox modes. Furthermore, the torsional mode at the 15th mode has 26 % frequency shift, and the lateral modes between the 21st and 30th modes show remarkable changes from 24 to 28 % similar to the lateral modes in the helical planetary geared rotor. On the other hand, axial modes of the spur planetary geared rotor are not sensitive to the density change due to the higher rigidity of the rotor system in the axial direction. Overall, the gearbox modes are more sensitive to the gear material density change compared to the other modes in both helical and spur planetary geared rotors. Another important observation is that the lateral modes are a bit more sensitive to the density change than the torsional and torsional-axial modes. Briefly, natural frequencies of both helical and spur planetary geared rotors decrease with respect to gear material density.

The mode shapes of the two extreme cases for the gear material density, which are 2700 kg/m^3 and 7800 kg/m^3, were compared using the modal assurance criteria as shown in Figure 5.11. There is a good mode shape agreement up to the 8th mode for the helical planetary geared rotor, however, making an assessment for the mode shape agreement after the 8th mode is so difficult due to the mode veering and the distortion between the modes. When looking at the MAC

comparison of the spur planetary geared rotor, there is a relatively good mode shape agreement up to the 20th mode. There is a lower agreement after the 20th mode where the mode veering and distortion between the modes are the reason for the lower agreement. Overall, the spur planetary geared rotor has a better mode shape agreement compared to the helical one.

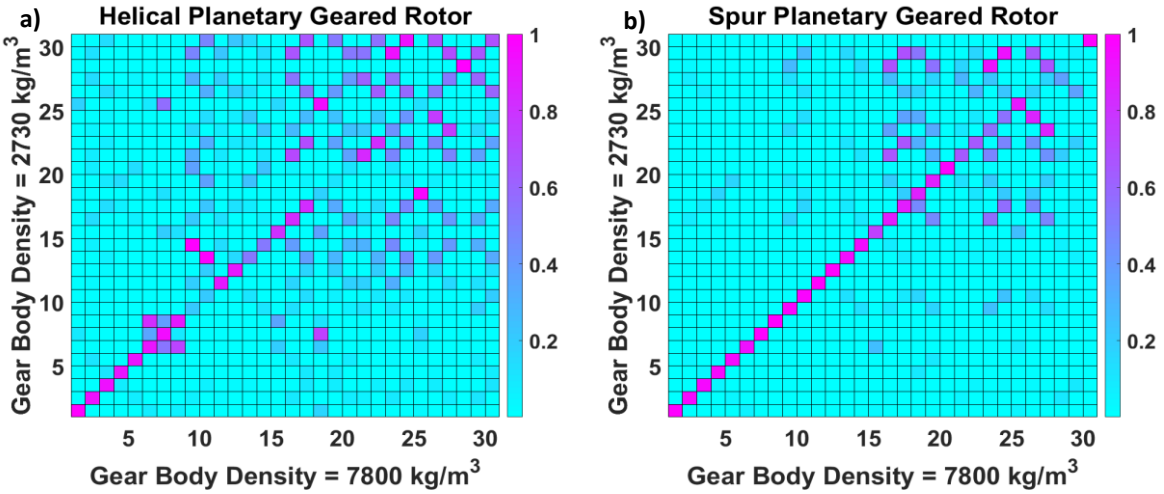

Figure 5.11 : MAC for gear material density, a) helical, b) spur.

5.3.2 Support stiffness

Support stiffness is an important parameter to control vibrations and modal parameters of rotor systems, and it has been shown in many rotor dynamics books [1–5]. Support stiffness effect on the modal behaviour of geared rotors [144] and planetary gearboxes [113,114] was investigated in some studies. In planetary gearboxes, the effect of the radial support stiffness of ring gears on the forced vibration response was also investigated by Li et al. [201]. Despite these studies, planetary gearbox support stiffness effect on the modal behaviour of planetary geared rotors is still not clear in the literature. Therefore, a parameter study for the planetary gearbox support stiffness is presented in this section.

There are four types of supporting structures in planetary gearboxes, which are the bearings of the ring gear, carrier, planet gears and sun gear. Baseline gearbox bearing stiffnesses given in Table 4.1 were reduced ten times for all gearbox bearings in the parameter study with the consideration of the bearing stiffness values of planetary gearboxes provided in the literature [81,96]. The frequency shifts between the baseline and 0.1 times baseline were computed for the first 30 modes of the helical and spur planetary geared rotors as given in Table 5.3. It should be noted that the corresponding vibration modes of both helical and spur planetary geared rotors for the baseline parameters were previously given in Table 5.1.

Table 5.3 : Vibration modes of the helical and spur planetary geared rotors for different support stiffness of planetary gearbox.

	Helical Planetary Geared Rotor				Spur Planetary Geared Rotor			
	ksup*0.1	Baseline ksup			ksup*0.1	Baseline ksup		
Mode #	Nat. Freq. [Hz]	Nat. Freq. [Hz]	Mode Type	Freq. Shift %	Nat. Freq. [Hz]	Nat. Freq. [Hz]	Mode Type	Freq. Shift %
1	0	0	Torsional	0	0	0	Torsional	0
2	87	114	Lateral	31	87	113	Lateral	30
3	87	114	Lateral	31	87	113	Lateral	30
4	90	115	Lateral	28	92	114	Lateral	24
5	90	115	Lateral	28	92	114	Lateral	24
6	150	220	Torsional - Axial	46	176	256	Torsional	45
7	218	301	Torsional - Axial	38	216	298	Axial	38
8	231	318	Torsional - Axial	37	227	311	Axial	37
9	107	322	Lateral	200	174	333	Lateral	91
10	107	322	Lateral	200	174	333	Lateral	91
11	174	333	Lateral	91	107	340	Gearbox	216
12	174	333	Lateral	91	107	340	Gearbox	216
13	209	346	Lateral	65	209	345	Lateral	65
14	209	346	Lateral	65	209	345	Lateral	65
15	192	466	Torsional - Axial	143	459	473	Torsional	3
16	304	508	Lateral	68	328	509	Lateral	55
17	304	508	Lateral	68	328	509	Lateral	55
18	457	595	Torsional - Axial	30	377	601	Lateral	59
19	377	601	Lateral	59	377	601	Lateral	59
20	377	601	Lateral	59	202	638	Gearbox	216
21	454	649	Lateral	43	456	655	Lateral	43
22	454	649	Lateral	43	456	655	Lateral	43
23	630	710	Lateral	13	635	727	Lateral	14
24	630	710	Lateral	13	635	727	Lateral	14
25	641	782	Torsional - Axial	22	669	789	Torsional	18
26	780	873	Lateral	14	750	880	Lateral	17
27	780	873	Lateral	14	789	880	Lateral	14
28	564	908	Gearbox	61	1008	948	Lateral	7
29	713	943	Lateral	32	937	948	Lateral	1
30	713	943	Lateral	32	670	1077	Gearbox	61

For both helical and spur planetary geared rotors, there are more than 10 % frequency shifts at all modes. The gearbox support stiffness effect on the natural frequencies was also plotted in Figure 5.12 for the modes between the 6^{th} and 25^{th} modes.

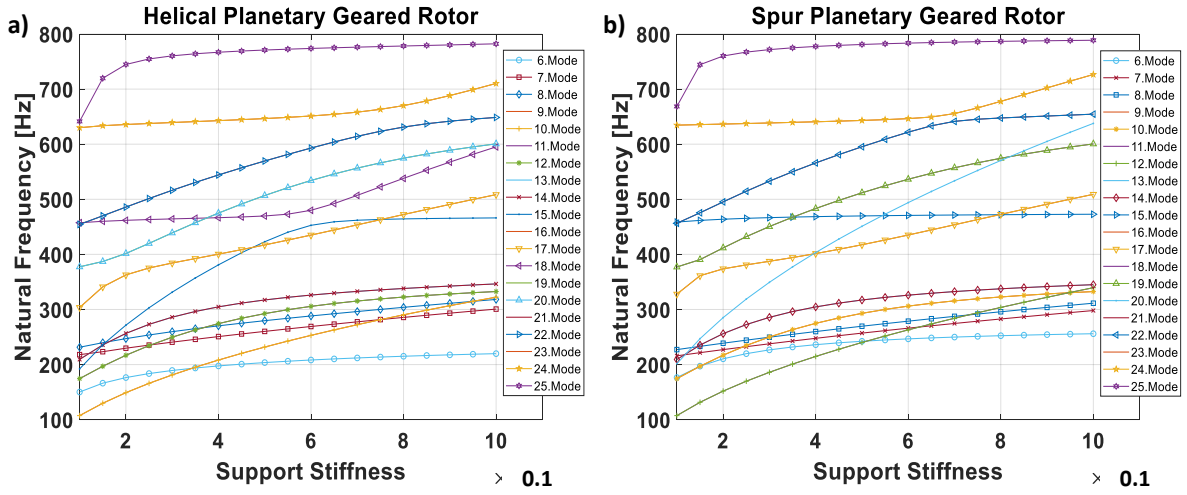

Figure 5.12 : Visualisation of sensitivity planetary geared rotor vibration modes to gearbox support stiffness, a) helical, b) spur.

As a general overview, the natural frequencies of both helical and spur planetary geared rotors increase with respect to support stiffness. There are significant frequency shifts, and the highest frequency shifts are seen at the gearbox modes in both gearbox types. It is also observed that the lateral modes are more affected than the torsional-axial modes in helical planetary geared rotors and the uncoupled torsional and axial modes in spur planetary geared rotors. Due to the significant frequency shifts, there may be mode veering at some modes and significant changes in the modal behaviour. Therefore, it is difficult to make individual assessments for all modes.

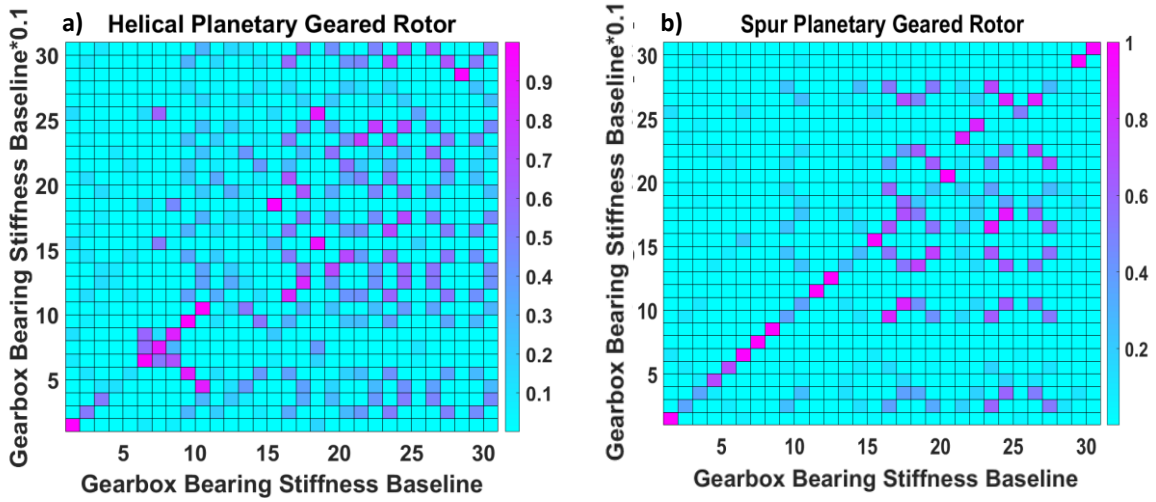

Figure 5.13 : MAC for gearbox support stiffness, a) helical, b) spur.

The MAC comparison between the baseline and 0.1 times baseline also shows lower mode agreement for the helical and spur planetary geared rotors due to the mode shape distortion and mode veering phenomenon. Overall, the spur planetary geared rotor has a slightly better mode agreement than the helical planetary geared rotor due to the mode coupling in the helical.

5.4 Planet gear parameter effects

5.4.1 Number of planet gears

Different number of planet gears are employed in planetary gearbox applications such as three, four, five, six and seven. The number of planet gears effect was investigated in some studies. For instance, Eritenel and Parker did modal analyses with their dynamic model for four and five planet gears, and they show the lowest ten vibration modes in their paper [81]. On the other hand, more research is required to investigate the number of planet gears effect on the modal behaviour of planetary geared rotors. For this purpose, a parameter study of the number of planet gears for the helical planetary geared rotor system is presented in this section. Two cases were determined as helical planetary geared rotors with three and five planets, and modal analyses were carried out for them. The results of the modal analyses are given in Table 5.4.

Table 5.4 : First 25 modes for the helical planetary geared rotors with three and five planets.

Mode #	Three Planets		Five Planets	
	Natural Frequency [Hz]	Mode Type	Natural Frequency [Hz]	Mode Type
1	0	Torsional	0	Torsional
2	114	Lateral	114	Lateral
3	114	Lateral	114	Lateral
4	115	Lateral	115	Lateral
5	115	Lateral	115	Lateral
6	197	Torsional - Axial	237	Torsional - Axial
7	300	Torsional - Axial	301	Torsional - Axial
8	316	Torsional - Axial	305	Lateral
9	332	Lateral	305	Lateral
10	332	Lateral	322	Torsional - Axial
11	340	Lateral	333	Lateral
12	340	Lateral	333	Lateral
13	351	Lateral	346	Lateral
14	351	Lateral	346	Lateral
15	465	Torsional - Axial	467	Torsional - Axial
16	509	Lateral	507	Lateral
17	509	Lateral	507	Lateral
18	602	Lateral	573	Torsional - Axial
19	602	Lateral	598	Lateral
20	622	Torsional - Axial	598	Lateral
21	652	Lateral	645	Lateral
22	652	Lateral	645	Lateral
23	719	Lateral	705	Lateral
24	719	Lateral	705	Lateral
25	780	Torsional - Axial	786	Torsional - Axial

Mode shapes of the helical planetary geared rotors with three and five planets were plotted for the first 25 modes as shown in Figure 5.14 and 5.15 where rigid body torsional, lateral and coupled torsional-axial modes can be clearly seen.

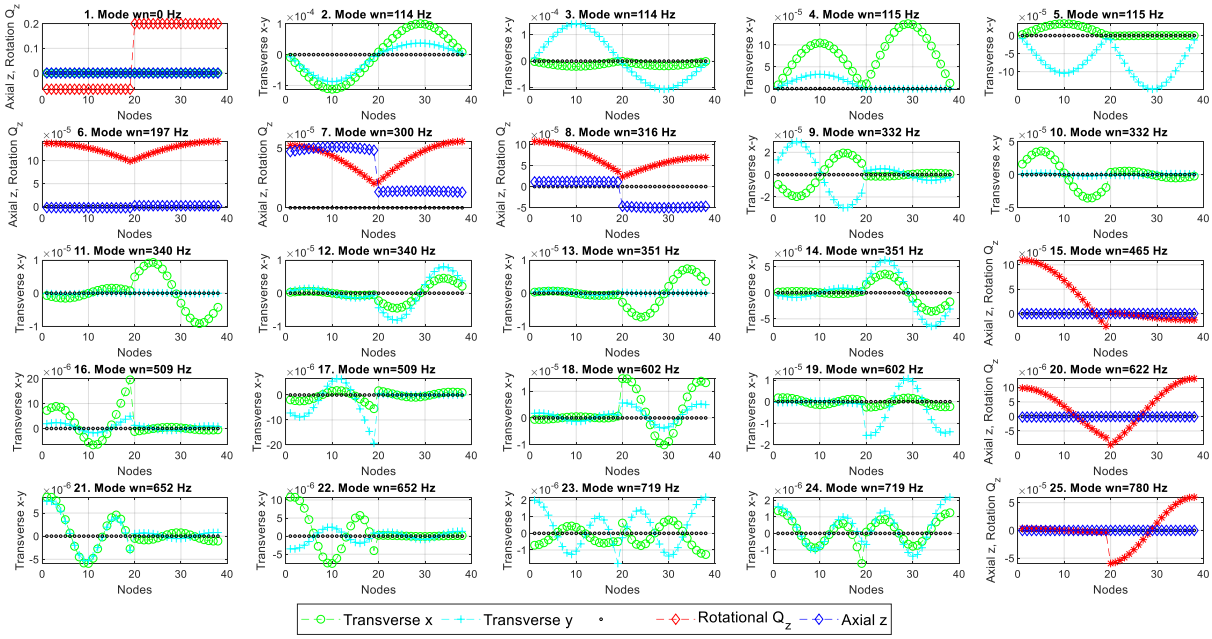

Figure 5.14 : Mode shapes of the helical planetary geared rotor with three planets.

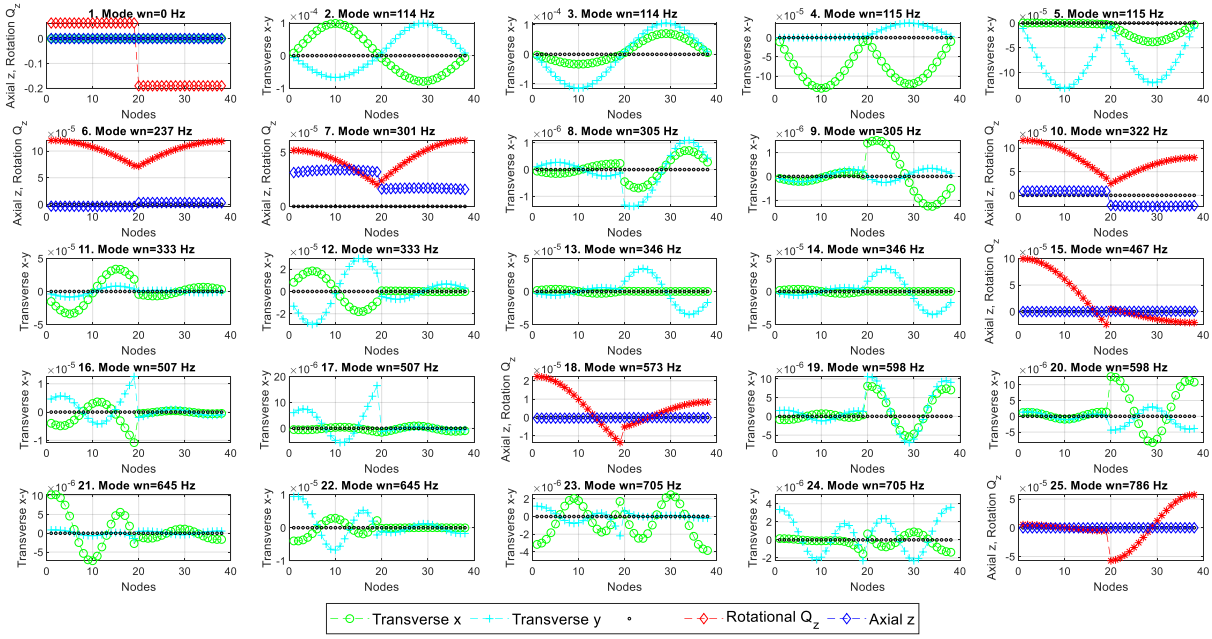

Figure 5.15 : Mode shapes of the helical planetary geared rotor with five planets.

From the three planets to the five planets, natural frequencies of the torsional-axial modes have an increasing tendency except for the 20th mode of the system with three planets at 622 Hz, which nearly corresponds to the 18th mode of the system with five planets at 573 Hz. On the

other hand, natural frequencies of the lateral modes have a decreasing tendency with respect to the number of planets except for the first four lateral modes which remain constant.

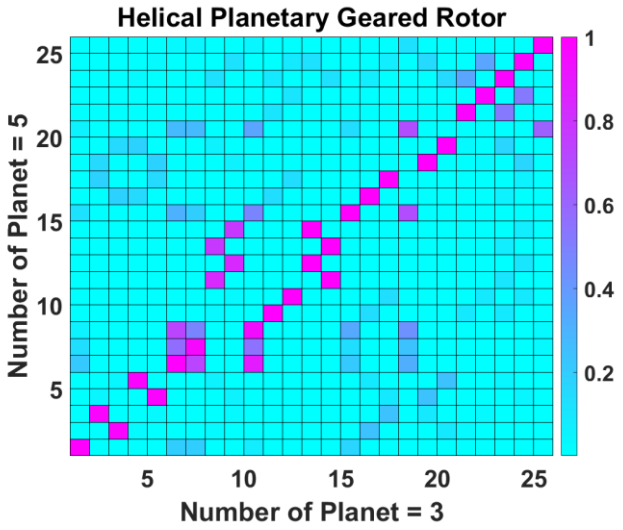

Figure 5.16 : MAC comparison between the helical planetary geared rotors with three and five planets.

The mode shapes of the helical planetary geared rotors with three and five planets were compared using the modal assurance criteria as seen in Figure 5.16. There is a good mode shape agreement up to the 8th mode, where the modes 2 and 3, and the modes 4 and 5 reverse their order because of the mode veering phenomenon. There are also good mode shape agreements at the modes 15, 16, 17, 21, 22, 23, 24, 25. In the rest, mode veering phenomenon occurs at some modes and lower mode shape agreements are observed due to the mode shape distortions. Overall, there is a good mode shape agreement except for some distorted mode shapes when mode veering phenomenon is taken into account.

5.4.2 Planet mistuning

Planetary gearboxes are ideally designed and manufactured with equally space planet gears. However, there can sometimes be positioning error between the planet gears due to the unequally spaced planets, which breaks the cyclic symmetry of the planetary gearbox structure. This phenomenon is also known as planet mistuning in the literature where there are some studies related to this phenomenon. For instance, vibration mode sensitivity of planetary gear [113] and general compound planetary gear [114] to planet mistuning, and modal behaviour of mistuned planetary gears [102] were investigated by researchers. All these studies were done for planetary gearboxes only. However, no research has been conducted yet to investigate planet mistuning effect on the modal behaviour of planetary geared rotors. Therefore, a

parameter study for the planet mistuning is presented in this section to understand the modal behaviour of mistuned planetary geared rotors. Planet mistuning amount range was determined from 0° (baseline) to 14° degrees for only one planet gear in the parameter study. The frequency shifts between the baseline 0° and 14° degrees were computed and plotted for the helical and spur planetary geared rotors as seen in Figure 5.17.

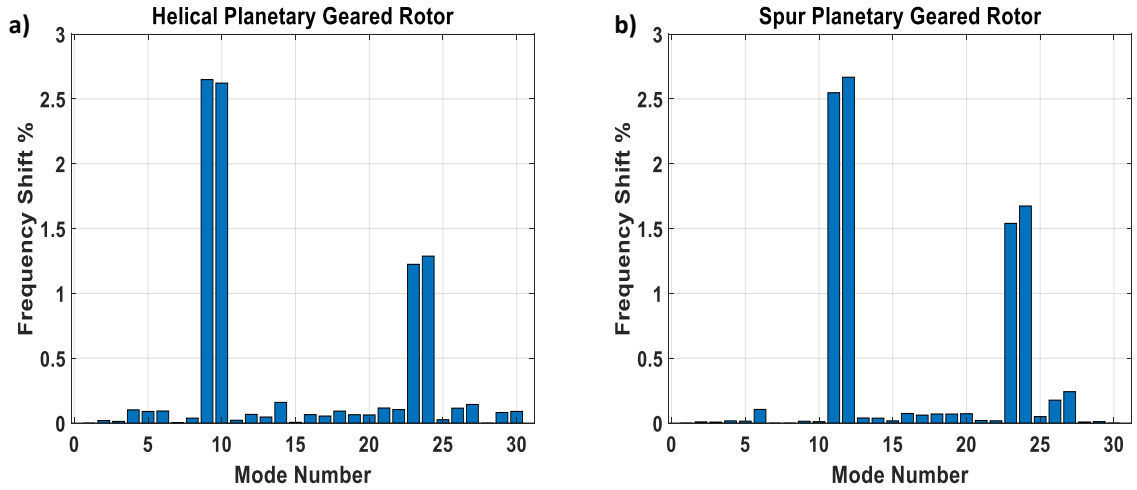

Figure 5.17 : Frequency shifts of planetary geared rotor vibration modes due to planet mistuning, a) helical, b) spur.

Natural frequency sensitivity of the helical and spur planetary geared rotors to the planet mistuning were also plotted for the modes between the 6th and 25th modes as shown in Figure 5.18. In general, there is no significant change in the natural frequencies as seen in Figures 5.17 and 5.18. The modes having more than 1 % frequency shift were investigated further for identifying the sensitive modes.

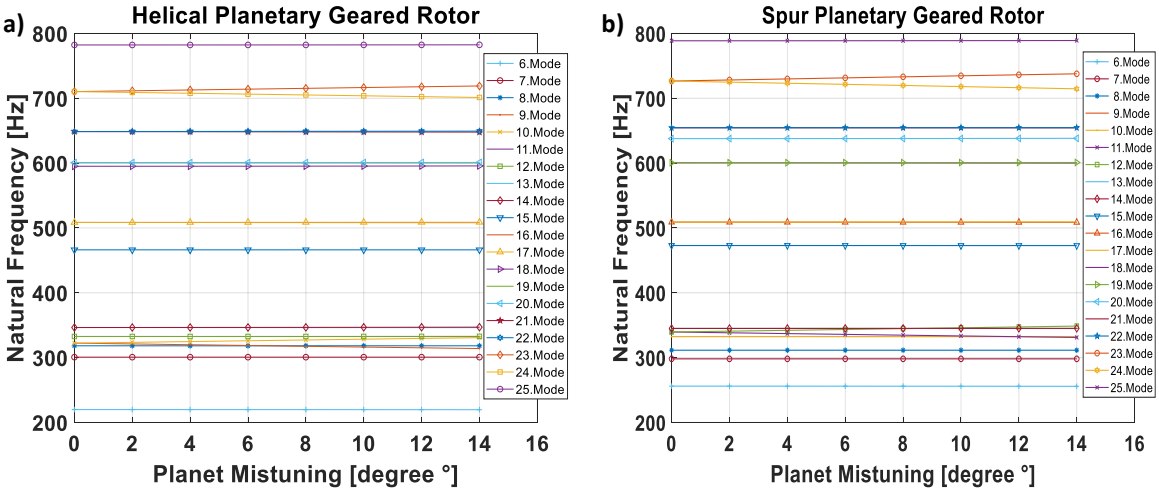

Figure 5.18 : Visualisation of sensitivity planetary geared rotor vibration modes to planet mistuning, a) helical, b) spur.

For the helical planetary geared rotor, the significant frequency shifts are seen at the 9th and 10th modes as 2.6 %, at the 23rd mode as 1.2 %, and at the 24th mode as 1.3 %. It should be noted that these modes are originally lateral if there is no planet mistuning. The torsional-axial modes are found to be barely affected by mistuning compared to the lateral modes, which is less than 1 %. For the spur planetary geared rotor, the significant frequency shifts are seen at the 11th and 12th gearbox modes as 2.5 % and 2.7 % respectively, and at the 23rd and 24th lateral modes as 1.5 % and 1.7 %, respectively. In the spur planetary geared rotor, it is found that the axial modes are not sensitive to the mistuning because of no geometric interaction of the mistuning in the axial direction. Furthermore, the torsional modes are barely affected compared to the lateral modes.

Due to the breaking cyclic symmetry of the planetary gearbox structure, the planet mistuning may result in lateral-torsional-axial coupling in helical planetary geared rotors and lateral-torsional coupling in spur planetary geared rotors. Mode shapes of the highest frequency shifting observed modes in the helical planetary geared rotor was plotted in Figure 5.19, showing the coupled lateral-torsional-axial modes due to the planet mistuning effect. As a result, modes of the mistuned helical planetary geared rotors are coupled in lateral, torsional and axial directions. Depending on the vibration mode sensitivity levels, the coupled lateral-torsional-axial modes can be clearly detected in their mode shapes.

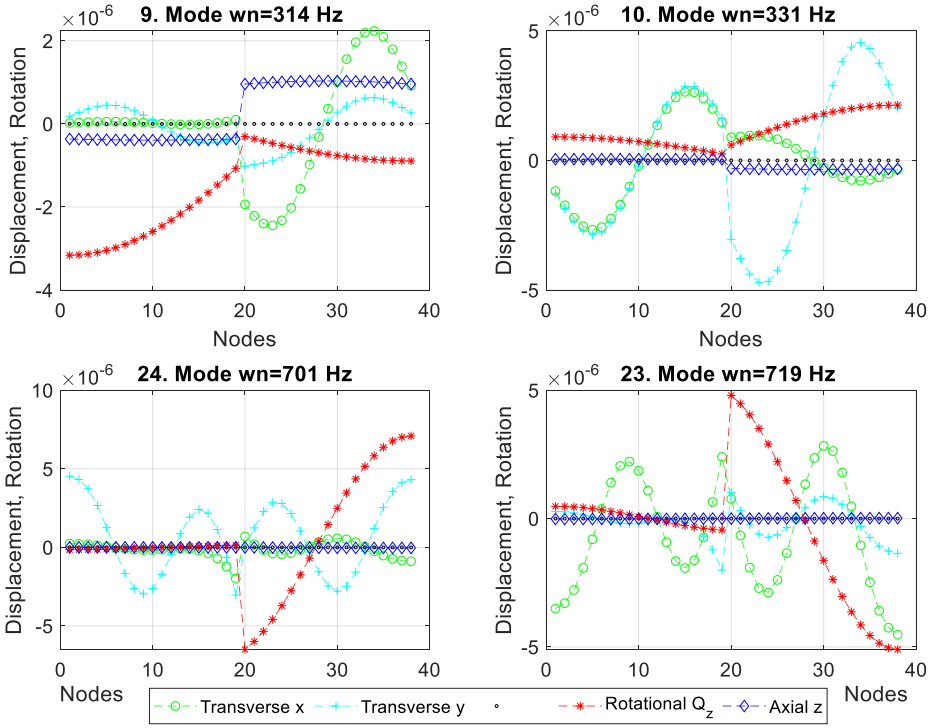

Figure 5.19 : Coupled lateral-torsional-axial vibration modes of the helical planetary geared rotor with unequally spaced planets.

The natural frequency shifts due to the planet mistuning were negligible in both helical and spur planetary geared rotors while it can directly affect their mode shapes. Mistuning can lead to an increase or decrease in the natural frequencies of the planetary geared rotors.

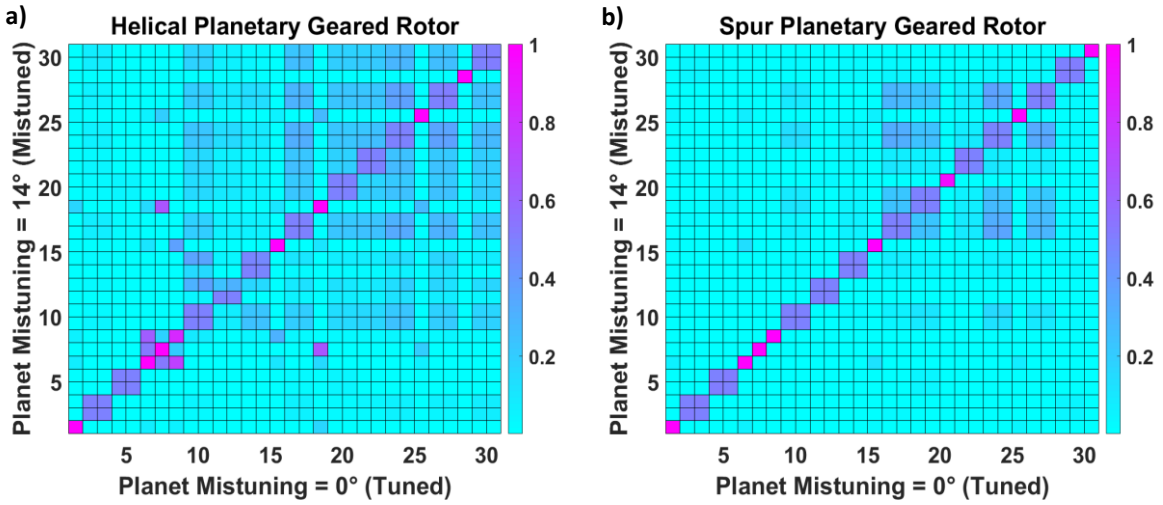

Figure 5.20 : MAC for planet mistuning, a) helical, b) spur.

Mode shapes of the tuned and mistuned cases were compared with MAC matrices for the helical and spur planetary geared rotors as seen in Figure 5.20. For the helical planetary geared rotor, there is nearly % 100 mode shape agreement at the torsional rigid body, torsional-axial and gearbox modes. In contrast, there is reduced MAC agreement at the lateral modes of the tuned system because of the occurrence of lateral-torsional-axial coupling at these modes in the mistuned case. For the spur planetary geared rotor, a good mode shape agreement can be observed at all torsional and axial modes and some gearbox modes. Lower mode shape agreements are also observed at the lateral modes of the tuned system due to the lateral-torsional coupling in the mistuned one. Briefly, the reduced MAC agreement highlights lateral-torsional-axial coupling in the helical one and lateral-torsional coupling in the spur one.

5.5 Discussion

Three main planetary gearbox parameters which are gear contact parameters, gearbox mass and support parameters and planet gear parameters are the main focus of this investigation to understand their effects on the modal behaviour of planetary geared rotors. The global rotor modes are going to be discussed here rather than the gearbox modes since the gearbox modes are isolated from the global system. In general, the first five modes of the spur and helical planetary geared rotors are found to be not sensitive to the parameter change except the support stiffness. Mass and support parameters have a significant effect on the modal behaviour of

planetary geared rotors in terms of natural frequency shifts and mode shape changes when compared with the gear contact parameters.

The torsional-axial modes of helical planetary geared rotors and the torsional modes of spur planetary geared rotors are more sensitive to two gear contact parameters, which are mesh stiffness and helix angle, than their lateral modes. The other gear contact parameter which is pressure angle does not have a significant effect on the vibration modes compared with the other two gear contact parameters. For the gear mesh stiffness and pressure angle parameters, the dominancy of torsional components in the torsional-axial modes of helical planetary geared rotors determine the vibration mode sensitivity level because the axial modes in spur planetary geared rotors are not affected by these contact parameters. As a result, the torsional modes are sensitive to gear mesh stiffness and pressure angle. Gear mesh stiffness is more influential at the higher lateral modes when looking at the frequency shifts and mode shape comparisons at these modes. Natural frequencies of planetary geared rotor systems increase with respect to the mesh stiffness, whereas they can increase or decrease with respect to the pressure angle and helix angle, depending on the vibration modes. For instance, natural frequencies of the global system may decrease with respect to the helix angle based on the dominancy of the torsional components in the coupled torsional-axial modes of helical planetary geared rotors. If axial components of the coupled torsional-axial modes are more dominant than the torsional one, the natural frequencies of the global system may increase vice versa. This reverse effect exists due to dropping of torsional mesh stiffness and rising of axial mesh stiffness with respect to the helix angle. Similarly, another reverse effect of the helix angle in the natural frequencies may also be seen at the lateral modes based on the dominancy between the transverse and tilting components. In general, the mode shapes of both spur and helical planetary geared rotors are not significantly affected by the gear contact parameters. On the other hand, gearbox mass (related to the material density) and support stiffness can significantly affect the modal behaviour of the system more than the gear contact parameters. Lateral vibration modes are found to be more sensitive to the gearbox mass and support stiffness compared with the other global modes (coupled torsional-axial, uncoupled torsional and uncoupled axial modes). The gearbox mass effect can noticeably be seen at higher modes while the support stiffness effect can be seen at both lower and higher modes. As a result, lower vibration modes, particularly the lower lateral modes, can be controlled by the gearbox bearing stiffnesses. To sum up, the torsional and coupled torsional-axial modes are more sensitive to the gear mesh stiffness and helix angle, whereas the lateral modes are more sensitive to the gear material density and

support stiffness. As a piece of general advice, it is useful to control the torsional and torsional-axial modes by changing the gear mesh stiffness and helix angle parameters and to control the lateral modes by changing the mass and support stiffnesses of the planetary gearbox.

Increasing the number of planet gears leads to an increase in the natural frequencies of the torsional-axial modes, whereas leading to a decrease in the natural frequencies of the lateral modes in general. It means that a planetary gearbox behaves more rigid in torsional-axial vibrations and more flexible in lateral vibrations with the increase in the number of planet gears. From the modal behaviour perspective, it could be suggested that different number of planet gears can be used in order to control the natural frequencies of the torsional-axial modes and lateral modes. It should also be noted that there is a reverse effect between the torsional-axial modes and lateral modes in terms of flexibility with respect to the number of planet gears. The planet mistuning study also shows that there are no significant frequency shifts due to the mistuning, which is nearly negligible. On the other hand, the planet mistuning results in coupled lateral-torsional-axial modes in helical planetary geared rotors and coupled lateral-torsional modes in spur planetary geared rotors due to the breaking cyclic symmetry in planetary gearboxes. Furthermore, original lateral modes in the tuned system are more sensitive to the planet mistuning. It is important to point out that unexpected axial vibrations can lead to lateral vibrations in the mistuned helical planetary geared rotor systems due to the coupled lateral-torsional-axial modes. For instance, the axial thrust forces in geared turbofan engines may excite their lateral modes and vice versa.

5.6 Concluding remarks

In this chapter, a comprehensive planetary gearbox parameter study including gear contact, gearbox mass and support, and planet gear parameters is conducted on the hybrid dynamic model of the planetary geared rotor system in order to investigate the parameter effects on the modal behaviour of helical and spur planetary geared rotors. Gear contact parameter study consists of investigating the mesh stiffness, pressure angle and helix angle effects. The parameter study for the planetary gearbox mass and support stiffness includes investigation of the gear material density and gearbox bearing stiffness effects. The planet gear parameter study also covers the number of planet gears and planet mistuning effects. The natural frequency sensitivity is determined by computing natural frequency maps and frequency shifts between the two extreme cases. For the mode shape comparison between the two cases, modal assurance criteria is used throughout this chapter.

Modal behaviours of both helical and spur planetary geared rotors are much more affected by mass and support parameters compared to the gear contact parameters. It is found that the torsional and coupled torsional-axial modes are more sensitive to the gear mesh stiffness and helix angle, whereas the lateral modes are more sensitive to the gear material density and support stiffness. The axial modes of spur planetary geared rotors, in general, are found to be less sensitive to the gearbox parameters except for the support stiffness. Higher frequency shifts, mode shape distortions and mode veerings can occur due to the change in planetary gearbox mass and support stiffness parameters.

The number of planet gear parameter study also reveals the reverse effect between the natural frequencies of the torsional-axial modes and lateral modes. With the increase in the number of planet gears, planetary gearbox becomes more rigid in the torsional-axial modes and more flexible in the lateral modes mostly. It is also important to point out that the planet mistuning results in coupled lateral-torsional-axial modes in helical planetary geared rotors and coupled lateral-torsional modes in spur planetary geared rotors, which is due to the breaking cyclic symmetric structure of the planetary gearbox (unequally spaced planets). However, the natural frequency shifts are nearly negligible because of the planet mistuning.

To conclude, the presented results highlight the sensitivity of the vibration modes based on the planetary gearbox parameters and the importance of investigating gearbox parameter effects on the modal behaviour of planetary geared rotor systems.

Chapter 6

6 Experimental modal analysis of planetary geared rotors

6.1 Introduction

In this chapter, the experimental lateral modal behaviour of an equally spaced spur planetary geared rotor system and its numerical model validation with the experimental modal analysis results are presented. The modal parameters which are natural frequencies, mode shapes and modal damping can be obtained experimentally with modal testing. For the lateral modal behaviour investigation, modal testing is carried out on a spur planetary geared rotor assembly and its input and output shafts. In the first part, the input and output shafts of the planetary geared rotor assembly are characterized by experimental modal analyses. Free-free impact hammer tests of the input and output shafts are done separately, and their modal testing procedure is shown explicitly. Their natural frequencies and mode shapes are then extracted from the experimental modal analyses to validate finite element modal analyses of the shafts. Hence, the modal behaviour and material properties of the two shafts are validated before starting the impact tests on the planetary geared rotor assembly. In the second part, the spur planetary geared rotor test rig is described, and the material and geometry properties of the planetary gearbox are provided. Free-free impact hammer tests are also conducted for the spur planetary geared rotor assembly. Its experimental modal analysis results and mode shape identification are then given. In the third part, the numerically computed modal analysis results of the planetary geared rotor assembly are validated with the experimental modal analysis results after updating the hybrid numerical model. In the final part, the experimental and numerical modal analysis results are discussed to understand the reason for the difference between them. Lastly, important findings of this chapter are given in the concluding remarks.

6.2 Modal testing

In modal testing, the force as an input excitation and acceleration as an output response are measured simultaneously, with a force transducer and an accelerometer, respectively. Input excitations can be generated with different tools such as shakers and hammers [26]. The main aim of modal testing is to compute the frequency response functions by dividing the output responses by the input excitations. The so-called frequency response function is written as

$$\alpha(\omega) = \frac{A(\omega)}{F(\omega)}. \tag{6.1}$$

where $A(\omega)$ and $F(\omega)$ represent the output response and input excitation in terms of acceleration, and force, respectively. Here, ω also represents the frequency of the signals. From measured frequency response functions, the modal parameters, which are natural frequencies, mode shapes, and modal damping, can easily be obtained [26]. In order to build a mathematical model of a system from measured data, an experimental route which is shown in Figure 6.1 is followed. The experimental and theoretical routes are exactly in opposite directions.

Figure 6.1 : Experimental route [26].

6.2.1 Experimental setup

In this section, independent modal testing of the input and output shafts, and the spur planetary geared rotor assembly were carried out using an impact hammer. A PCB Piezotronics impact hammer and single-axis ICP accelerometers for measuring the force and acceleration data respectively, and a Data Physics SignalCalc Ace signal analyser for the data acquisition were used as the basic modal testing equipment as seen in Figure 6.2.

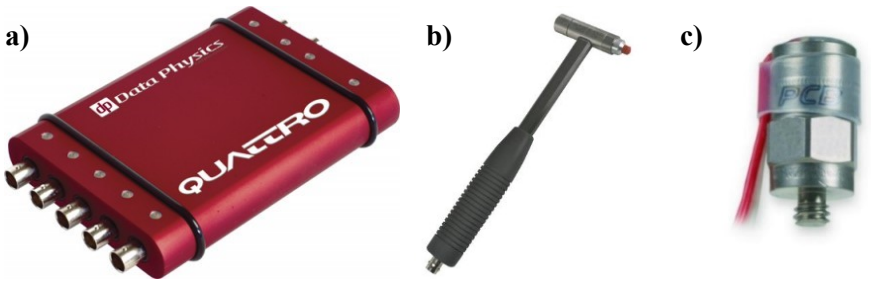

Figure 6.2 : Testing equipment, a) SignalCalc Ace signal analyser [Source: Data Physics] b) PCB impact hammer, c) PCB single axis accelerometer [Source: PCB Piezotronics].

After doing some initial tests with rubber, plastic and metal hammer tips, a plastic hammer tip was decided to be chosen for the modal testing of the input shaft, output shaft and spur planetary geared rotor in their lateral directions, since it gave the best balance between the frequency bandwidth and energy transfer. Both rubber and metal tips have advantages and disadvantages of vibration testing [26]. Plastic hammer tips stand between rubber and metal tips in terms of maximum excitation frequency and maximum energy transfer to structures. More energy can be given to structures with a rubber hammer tip, whereas it cannot excite higher frequencies. Conversely, a metal hammer tip can excite higher frequencies while less energy can be transferred to structures with a metal tip. Therefore, a plastic hammer tip was used for the modal testing of the shafts and planetary geared rotor assembly.

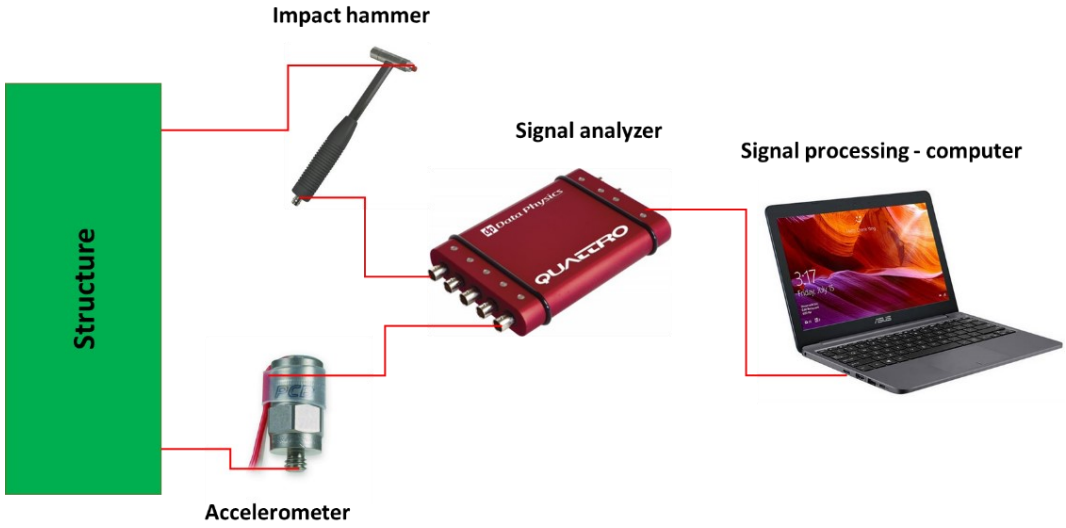

Figure 6.3 : Experimental setup.

The experimental setup for the impact hammer test is shown in Figure 6.3. Here, the accelerometer and impact hammer are connected to the signal analyser as input channels, and a computer is connected to the signal analyser as the output channel for the signal processing. Force and acceleration are measured from the structure via the force transducer on the impact hammer and the accelerometer respectively.

6.2.2 Shafts

Two steel homogenous and circular shafts containing two segments with varying cross-sections were manufactured for both input and output shafts. Both shafts have slightly different lengths and diameters, and the geometrical details of the input and output shafts such as the lengths and diameters of the two segments are shown in Figure 6.4. For the input shaft, the length of its longer and shorter segments are 570 mm and 30 mm, and their diameters are 16 mm and 14

mm respectively. For the output shaft, the longer segment has 570 mm length and 15 mm diameter whereas the shorter segment has 17 mm length and 14 mm diameter.

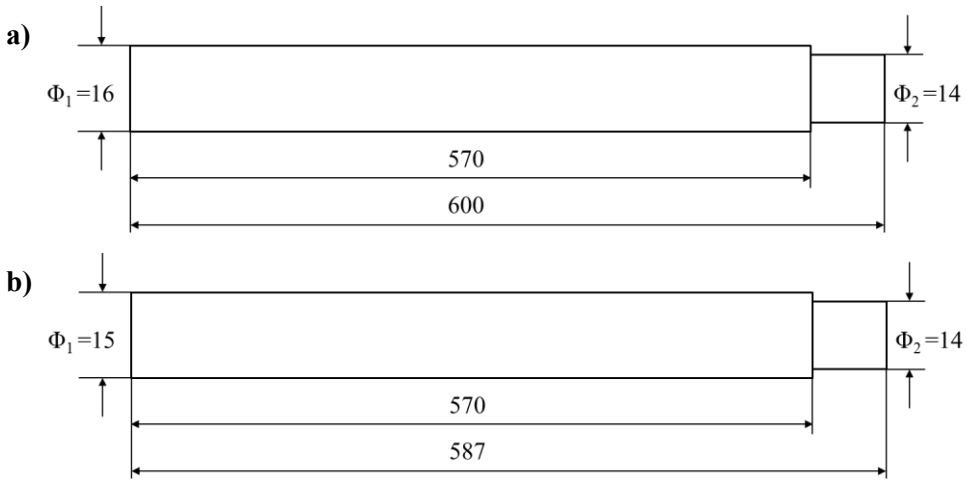

Figure 6.4 : Technical drawings, a) input shaft, b) output shaft.

The material properties of the input and output shafts are presented in Table 6.1. The material densities of the shafts were computed by measuring their mass and volume. Here, the Young`s and shear modulus of the shafts were also determined based on the experimental modal analysis results, presented in this section.

Table 6.1 : Material properties of the steel shafts.

Parameter	Input shaft	Output shaft
Density [kg/m^3]	7950	7850
Young`s modulus [GPa]	190	208
Shear modulus [GPa]	74	80

The input and output shafts were divided into roughly twelve equal segments for their impact hammer tests, resulting in thirteen measurement locations as seen in Figure 6.5. The shafts were suspended with elastic cords from their left and right sides. In the input shaft test, suspension locations were between the measurement locations 3 and 4 at its left side, and between the measurement locations 11 and 12 at its right side. In the output shaft test, suspension locations were determined to be between the measurement locations 3 and 4 at its left side, and between the measurement locations 10 and 11 at its right side.

The modal behaviour of homogenous and cyclically symmetric structures in both the horizontal (y) and vertical (x) directions should ideally be the same due to the presence of orthogonal modes. Therefore, the impact hammer tests for the input and output shafts were repeated in both the horizontal (y) and vertical (x) directions by measuring the excitation and response

signals in the same directions. When exciting the shafts horizontally, the acceleration signals were measured in the horizontal direction. Similarly, the acceleration signals were measured in the vertical direction when exciting the shafts vertically. For both the input and output shafts, the excitation and response signals were collected with 2048 Hz sampling frequency in the signal analyser since the first four modes were aimed to capture. Here, the maximum frequency was set as 800 Hz; hence the sampling ratio became 2.56. Due to negligible internal damping inside the shafts, the measurement periods for collecting the data were set as 16 and 32 seconds for the input and output shafts respectively, which were found to be sufficient to allow the response to decay. As a result, the frequency resolution became 0.0625 Hz and 0.03125 Hz, respectively. In order to improve the measurement accuracy and data quality, exponential windowing functions and averaging techniques were applied to the time data of the two shafts. The excitation and response signals were measured simultaneously three times, and the collected signals were then averaged. Exponential windowing was needed to minimize leakage on the signal by creating artificial damping [26].

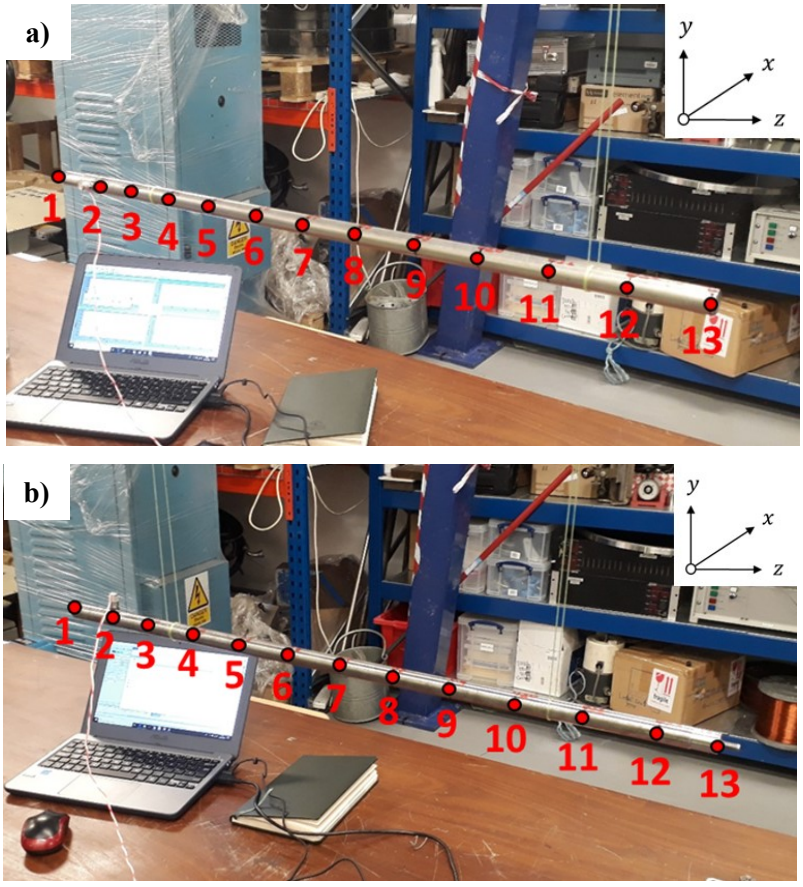

Figure 6.5 : Modal testing setup, a) input shaft, b) output shaft.

The shafts were excited by the impact hammer at the measurement locations from 1 to 13 as shown in Figure 6.5. Throughout the impact hammer test of the two shafts, the acceleration

responses were measured with the accelerometer at the measurement location 2, which was kept constant. The excitation location was changed by moving the impact hammer from the measurement locations 1 to 13. For each test, 13 frequency response functions were measured in total by doing impact hammer tests at 13 different measurement locations. The point FRFs were also measured at the measurement location 2, and the cross FRFs were measured at the rest of the measurement locations. It should be noted that the shafts were excited from the opposite direction at their point FRF locations.

Experimental modal behaviour

The frequency response functions (FRFs) of input and output shafts in terms of accelerance were computed using the force excitation signal and acceleration response signal in vertical (x) and horizontal (y) directions. They were plotted up to 800 Hz for the first two elastic modes as seen in Figures 6.6 and 6.7, respectively, where the peak frequencies are also indicated.

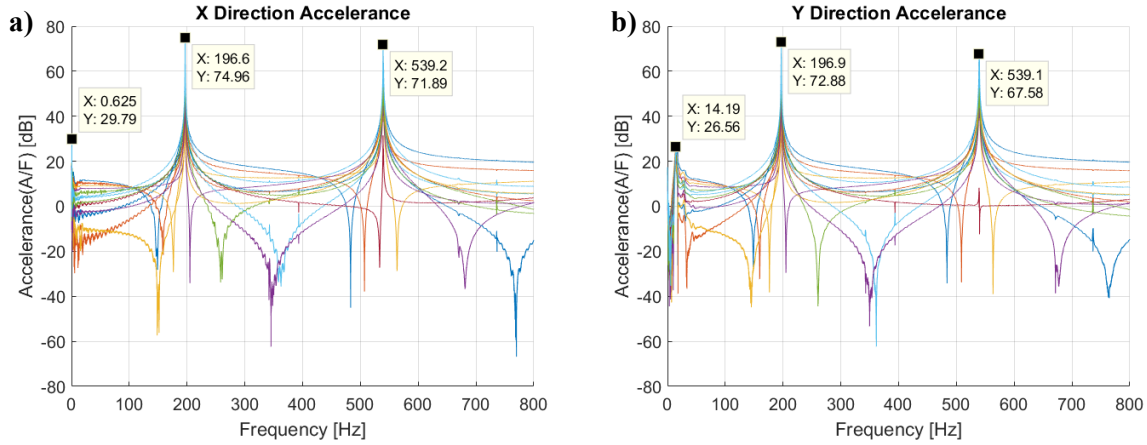

Figure 6.6 : Input shaft accelerance, a) horizontal direction, b) vertical direction.

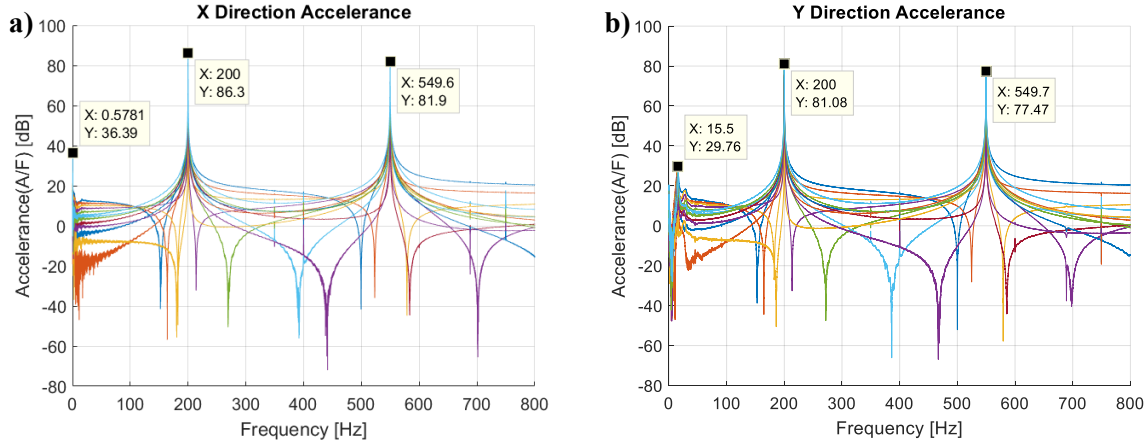

Figure 6.7 : Output shaft accelerance, a) horizontal direction, b) vertical direction.

For the input shaft, the peak frequencies were detected in the frequency response functions at 197 Hz and 539 Hz in both of the horizontal “x” and vertical “y” directions. Similarly, the peak frequencies were detected at 200 Hz and 550 Hz in the horizontal “x” and vertical “y” direction FRFs for the output shaft. It is important to point out that these peak frequencies represent the natural frequencies of lateral vibration modes (elastic modes) of the shafts. The natural frequencies of the shafts in their horizontal “x” and vertical “y” directions are found to be same, which proves the homogenous and cyclically symmetric structure of the shafts. Furthermore, the peak frequencies at 0.6 Hz and 14.2 Hz in the FRFs of the input shaft represent the rigid body modes in the “x” and “y” directions respectively. Similarly, the peak frequencies at 0.6 Hz and 15.5 Hz in the FRFs of the output shaft represent the rigid body modes in the “x” and “y” directions, respectively.

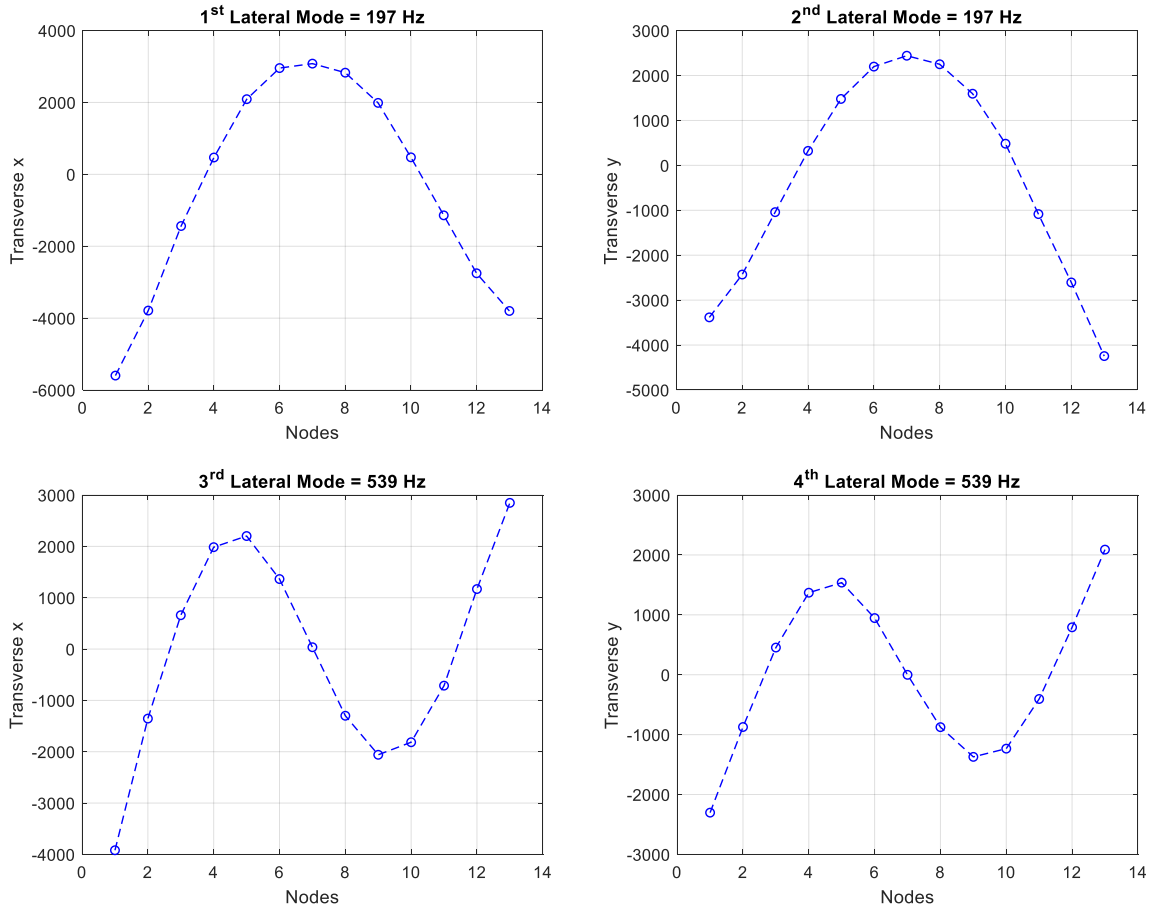

Figure 6.8 : Lateral modes of the input shaft.

Lateral mode shapes of the input and output shafts in the horizontal “x” and vertical “y” directions were plotted using the measured frequency response functions in Figures 6.8 and 6.9 respectively. In total, four elastic lateral modes were found for both the input and output shafts up to 800 Hz. For the input shaft, the first and second modes were found to be at 197 Hz, and

the third and fourth modes were found to be at 539 Hz. For the output shaft, the first and second modes were found to be at 200 Hz, and the third and fourth modes were found to be at 550 Hz. Experimentally, lateral vibration modes of the shafts in transverse directions “x” (horizontal) and “y” (vertical) are clearly seen in these figures.

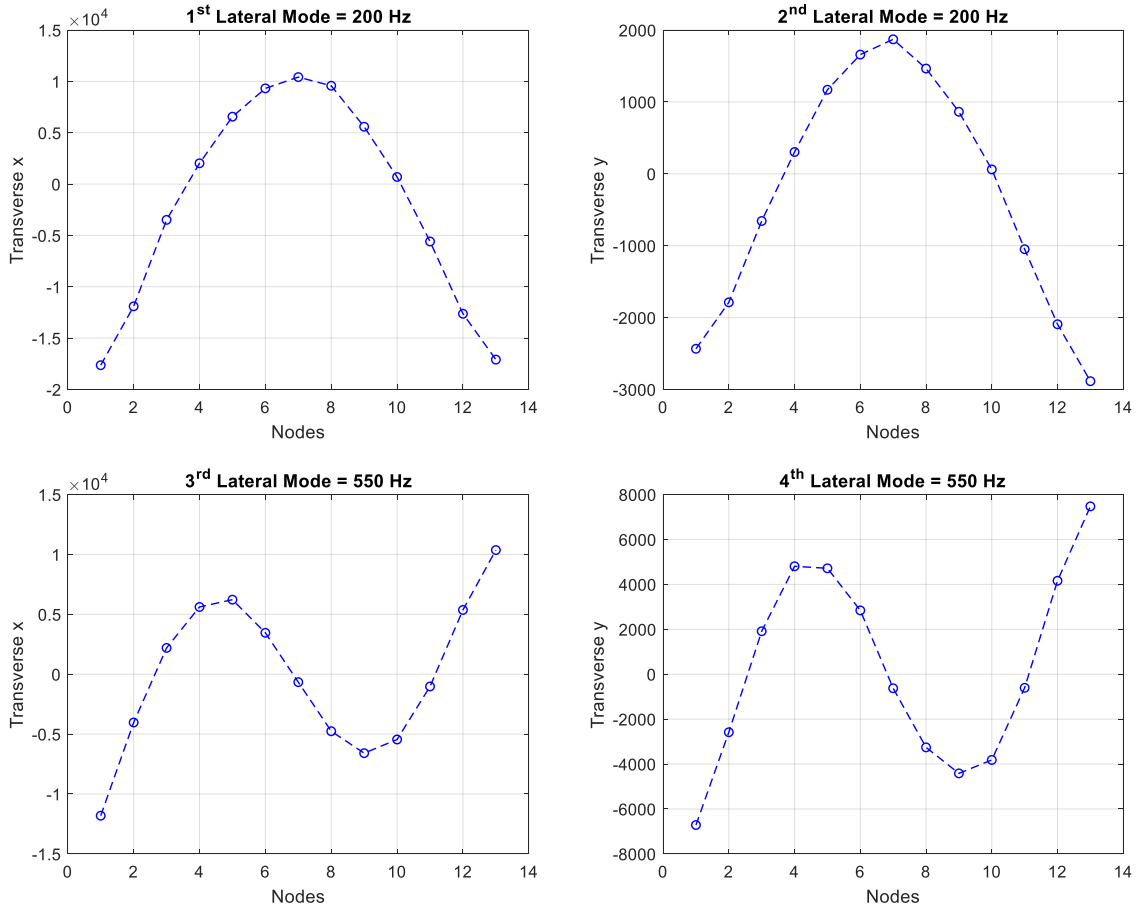

Figure 6.9 : Lateral modes of the output shaft.

Numerical modal behaviour

After obtaining the natural frequencies and mode shapes experimentally, numerical modal analyses of the input and output shafts were performed using the Abaqus finite element software. The finite element models of the two shafts were created with 3D solid deformable elements in Abaqus, where beam elements are not used because of the varying cross-section of the shafts. With the modal analysis tool in Abaqus, the natural frequencies of the first and second lateral modes were computed as 196.9 Hz, and the natural frequencies of the third and fourth lateral modes were computed as 539.4 Hz in the horizontal “x” and vertical “y” directions for the input shaft. Similarly, the natural frequencies of the first and second lateral modes were computed as 200.5 Hz, and the natural frequencies of the third and fourth lateral modes were computed as 550.6 Hz in the horizontal “x” and vertical “y” directions for the

output shaft. The computed natural frequencies are the same in the horizontal "x" and vertical "y" directions because of the homogenous and cyclically symmetric structure of the input and output shafts. The numerically computed mode shapes in Abaqus finite element software are also shown in Figure 6.10 and Figure 6.11 for the input and output shafts, respectively.

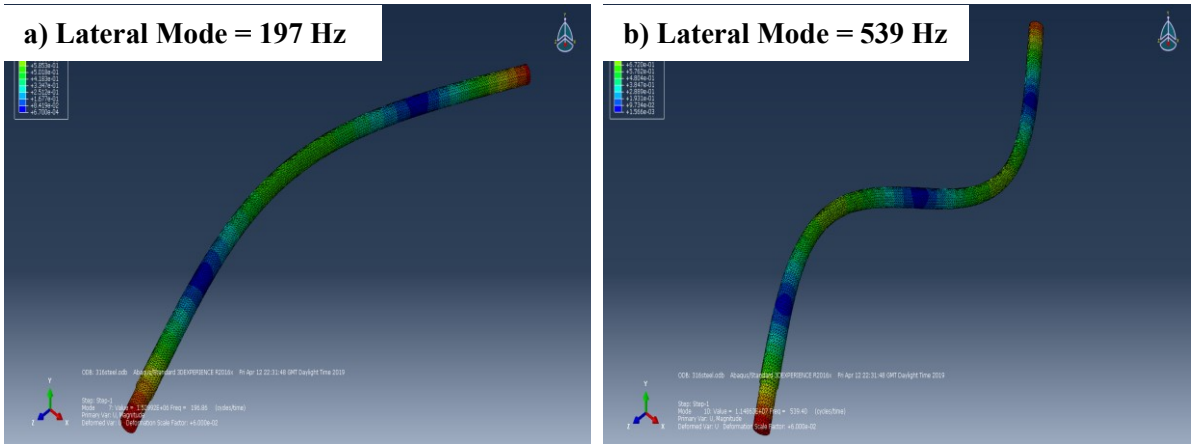

Figure 6.10 : Numerical modal analysis of the input shaft, a) first and second lateral modes, b) third and fourth bending modes.

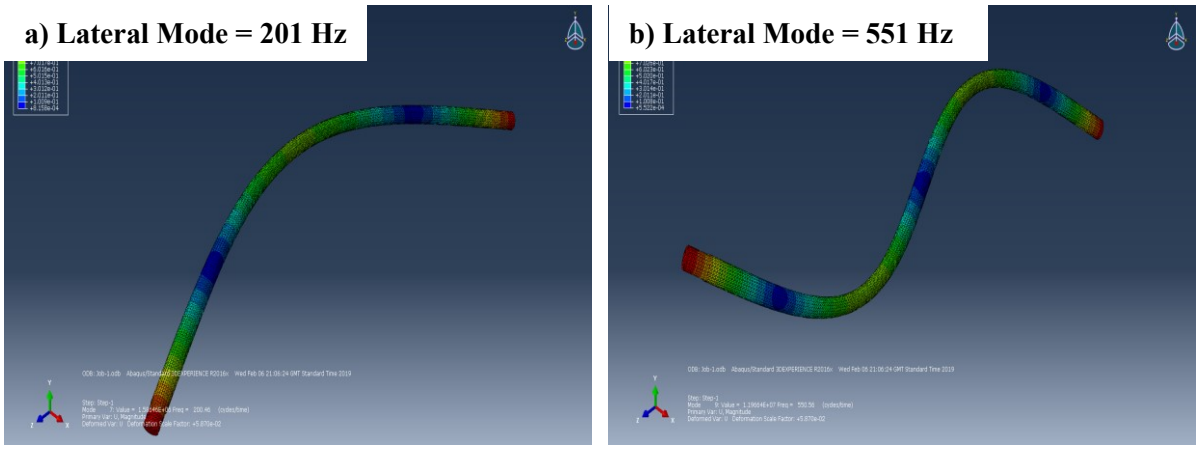

Figure 6.11 : Numerical modal analysis of the output shaft, a) first and second lateral modes, b) third and fourth bending modes.

Table 6.2 : Comparison of natural frequencies of shafts.

	Input Shaft			Output Shaft		
Elastic Lateral Mode #	Numerical Nat. Frequency [Hz]	Experimental Nat. Frequency [Hz]	Error %	Numerical Nat. Frequency [Hz]	Experimental Nat. Frequency [Hz]	Error %
1	196.9	196.6	0.15	200	200.5	0.25
2	196.9	196.9	0.00	200	200.5	0.25
3	539.4	539.1	0.06	549.6	550.6	0.18
4	539.4	539.2	0.04	549.7	550.6	0.16

The numerical modal analysis results in terms of natural frequencies and mode shapes are compared with the experimental modal analysis results as shown in Table 6.2. They are entirely consistent with each other, and the errors between them are negligible at a deviation of 0.25 %. Briefly, the numerically obtained first four elastic lateral modes of the shafts have been validated with the experimental modal analyses.

6.2.3 Planetary geared rotor

A planetary geared rotor test rig was built, and impact hammer tests were performed. The main motivation for building a test rig was to understand the modal behaviour of planetary geared rotors experimentally and then update the model parameters. Therefore, the experimental studies conducted on the planetary geared rotor test rig is a novel aspect of this project.

Despite some experimental studies in the literature to investigate the dynamic and modal behaviour of geared rotors, there are insufficient studies to understand the experimental modal behaviour of planetary geared rotors [52,162–165]. Among these studies, only Saxena et al. [165] carried out FRF measurements on a basic single-stage geared rotor system to detect lateral vibration modes. They also validated their finite element vibration analyses with experimental results. Furthermore, Wang et al. [166] conducted research on lateral-torsional coupled dynamic behaviour of a two-stage planetary geared rotor system for the non-rotating (static) case. This is the only experimental study which investigates the modal behaviour of planetary geared rotors. In this study, the torsional vibration modes were determined with a harmonic response analysis using spinning tests, whereas lateral vibration modes were determined with an experimental modal analysis using impact hammer tests.

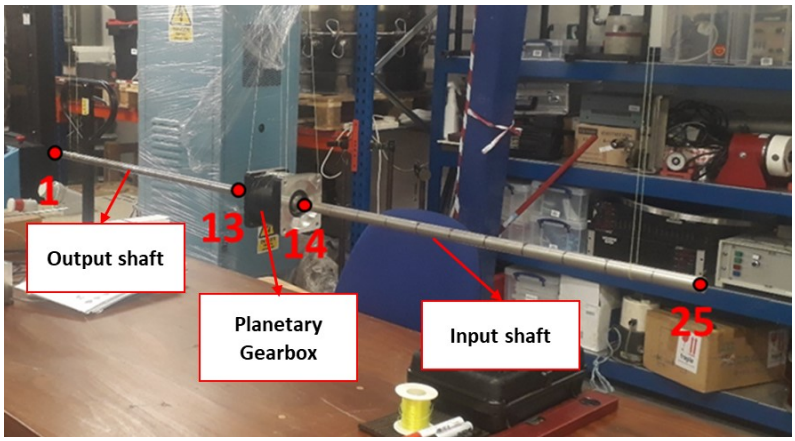

Figure 6.12 : Planetary geared rotor assembly.

The planetary geared rotor assembly basically consists of an input shaft, an output shaft and a spur planetary gearbox as seen in Figure 6.12. The input and output shafts are directly

connected to the planetary gearbox via interference-fit and screw connections respectively, which makes the coupling between the gearbox and shafts nearly rigid. Both the interference-fit and the screw add additional joints to the system, but their impact was considered small compared to the effect of the planetary gearbox itself. In this planetary geared rotor assembly, the material and geometry properties of the input and output shafts were assumed to be those presented in Table 6.1. A Nema 34 86PX single-stage spur planetary gearbox was purchased from the market for this assembly as shown in Figure 6.13. The housing of this planetary gearbox (two sides flanges) was made of Aluminium whereas the sun and planet gears were made of steel. The parameters of the spur planetary gearbox are presented in Table 6.3.

Figure 6.13 : Spur planetary gearbox, a) front view, b) rear view, c) isometric view.

Table 6.3 : Spur planetary gearbox parameters.

Parameter	Value
Gearbox mass [kg]	1.59
Housing material density [kg/m^3]	2700
Gear material density [kg/m^3]	7800
Number of planets	3
Speed ratio	4

The Nema 34 86PX planetary gearbox was disassembled for inspection, as seen in Figure 6.14. It is clearly seen that the spur planetary gearbox consists of a sun gear, three planet gears and a carrier. Lubrication between the gear teeth is provided by grease.

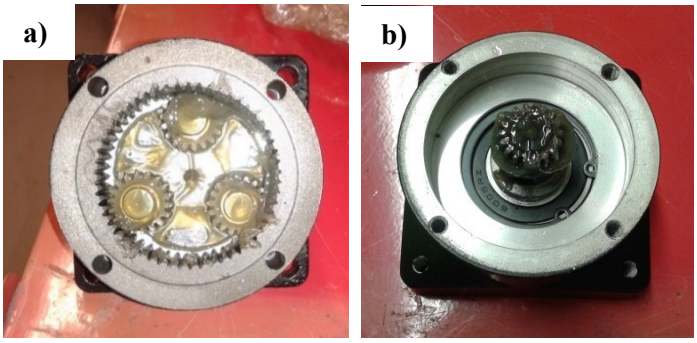

Figure 6.14 : Disassembled spur planetary gearbox, a) planet gears view, b) sun gear view.

The technical drawing of the Nema 34 86PX planetary gearbox is shown in Figure 6.15. The output shaft on the planetary gearbox has 16 mm diameter, and the hole diameter inside the planetary gearbox for the input shaft is 14 mm.

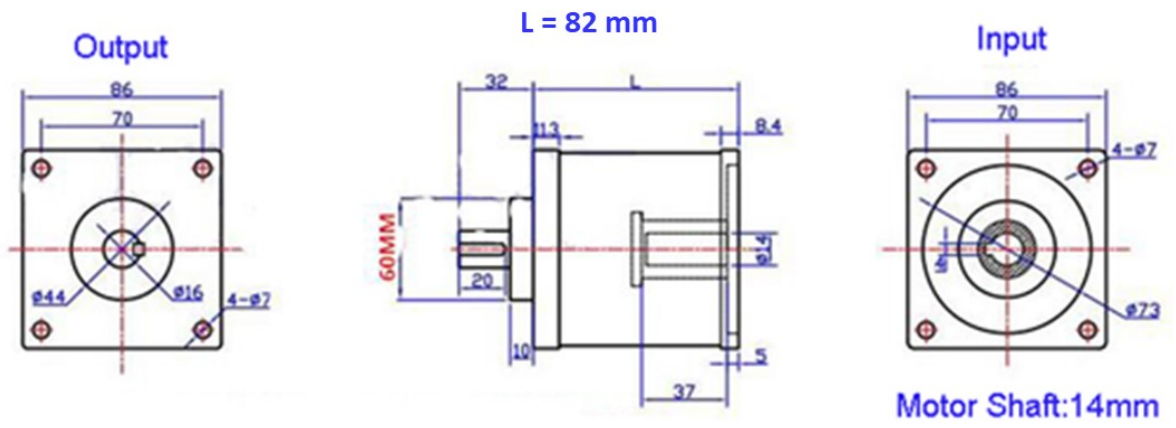

Figure 6.15 : Technical drawing of the spur planetary gearbox.

The planetary gearbox housing has a square cross-section, and its length is 86 mm. Total height of the planetary gearbox with the output shaft is 114 mm. After the disassembly of the planetary gearbox, the gears and carrier geometry were also measured, which are presented in Table 6.4.

Table 6.4 : Geometry of the gears and carrier.

Parameter	Carrier	Ring	Planets	Sun
Length [mm]	5	80	7	15
Outer Diameter [mm]	50	86	20	20
Inner Diameter [mm]	0	56	12	12

The planetary geared rotor assembly was divided into twenty-four equal segments approximately for the impact hammer test, creating twenty-five measurement locations as seen in Figures 6.12 and 6.16. The planetary geared rotor assembly was suspended with elastic cords from the right side of the input shaft and the left side of the output shaft. Its suspension locations are between the measurement locations 2 and 3 at the left side, and between the measurement locations 23 and 24 at the right side.

In order to identify the lateral modal behaviour of the planetary geared rotor, impact hammer tests were carried out by measuring the acceleration response signal in the horizontal (y) and vertical (x) directions with two single-axis accelerometers simultaneously. Basically, when exciting the structure horizontally, the acceleration signal was measured from the horizontal and vertical directions. Likewise, the acceleration signal was measured in the two directions

when exciting the structure vertically. Similar to the impact hammer tests of the shafts, the excitation and response signals were collected with 2048 Hz sampling frequency for 800 Hz maximum frequency in the signal analyser, making the sampling ratio 2.56. The planetary gearbox had relatively high damping compared to the shafts because of the lubrication grease inside the gearbox housing. Therefore, the measurement period was set as 4 seconds for collecting data, which was found to be sufficient after performing initial impact hammer tests. Thus, the frequency resolution during the impact hammer tests became 0.25 Hz. An exponential window and three averages were used for better data quality and measurement accuracy.

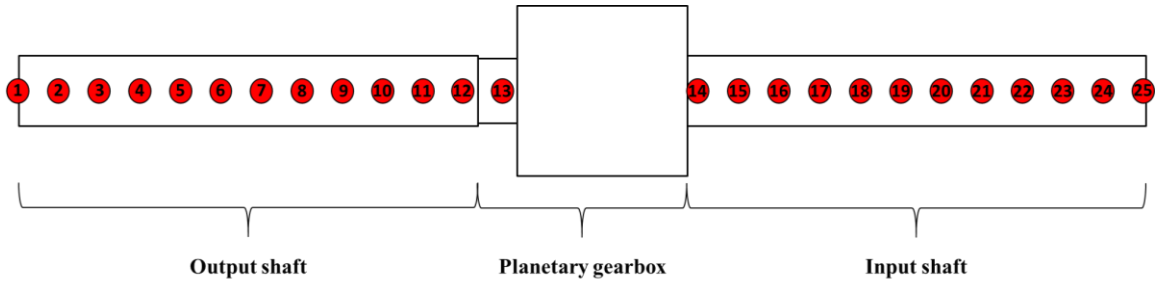

Figure 6.16 : Hammer testing nodes on the spur planetary geared rotor.

The planetary geared rotor assembly was excited by the impact hammer at the measurement locations from 1 to 25 as shown in Figure 6.16. The acceleration responses in the horizontal (x) and vertical (y) directions were measured simultaneously with two accelerometers at the constant measurement location 2. Only the excitation locations were changed by moving the hammer from the measurement locations 1 to 25 and repeating the tests in both horizontal and vertical locations. In total, fifty frequency response functions were measured with the impact hammer tests at twenty-five different measurement locations. The point FRFs were measured at the measurement location 2, and the cross FRFs were measured at the rest of the measurement locations. It should be noted that the planetary geared rotor assembly was excited from the opposite direction at its point FRF location.

Experimental vertical modal behaviour

The accelerance FRFs were computed using the force excitation signal in the vertical direction (y) and acceleration response signals in the horizontal (x) and vertical (y) directions in order to plot the 3D lateral mode shapes. The horizontal (x) and vertical (y) acceleration responses with respect to the vertical (y) excitation up to 500 Hz are shown in Figures 6.17 and 6.18, respectively. Six peak frequencies are indicated in each figure, representing the lateral resonant frequencies.

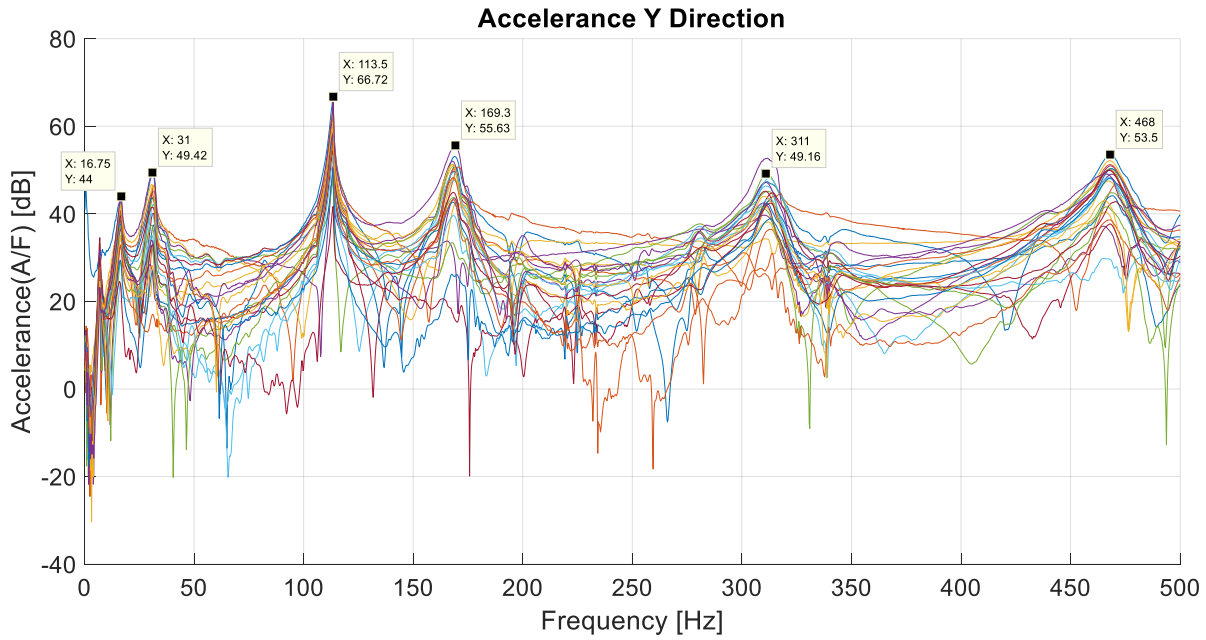

Figure 6.17 : Vertical (y) excitation, vertical (y) response.

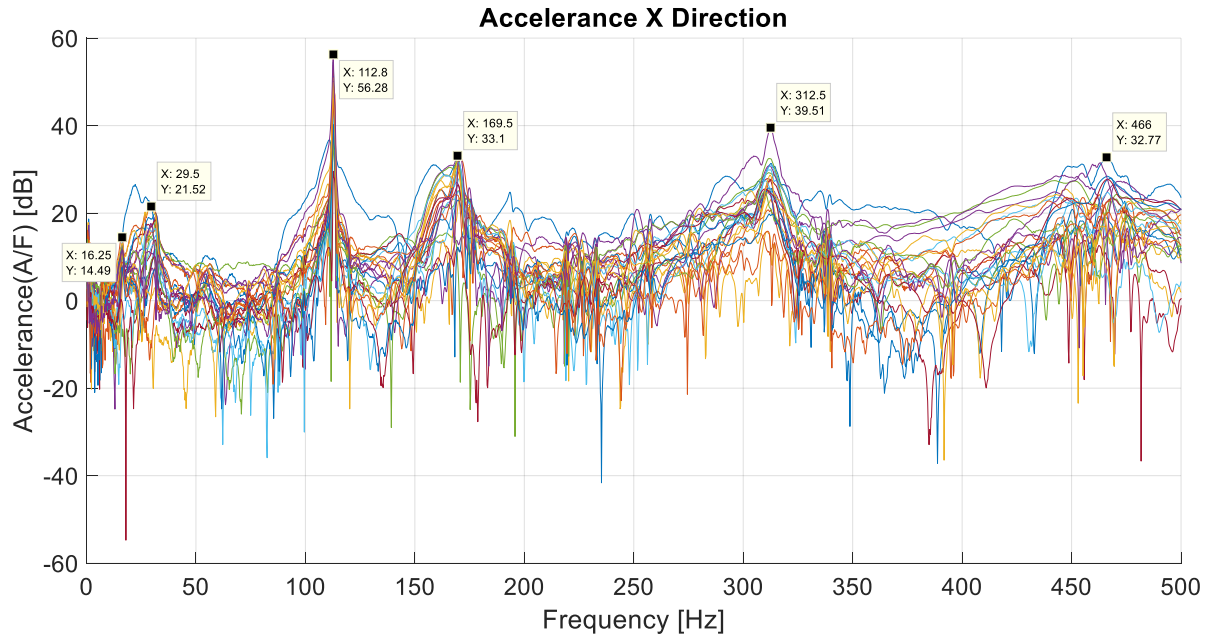

Figure 6.18 : Vertical (y) excitation, horizontal (x) response.

The 3D lateral mode shapes of the planetary geared rotor were plotted using the measured frequency response functions in the horizontal “x” and vertical “y” directions, as seen in Figure 6.19. In total, six lateral modes were detected up to 500 Hz. The first, second, third, fourth, fifth and sixth lateral modes were found to be at 16 Hz, 30 Hz, 114 Hz, 168 Hz, 305 Hz and 468 Hz, respectively. Among these lateral vibration modes, the third and fifth modes are identified as “out of phase” modes whereas the second, fourth and sixth modes are identified

as “in phase” modes. It should be noted that the first mode is the rigid body mode and the rest of them are the elastic modes. When looking at the mode shapes, the vibrational motion of the input and output shafts are in the same direction for the in phase modes, and they are in the opposite direction for the out of phase modes. Therefore, “in phase” and “out of phase” mode definitions are used for the lateral mode shapes.

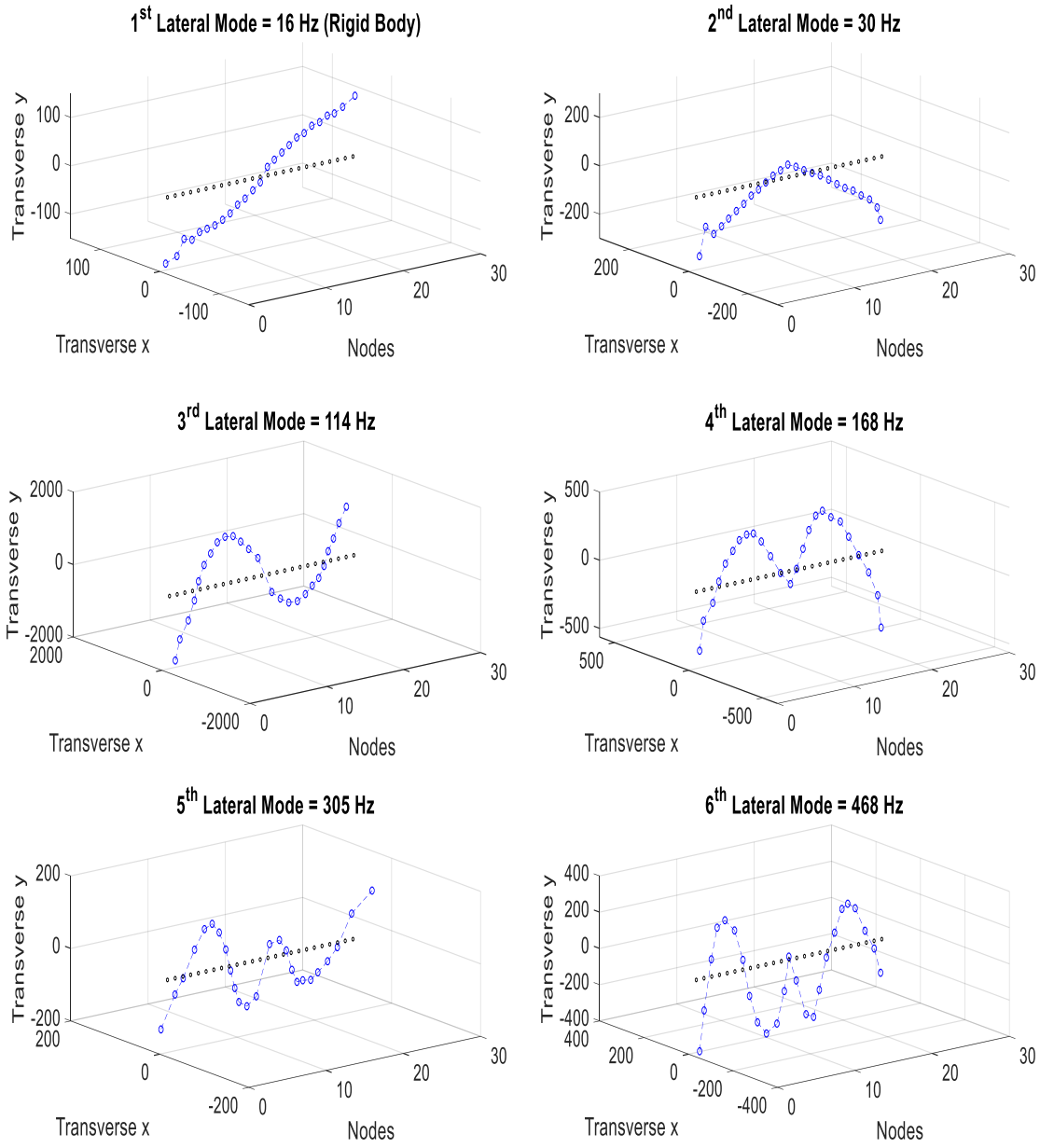

Figure 6.19 : Vertical (y) excitation 3D mode shapes.

Experimental horizontal modal behaviour

The accelerance FRFs were computed using the force excitation signal in the horizontal direction (x) and acceleration response signals in the vertical (x) and horizontal (y) directions for plotting the 3D lateral mode shapes. The horizontal and vertical acceleration responses with

respect to the horizontal excitation were plotted up to 500 Hz as seen in Figures 6.20 and 6.21 respectively. Six peak frequencies are indicated in each figure. These peak frequencies represent the lateral resonant frequencies.

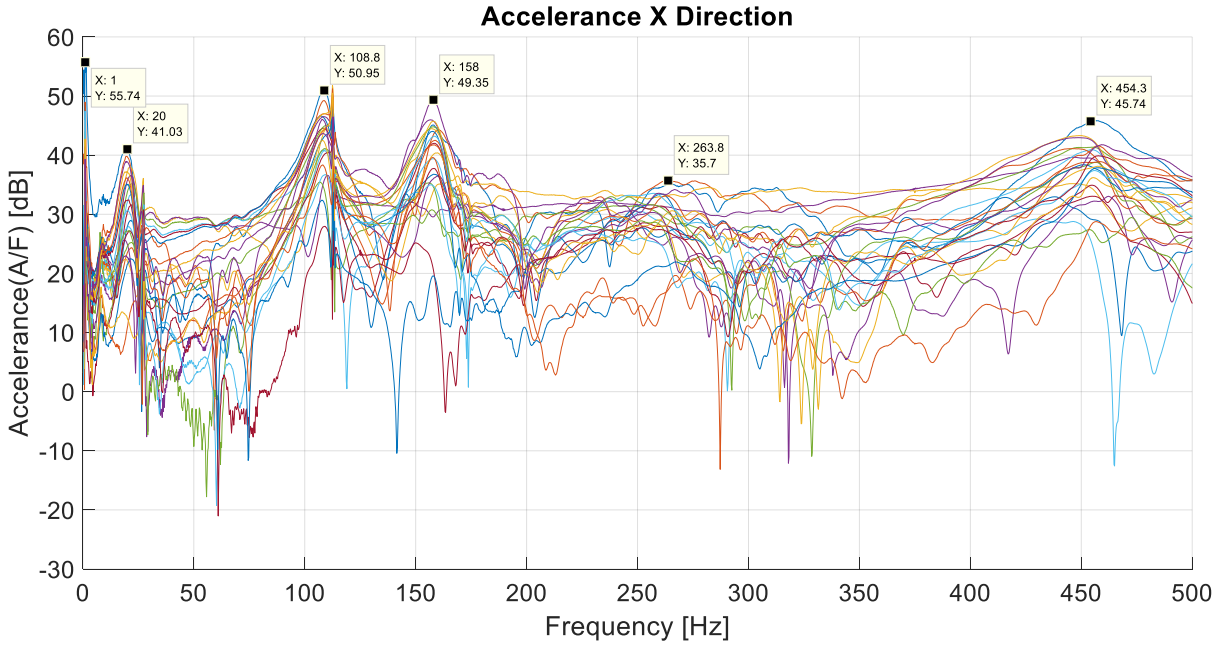

Figure 6.20 : Horizontal (x) excitation, horizontal (x) response.

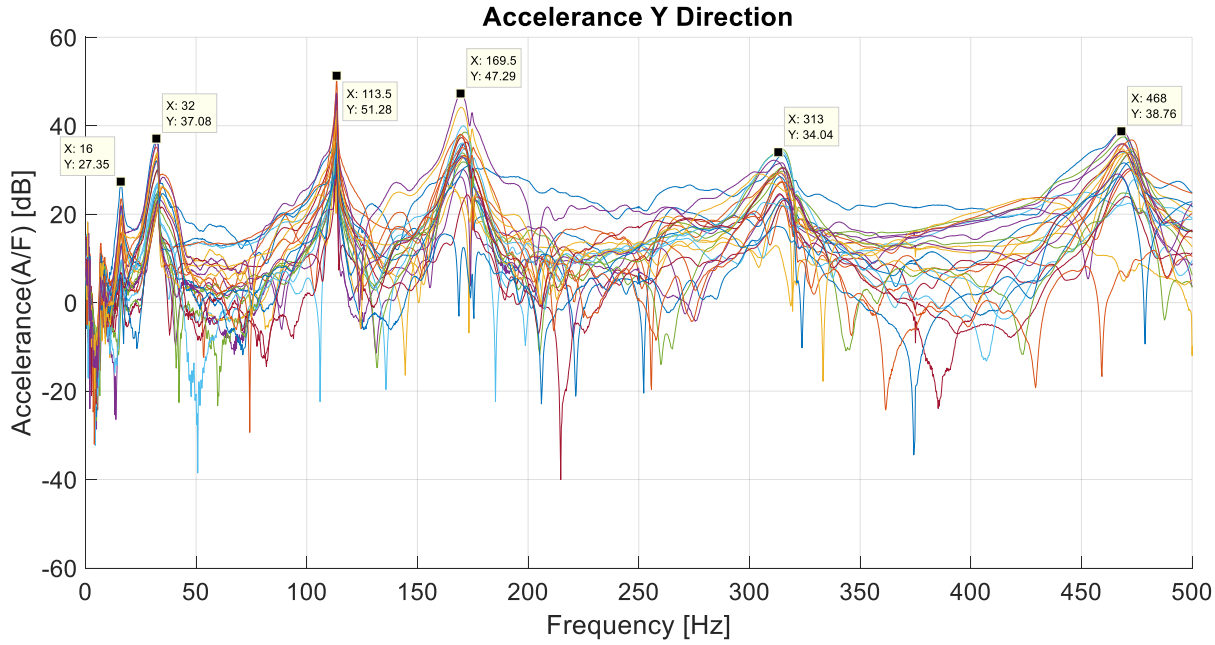

Figure 6.21 : Horizontal (x) excitation, vertical (y) response.

The 3D lateral mode shapes of the planetary geared rotor were plotted using the measured frequency response functions in the horizontal “x” and vertical “y” directions, as seen in Figure 6.22. In total, six lateral vibration modes were detected up to 500 Hz. The first, second, third,

fourth, fifth and sixth lateral vibration modes were found to be at 1 Hz, 20 Hz, 109 Hz, 158 Hz, 264 Hz, and 454 Hz, respectively. These are the elastic modes except for the first mode, which represents the rigid body mode. Similar to the experimental vertical modal behaviour, the third and fifth modes are identified as out of phase mode, and the second, fourth and sixth modes are identified as in phase mode when looking at the mode shapes in Figure 6.22.

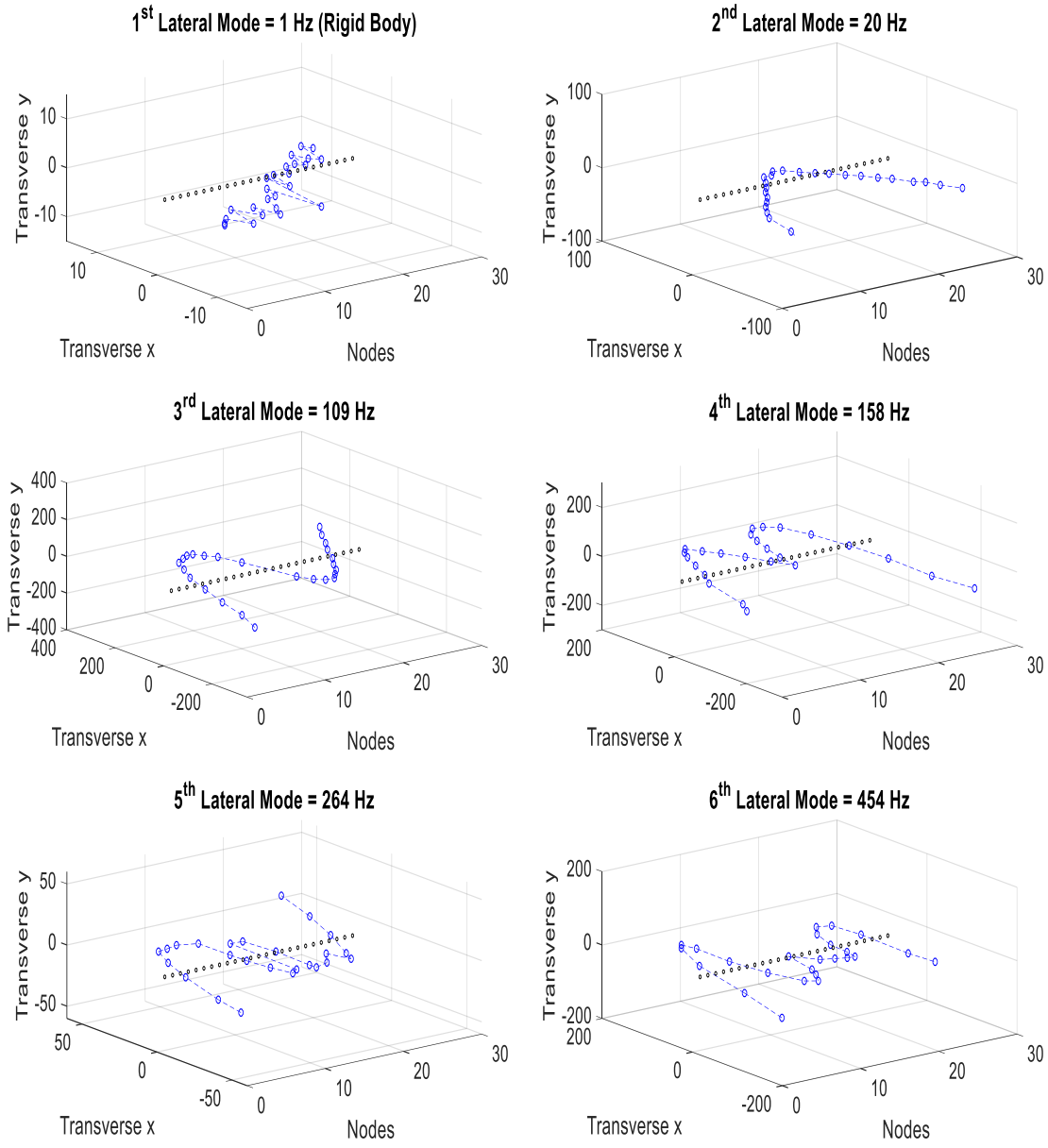

Figure 6.22 : Horizontal (x) excitation 3D mode shapes.

The natural frequencies of the lateral vibration modes were previously found to be same in vertical and horizontal directions for the shafts due to their homogenous and cyclically symmetric structures. However, they are not found to be the same for the planetary geared rotor assembly owing to the anisotropic stiffness parameters inside the planetary gearbox.

6.3 Dynamic model update and validation

The main aim of performing modal testing is to determine the modal parameters such as natural frequencies, mode shapes and modal damping. The modal parameters can also be computed via numerical approaches such as lumped parameter and finite element methods without doing experiments. However, it is crucial to use real system parameters such as stiffness, mass and damping in order to compute correct modal parameters. This can be achieved by updating the system parameters in the numerical models using the experimental data. Then, the updated model can be validated with the experimental results. Model updating based on experiments is a significant topic in vibration engineering since time and costs could be reduced by using the correct dynamic models instead of expensive experiments.

6.3.1 Model update

In most of the real planetary geared rotor applications, the shafts and planetary gearbox are grounded via their bearings. A typical planetary geared rotor system was previously presented in Chapter 3, where the detail of the planetary geared rotor model is seen in Figures 3.1 and 3.5. On the other hand, planetary geared rotor systems can be subjected to platform motions in some engineering applications, for instance in offshore wind turbines [202]. This phenomenon is described as base motion in the literature [203]. Similar to the base motion phenomenon, the planetary geared rotor assembly is also not grounded in the free-free modal analysis. Therefore, the dynamic model presented in Chapter 3 needs to be updated for the free-free motion.

First of all, the lumped parameter model of the planetary gearbox model given in Figure 3.3 has been updated to determine its bearing characteristics. In the free-free impact hammer test of the planetary geared rotor assembly, central members of the planetary gearbox which are the ring gear, sun gear and carrier are not grounded. The ring gear is rigidly fixed on the gearbox housing, and it moves with the movement of the gearbox housing. Due to no grounded support on the gearbox housing and the rigid connection between the ring gear and gearbox housing, the ring gear is assumed to be not supported, which makes its support stiffness and damping parameters zero if the elastic cord stiffness is neglected. On the other hand, the sun gear and carrier are attached to the gearbox housing via their bearings. Hence, the sun gear and carrier move in relation to the gearbox housing. Due to these relative motions, the strain energy equation of the bearings for the central members expressed in Equation 3.33 in section 3.3.2 requires a model update for the displacement terms. For this purpose, strain energies of the central members are rewritten as

$$V_h = \frac{1}{2}\sum_{h=1}^{3} k_{xh}(x_h - x_r)^2 + k_{yh}(y_h - y_r)^2 + k_{zh}(z_h - z_r)^2 + k_{\theta_{xh}}(\theta_{xh} - \theta_{xr})^2 + k_{\theta_{yh}}\left(\theta_{yh} - \theta_{yr}\right)^2 + k_{\theta_{zh}}(\theta_{zh} - \theta_{zr})^2. \quad \textbf{(6.2)}$$

Apart from updating the strain energy equation of the central members, total kinetic energy ($T = T_h + T_p$), the strain energy equation of the planet gear bearings (V_p) and the gear mesh strain energy equation (V_m) of the planetary gearbox remain unchanged. Therefore, a change in just the total potential energy equation is experienced. It is also important to point out that the planetary gearbox housing mass is added to the ring gear mass in the dynamic model because of the rigid connection between them. With the updated energy equations, the new planetary gearbox equation of motion can be derived again using the Lagrange`s equations of the second kind, similar to the Eq. 3.43.

System parameters of the planetary geared rotor system have been updated with the modal testing results presented in section 6.2. The updated system parameters are given in Table 6.5, where the geometry properties of the planetary geared rotor system were previously given in section 6.2. It should be noted that the lengths of the output and input shafts have been updated after the assembly because of their connection to the planetary gearbox. Material properties of the shafts were also directly taken from Table 6.1. Furthermore, bearing stiffness and damping parameters of the input and output shafts were set to be zero since the shafts are not grounded in the free-free experimental modal analysis. Internal damping of the input and output shafts were also not considered since it was negligible. Although the damping inside the planetary gearbox is one of the important unknown parameters, it was assumed to be zero. Planetary gearbox damping is neglected because the model updating is based on the natural frequencies and mode shapes. Among the gear contact parameters, the helix angle was exactly defined as zero because of the spur gears inside the planetary gearbox. Moreover, the transverse pressure angle and mesh stiffness values in Table 6.5 were determined with several numerical iterations in “GEAROT” by obeying their standard values in gear applications. These standard gear parameter values can also be found in references [191,200].

Table 6.5 : Updated model parameters of the planetary geared rotor system.

Parameter	Output Shaft	Input Shaft	Carrier	Ring	Planets	Sun
Length [m]	0.621	0.570	0.005	0.080	0.007	0.015
Outer Diameter [m]	0.015	0.016	0.050	0.086	0.02	0.02
Inner Diameter [m]			0	0.056	0.012	0.012
Material density [kg/m^3]	7850	7950	7800	7800	7800	7800
Young`s modulus [GPa]	208	190				
Shear modulus [GPa]	80	74				
Proportional damping α_1 constant	0	0	0	0	0	0
Proportional damping α_2 constant	0	0	0	0	0	0
Bearing radial stiffness (x) [kN/mm]	0	0	4.735	0	47.35	0.4735
Bearing radial stiffness (y) [kN/mm]	0	0	13.42	0	134.2	1.342
Bearing axial stiffness (z) [kN/mm]	0	0	5	0	50	0.5
Bearing tilting stiffness (θ_x) [kN.m/rad]	0	0	9.47	0	94.7	0.947
Bearing tilting stiffness (θ_y) [kN.m/rad]	0	0	26.84	0	268.4	2.684
Bearing torsional stiffness [N.m/rad]	0	0	0	0	0	0
Bearing radial damping [N/(m/s)]	0	0	0	0	0	0
Bearing axial damping [N/(m/s)]	0	0	0	0	0	0
Bearing tilting damping [N.m/(rad/s)]	0	0	0	0	0	0
Bearing torsional damping [N.m/(rad/s)]	0	0	0	0	0	0
Helix angle β [deg]				0	0	0
Transverse pressure angle ϕ [deg]				25	25	25
Mesh Stiffness [N/m]				10^8	10^8	10^8
Number of planets					3	

Prediction of the bearing stiffness values is one of the most challenging parts of model updating owing to the nonlinear, time-varying and load-dependent behaviour of bearings. It is known that the bearing stiffness can increase with respect to the load on the bearings, leading to hardening spring behaviour [3]. The weight of the planetary geared rotor system leads to an increase in the bearing stiffnesses in the vertical direction. Therefore, the radial and tilting bearing stiffness values were updated in the vertical and horizontal directions individually. As seen in Table 6.5, the bearing stiffnesses in the vertical (x) direction are higher than the bearing stiffnesses in the horizontal (y) direction. Moreover, all members of the planetary gearbox (carrier, ring gear, sun gear and planet gears) were able to rotate freely due to not having grounded bearings. Therefore, the torsional stiffnesses of the planetary gearbox bearings were set to zero. The bearing and gear mesh stiffness parameters of the planetary gearbox were the main unknowns in the experimental setup. Briefly, values of the bearing stiffnesses, gear mesh stiffnesses, transverse pressure angles in Table 6.5 were determined with several numerical iterations in “GEAROT” after comparing them with the experimental modal analysis results.

6.3.2 Model validation

After updating the dynamic model with the parameters from Table 6.5, a numerical modal analysis of the planetary geared rotor assembly was carried out in the "GEAROT" software for an undamped non-rotating (static) case. The input and output shafts were modelled with 48 Timoshenko beam elements. For the output and input shafts, 25 and 23 beam elements were used respectively due to their different lengths in the assembly.

Numerical modal analysis results are presented for the first twelve modes in Table 6.6. Similar to the experimental modal behaviour of the planetary geared rotor assembly, the elastic lateral vibration modes of the planetary geared rotor are identified as "out of phase" and "in phase". 2D mode shapes of the lateral vibration modes are shown in Figure 6.23, where the horizontal and vertical displacements are seen separately. In order to see the lateral vibration modes in 3D space, the 3D mode shapes were also plotted in Figure 6.24, where the horizontal and vertical modal behaviour of the planetary geared rotor system for the lateral vibration modes are clearly seen. It is worth stating that both Figures 6.23 and 6.24 reveal the out of phase and in phase mode when looking at mode shapes.

Table 6.6 : Experimental and numerical natural frequency comparison of the spur planetary geared rotor.

Lateral Mode #	Experimental Nat. Frequency [Hz]	Numerical Nat. Frequency [Hz]	Mode Type	Error %
1	1	0	Rigid Body	--
2	16	0	Rigid Body	--
3	20	21	In Phase	4.8
4	30	29	In Phase	3.4
5	109	121	Out of Phase	9.9
6	114	124	Out of Phase	8.1
7	158	161	In Phase	1.9
8	168	169	In Phase	0.6
9	264	264	Out of Phase	0.0
10	305	304	Out of Phase	0.3
11	454	431	In Phase	5.3
12	468	464	In Phase	0.9

Experimental and numerical natural frequencies for the lateral vibration modes were also compared with the error percentage as shown in Table 6.6. It is clearly seen that the error percentages are less than 10 % for the elastic lateral modes, which include in phase and out of phase modes. It is important to point out that experimentally detected in phase and out of phase

lateral vibration modes are substantially captured with the numerical modal analysis, highlighting the achievement of the “GEAROT” in numerical modal analysis.

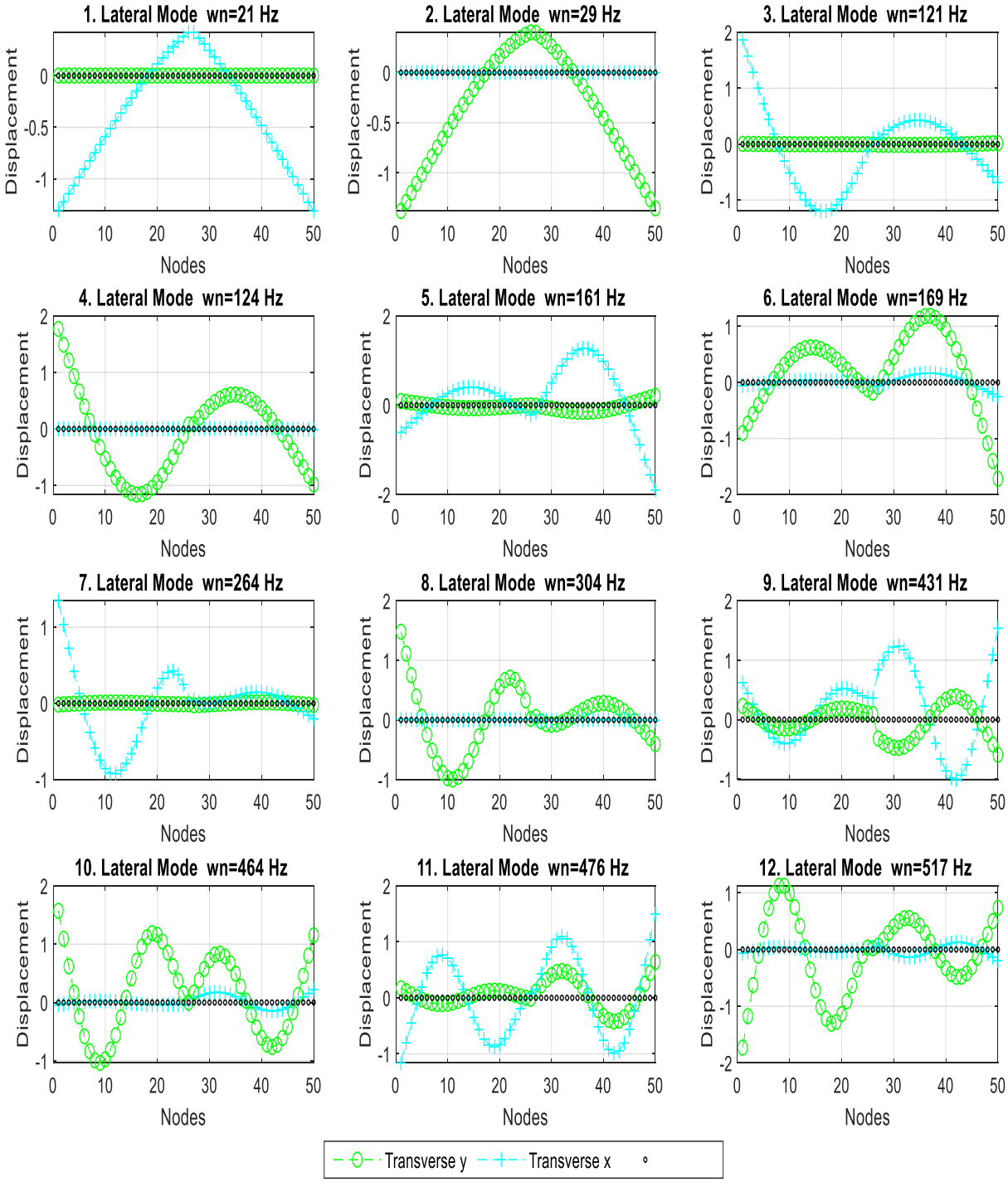

Figure 6.23 : 2D numerical elastic lateral mode shapes.

On the other hand, the numerical model could not predict the first two lateral modes, which are the rigid body modes, correctly in terms of natural frequencies because of the numerical assumptions. Basically, the stiffnesses of the elastic cords used in the impact hammer tests

were not included in the free-free numerical model analysis while the experiments were carried out using the elastic cords. Therefore, the numerical and experimental natural frequencies for the rigid body modes cannot be matched, and the error between them is not specified in Table 6.6.

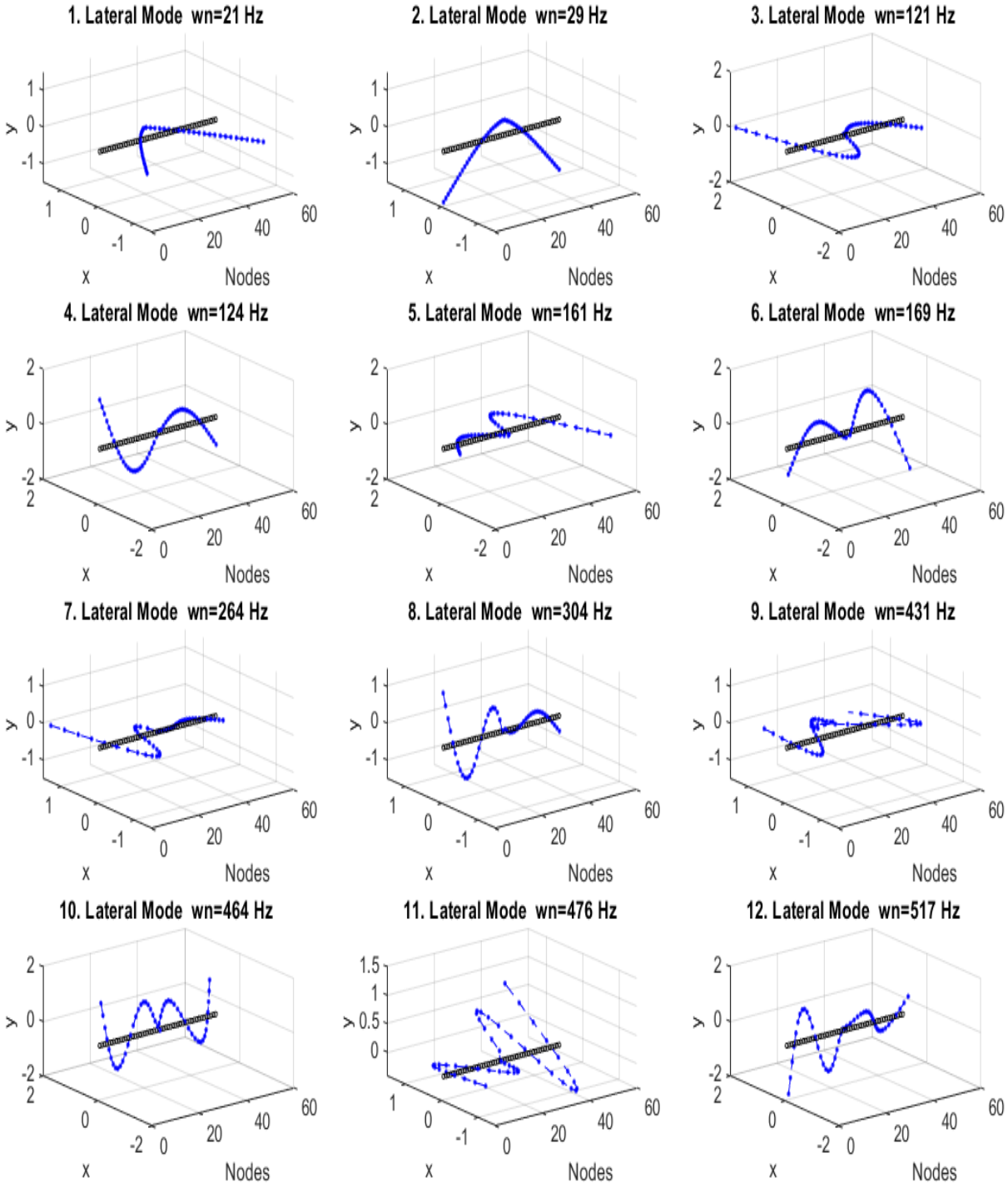

Figure 6.24 : 3D numerical elastic lateral mode shapes.

6.4 Discussion

A better understanding of the lateral modal behaviour of spur planetary geared rotors using experimental modal analysis and dynamic model updating with the experimental results were the main aims of this study. To achieve this goal, impact hammer tests on the spur planetary geared rotor assembly and its components, which are the input and output shafts, were carried out separately.

The planetary gearbox acts as a rigid mass on the rotor system, and its structure is different to a rotating flexible shaft element. Therefore, an impact hammer test was not performed for the planetary gearbox. Experimental and numerical modal analyses were successfully achieved to compute the natural frequencies and mode shapes for the input and output shafts with the impact hammer tests and finite element analyses in Abaqus, respectively. The numerically computed first four elastic lateral vibration modes of the input and output shafts are consistent with the experimental modal analysis. The errors between the numerical and experimental results in terms of natural frequencies and mode shapes are negligible. The impact hammer tests of components (shafts) are required to confirm their material and modal properties before the impact hammer test of the coupled structures (planetary geared rotor assembly).

For the planetary geared rotor assembly, experimental modal analysis was performed after the impact hammer tests. The hybrid numerical model was validated with the experimental modal analysis using the known and estimated system parameters. In the hybrid numerical model, only the strain energy equations of the bearings of the ring gear, carrier and sun gear were updated for the free-free modal analysis because of the free-free motion of the planetary gearbox. The lateral vibration modes of the planetary geared rotors are clearly divided into two groups as “out of phase” and “in phase”, which appear in both the numerical and experimental modal analyses. It has been found that the natural frequencies of the planetary geared rotor are slightly different in the vertical and horizontal directions, while they were found to be same in the vertical and horizontal directions for the shafts because of their homogenous and cyclically symmetric structures. When the planetary geared rotor assembly is hung from close to the edges of the shafts, the gearbox starts to sag in the vertical direction due to its heavy mass. Therefore, loads on the gearbox bearings increase with sagging, leading to increases in bearing stiffnesses in the vertical direction (hardening spring behaviour). Different hanging configurations were also tried to investigate the sagging effect on the lateral vibration modes in vertical directions

by measuring horizontal levels with a tubular spirit level. It has been found that the natural frequencies of the lateral vibration modes increase with the level of sagging.

Validation of the numerical modal analysis of planetary geared rotor with the experimental modal analysis is found to be very difficult due to the unknown system parameters and numerical assumptions. In terms of natural frequencies, the maximum error between the numerical and experimental results is found to be less than 10 % after dynamic model updating. Regarding the mode shapes, the experimentally found first two lateral modes, which are rigid body modes, could not be computed correctly in terms of natural frequencies with the numerical modal analysis because of not including elastic cord stiffnesses in the free-free numerical modal analysis. On the other hand, computing the rigid body modes were not the main priority compared with the elastic modes. Among the gearbox parameters, the gear mesh stiffness, gear pressure angle, bearing stiffness, damping inside gearbox and gearbox housing rotary inertia were unknown parameters. Gear teeth contacts and gearbox bearings have nonlinear and time-varying features in reality, therefore the constant stiffness value assumption for the meshes and bearings is a weakness in the numerical model. Furthermore, hardening spring behaviour of the bearings is another difficulty in the bearing stiffness prediction. The interference-fit and screw connections between the shafts and the planetary gearbox also create additional unknown contact stiffnesses in the assembly. Due to the complex structure of the planetary gearbox, rotary inertia of the gearbox housing is an unknown parameter, and the housing mass is added onto the ring gear as a basic assumption. Briefly, all these unknown parameters and numerical assumptions make the model validation of the planetary geared rotor assembly very difficult.

6.5 Concluding remarks

Experimental investigation of the lateral modal behaviour of a spur planetary geared rotor system and the validation of the numerical modal analysis were the main aims of this chapter. Free-free impact hammer tests were carried out for the planetary geared rotor assembly and its shafts separately. Independent modal analyses of the shafts are required to validate their material properties. Numerical modal analysis of the shafts and planetary geared rotor assembly for the free-free boundary conditions were conducted with finite element analysis in Abaqus and updated hybrid numerical model in “GEAROT”, respectively.

Both experimental and numerical free-free modal analysis of the input and output shafts were found to be consistent in terms of natural frequencies and mode shapes for the first four lateral

vibration modes, validated with a high level of accuracy. On the other hand, the numerical modal analysis of the planetary geared rotor assembly was validated substantially with the experimental modal analysis for the first twelve modes due to the unknown gearbox parameters such as stiffness, damping and inertia, and numerical assumptions. Based on the numerical modal analysis of planetary geared rotors, the lateral vibration modes were identified as “in phase” and “out of phase”, and they were validated with the experimental modal analysis. Basically, the input and output shafts move in the same direction in “in phase lateral modes” whereas they move in opposite directions in “out of phase lateral modes” during a vibration cycle. The planetary geared rotor assembly has different natural frequencies in the horizontal (x) and vertical (y) directions. The natural frequencies in the vertical direction were found to be higher than the natural frequencies in the horizontal direction because of the loads on the gearbox bearings in free-free experimental modal analysis of the planetary geared rotor system. Gearbox sagging on the rotor system due to its own weight leads to increased loads on the bearings, and as a result, increasing bearing stiffnesses in the vertical direction. Briefly, a planetary gearbox can provide higher stiffness value in the vertical direction than the horizontal direction when it sags on a rotor system.

In conclusion, there is a reasonable correlation between the experimental and numerical results of the planetary geared rotor assembly when the unknown system parameters and numerical assumptions are taken into account. The “out of phase” and “in phase” mode shape definition is thought to be one of the important findings of this research project.

Chapter 7

7 Conclusions and Recommendations

7.1 Conclusions

The main objectives of this research project were understanding the coupled dynamic behaviour of planetary geared rotor systems with numerical and experimental studies, and the numerical investigation of planetary gearbox parameter effects on the modal behaviour of planetary geared rotor systems. These objectives were achieved by developing a rotor dynamics software called “GEAROT” for the numerical studies and a planetary geared rotor test rig for the experimental studies. The summary of this research project and its main findings are provided below.

Within the numerical studies, a six degrees of freedom hybrid dynamic model of a planetary geared rotor system was created by taking gyroscopic effects into account in “GEAROT” rotor dynamics software, where the planetary gearbox and rotor system were modelled using the lumped parameter and finite element methods, respectively. In the finite element model of the rotor system, the shafts and bearings were assumed to be flexible and modelled with 1-D rotating Timoshenko beam elements and uncoupled flexible spring elements, respectively. In the lumped parameter model of the planetary gearbox, the carrier and gear wheels were assumed to be rigid while assuming the gear contacts as flexible. After having defined the energy equations for the rotor-bearing system and planetary gearbox, the system equation of motions was obtained using the Lagrange`s equations. Then, the coupled modal behaviour of both spur and helical planetary geared rotor systems and the gearbox parameters effects on the vibration modes of the planetary geared rotor system were investigated with linear modal analyses. Given the detected strong influence of the planetary gearbox on the rotor dynamics, and the significant uncertainty surrounding the input parameters for the planetary gearbox, the

parameter study was conducted to identify the most sensitive parameters and highlight their impact on a planetary geared rotor system. The sensitivity of planetary geared rotor vibration modes to the gearbox parameters was determined by computing the frequency shifts and comparing the mode shapes between the two extreme cases using the modal assurance criteria. In the planetary gearbox parameter study, sensitivity analyses of vibration modes were conducted for the gear contact parameters such as gear mesh stiffness, gear helix angle and gear pressure angle, gearbox mass and support parameters such as gear material density and support stiffness, and planet gear parameters such as number of planet gears and planet mistuning (positioning error of planet gears). To quantify the coupling level between the rotor system and planetary gearbox, the modal energy analysis was used, revealing the planetary gearbox effect on the modal behaviour of the global rotor system numerically. Gyroscopic effects of the planetary gearbox on the vibration modes of the planetary geared rotor system at higher speeds were also investigated. All numerical analyses in this thesis were carried out in the so-called "GEAROT" rotor dynamics software, which has been developed during this research project and one of the important outcomes of the project.

Within the experimental studies, a spur planetary geared rotor test rig was designed for the lateral modal behaviour investigation of planetary geared rotor systems. Before starting the impact tests on the spur planetary geared rotor assembly, the numerical modal analyses of the input and output shafts were undertaken in Abaqus finite element software. Following, free-free impact hammer tests were undertaken on the shafts so as to validate their material properties and modal behaviour. After completing the independent modal analyses of the shafts, free-free impact hammer tests were carried out on the spur planetary geared rotor assembly to validate the numerical modal analyses results in "GEAROT" rotor dynamics software, where the hybrid numerical model had been updated for representing the spur planetary geared rotor system in the free-free impact hammer test. Finally, the numerically identified lateral modal behaviour of the spur planetary geared rotor system was successfully validated with the experimental modal analysis results.

For clarification, the main original contributions of this research project are listed in detail below:

- A six degrees of freedom hybrid dynamic model of a planetary geared rotor system has been proposed using the finite element and lumped parameter method for the first time. The proposed hybrid dynamic model of planetary geared rotor systems can be employed for their multi-purpose rotor dynamic analyses. It is absolutely necessary to

incorporate a reasonably detailed planetary gearbox model in the rotor system in order to obtain an accurate dynamic response prediction of a planetary geared rotor system.

- Vibration modes of the helical planetary geared rotors are identified as coupled torsional-axial, lateral and gearbox modes, whereas they are classified as axial, torsional, lateral and gearbox modes in the spur planetary geared rotors. Torsional and axial vibrations of the planetary geared rotors are coupled in helical planetary geared rotors because of the gear helix angle effect. It is also found that there is no axial vibration transmission between the input and output shafts in spur planetary geared rotors due to the uncoupled axial modes. Gearbox modes in both spur and helical planetary geared rotors are found to be completely isolated from the shafts because of no dynamic interaction between the shafts and gearbox at these modes, where no displacement and rotation occur on the shafts.

- The modal energy analysis highlights the numerical influence level of the planetary gearbox on the global vibration modes of the planetary geared rotor system. The planetary gearbox has higher modal energy in some global modes (except the gearbox modes) of the planetary geared rotor system, where the natural frequencies computed from the independent modal analyses of the planetary geared rotor system and planetary gearbox are found to be close to each other. This phenomenon explicitly reveals the dominancy of the gearbox at these modes. The entire modal energy of the planetary geared rotor system is stored in the planetary gearbox at the gearbox modes; thus, no coupling between the shafts and gearbox occurs.

- At higher speeds, the global backward and forward lateral modes of the planetary geared rotor system in which the planetary gearbox has higher modal energy can experience significant gyroscopic effects due to the gearbox members, leading to significant changes in natural frequencies of the planetary geared rotor system.

- The planetary gearbox mass and support parameters are found to be more influential than the gear contact parameters to control the modal parameters of both helical and spur planetary geared rotors in terms of their natural frequencies and mode shapes. The coupled torsional-axial modes of helical planetary geared rotors and the torsional modes of spur planetary geared rotors are more sensitive to the gear mesh stiffness and helix

angle whereas their lateral vibration modes are more sensitive to the gear material density and support stiffness.

- The axial vibration modes of spur planetary geared rotors are found to be less sensitive to the gearbox parameters such as gear mesh stiffness, gear pressure angle, gear material density and planet gear mistuning, whereas these vibration modes can be effectively controlled with the axial support stiffnesses.

- The parameter study for the number of planet gears shows the reverse effect between the natural frequencies of the torsional-axial modes and lateral modes. Increasing number of planet gears leads to an increase in natural frequencies of torsional-axial modes while decreasing natural frequencies of lateral modes. Briefly, planetary gearboxes behave more rigid in the torsional-axial modes and softer in the lateral modes with respect to the increase in the number of planet gears.

- The parameter study for planet gear mistuning reveals that the mistuning leads to coupled lateral-torsional-axial modes in helical planetary geared rotors and coupled lateral-torsional modes in spur planetary geared rotors. These coupled vibration modes occur in the mistuned planetary geared rotors because unequally spaced planets break the cyclic symmetric structure of the planetary gearbox. On the other hand, the planet mistuning effect on the natural frequencies is found to be negligible.

- Experimental modal analysis of the planetary geared rotor assembly reveals that the lateral vibration modes can be divided into two groups as “in phase” and “out of phase”. Similarly, these lateral modes are observed in the numerical modal analysis of planetary geared rotors. When looking into the movement of the input and output shafts during a vibration cycle, both shafts move in the same direction in “in phase” lateral modes, while moving in the opposite direction in “out of phase” lateral modes.

- Numerical lateral modal behaviour of the planetary geared rotor assembly is satisfactorily validated with the experimental modal analysis. Both numerically and experimentally obtained lateral mode shapes are found to be consistent with high accuracy. There are slight differences between the numerically and experimentally

obtained natural frequencies at some lateral modes because of the unknown gearbox parameters and numerical assumptions.

- In the experimental modal analysis of the planetary geared rotor assembly, natural frequencies of the lateral modes are found to be higher in the vertical direction than the horizontal direction, which implies the unsymmetrical dynamic structure of the system and having higher stiffness in the vertical direction. Basically, planetary gearbox sagging on the rotor assembly causes higher loads on the gearbox bearings in the vertical direction, resulting in stiffening effect in the vertical direction. Consequently, a planetary geared rotor system can behave more rigid in the vertical direction due to the higher vertical loads on its bearings.

As a final statement, the planetary gearbox and shafts cannot be considered separately in a geared rotor system for a correct dynamic response prediction.

7.2 Future Recommendations

During this PhD research project, some topics in the investigation of planetary geared rotor dynamics have been considered as potential research areas. The following topics are suggested for further studies:

i. Analysing parameter sensitivity of planetary geared rotor vibration modes using modal energy analysis.

ii. Forced vibration response analysis of planetary geared rotors due to the imbalance of gears and the gear transmission error excitation.

iii. Investigation of the nonlinear gear backlash effect on the modal behaviour and vibration responses of geared rotor systems.

iv. Modifying the hybrid dynamic model of the planetary geared rotor system by considering the flexibility of gear bodies.

v. Investigation of the planetary gearbox damping effect on the modal behaviour of planetary geared rotor systems.

vi. Torsional vibration analysis of a planetary geared rotor system by using a continuous system model.

vii. Forced and free vibration analysis of planetary geared rotor systems under variable operating temperature.

viii. Modal analyses of planetary geared rotors with different gear materials.

ix. Comparison of the dynamic response of planetary geared rotor systems with rotating carrier-fixed ring and rotating ring gear-fixed carrier planetary gearbox configurations.

x. Aeroelastic dynamic analysis and modal behaviour investigation of a planetary geared fan system.

References

[1] A. Muszynska, Rotordynamics, CRC Press, 2005. doi:10.1201/9781420027792.

[2] G. Genta, Dynamics of rotating systems, Springer Science & Business Media, 2007.

[3] M.I. Friswell, J.E.T. Penny, S.D. Garvey, A.W. Lees, Dynamics of Rotating Machines, Cambridge University Press, Cambridge, 2010. doi:10.1017/CBO9780511780509.

[4] J.S. Rao, History of Rotating Machinery Dynamics, Springer Netherlands, Dordrecht, 2011. doi:10.1007/978-94-007-1165-5.

[5] Y. Ishida, T. Yamamoto, Linear and Nonlinear Rotordynamics, Wiley-VCH Verlag GmbH & Co. KGaA, Weinheim, Germany, 2012. doi:10.1002/9783527651894.

[6] C.G. Cooley, R.G. Parker, A Review of Planetary and Epicyclic Gear Dynamics and Vibrations Research, Appl. Mech. Rev. 66 (2014) 040804. doi:10.1115/1.4027812.

[7] J. Yang, L. Dai, Survey of dynamics of planetary gear trains, Int. J. Mater. Struct. Integr. 1 (2008) 302–322.

[8] A. Kahraman, R. Singh, Non-linear dynamics of a spur gear pair, J. Sound Vib. 142 (1990) 49–75. doi:10.1016/0022-460X(90)90582-K.

[9] H. Nevzat Özgüven, D.R. Houser, Mathematical models used in gear dynamics—A review, J. Sound Vib. 121 (1988) 383–411. doi:10.1016/S0022-460X(88)80365-1.

[10] J. Wang, R. Li, X. Peng, Survey of nonlinear vibration of gear transmission systems, Appl. Mech. Rev. 56 (2003) 309–329.

[11] S.S. Sutar, S. V Kadam, Dynamic Analysis of Geared Rotors - A Review, Int. J. Emerg. Technol. Adv. Eng. 2 (2012) 422–424.

[12] M. Li, T. Sun, H. Hu, Review on dynamics of geared rotor-bearing systems, J. Vib. Eng. 15 (2002) 249–261.

[13] F.C. Nelson, Rotor dynamics without equations, Int. J. COMADEM. 10 (2007) 2–10.

[14] B.O. Al-Bedoor, Modeling the coupled torsional and lateral vibrations of unbalanced rotors, Comput. Methods Appl. Mech. Eng. 190 (2001) 5999–6008. doi:10.1016/S0045-7825(01)00209-2.

[15] T.H. Patel, A.K. Darpe, Coupled bending-torsional vibration analysis of rotor with rub and crack, J. Sound Vib. 326 (2009) 740–752. doi:10.1016/j.jsv.2009.05.020.

[16] T. Szolc, On the Discrete–Continuous Modeling of Rotor Systems for the Analysis of Coupled Lateral Torsional Vibrations, Int. J. Rotating Mach. 6 (2000) 135–149. doi:10.1155/S1023621X00000130.

[17] Ö. Turhan, G. Bulut, Linearly coupled shaft-torsional and blade-bending vibrations in multi-stage rotor-blade systems, J. Sound Vib. 296 (2006) 292–318.

doi:10.1016/j.jsv.2006.03.010.

[18] S.Y. Yoon, Z. Lin, P.E. Allaire, Introduction to Rotor Dynamics, in: Control Surge Centrif. Compressors by Act. Magn. Bear., Springer, 2013: pp. 17–55. doi:10.1007/978-1-4471-4240-9_2.

[19] O. Cakmak, K.Y. Sanliturk, A dynamic model of an overhung rotor with ball bearings, Proc. Inst. Mech. Eng. Part K J. Multi-Body Dyn. 225 (2011) 310–321. doi:10.1177/1464419311408949.

[20] Y. Li, H. Cao, L. Niu, X. Jin, A General Method for the Dynamic Modeling of Ball Bearing–Rotor Systems, J. Manuf. Sci. Eng. 137 (2015) 021016. doi:10.1115/1.4029312.

[21] D.L. Thomas, J.M. Wilson, R.R. Wilson, Timoshenko beam finite elements, J. Sound Vib. 31 (1973) 315–330. doi:10.1016/S0022-460X(73)80276-7.

[22] H.D. Nelson, A Finite Rotating Shaft Element Using Timoshenko Beam Theory, J. Mech. Des. 102 (1980) 793. doi:10.1115/1.3254824.

[23] S. Jones, Finite element for the analysis of rotor-dynamic systems that include gyroscopic effects, (2005).

[24] F. Tisseur, K. Meerbergen, The Quadratic Eigenvalue Problem, SIAM Rev. 43 (2001) 235–286. doi:10.1137/S0036144500381988.

[25] M. Berhanu, The polynomial eigenvalue problem, University of Manchester, 2005.

[26] D.J. Ewins, Modal testing: theory, practice, and application, Research Studies Press, 2000.

[27] E.S. Gutiérrez-Wing, Modal Analysis of Rotating Machinery Structures, Vib. Univ. Technol. Cent. (2003) 169. doi:10.1007/BF02916201.

[28] C.L. Kessler, Complex modal analysis of rotating machinery, (1991) 111. doi:10.4271/1999-01-1835.

[29] I. Bucher, D.J. Ewins, Modal analysis and testing of rotating structures, Philos. Trans. R. Soc. London. Ser. A Math. Phys. Eng. Sci. 359 (2001) 61–96. doi:10.1098/rsta.2000.0714.

[30] C. Lee, A complex modal testing theory for rotating machinery, Mech. Syst. Signal Process. 5 (1991) 119–137. doi:10.1016/0888-3270(91)90019-2.

[31] G.H. Golub, H.A. Van der Vorst, Eigenvalue computation in the 20th century, J. Comput. Appl. Math. 123 (2000) 35–65.

[32] Z. Zheng, G. Ren, F.W. Williams, The eigenvalue problem for damped gyroscopic systems, Int. J. Mech. Sci. 39 (1997) 741–750.

[33] W.R. Ferng, W.-W. Lin, C.-S. Wang, Numerical algorithms for undamped gyroscopic systems, Comput. Math. with Appl. 37 (1999) 49–66. doi:10.1016/S0898-1221(98)00241-7.

[34] J. Qian, W.W. Lin, A numerical method for quadratic eigenvalue problems of gyroscopic systems, J. Sound Vib. 306 (2007) 284–296. doi:10.1016/j.jsv.2007.05.009.

[35] F. Republic, Review Complex Article Eigenvalue Problems, 85 (1989).

[36] D. Kressner, Numerical Methods for General and Structured Eigenvalue Problems,

(2005).

[37] Y. Saad, Numerical Methods for Large Eigenvalue Problems: Revised Edition, SIAM, 2011.

[38] Z. Bai, Progress in the numerical solution of the nonsymmetric eigenvalue problem, Numer. Linear Algebr. with Appl. 2 (1995) 219–234.

[39] E. Anderson, Z. Bai, J. Dongarra, A. Greenbaum, A. McKenney, J. Du Croz, S. Hammerling, J. Demmel, C. Bischof, D. Sorensen, LAPACK: A portable linear algebra library for high-performance computers, in: Proc. 1990 ACM/IEEE Conf. Supercomput., IEEE Computer Society Press, 1990: pp. 2–11.

[40] D.J. Inman, Engineering vibration, Prentice Hall New Jersey, 2008.

[41] R. Kannan, S. Hendry, N.J. Higham, F. Tisseur, Detecting the causes of ill-conditioning in structural finite element models, Comput. Struct. 133 (2014) 79–89.

[42] J.D. Smith, Gear noise and vibration, CRC Press, 2003.

[43] Ö.S. Şener, H.N. Özgüven, Dynamic analysis of geared shaft systems by using a continuous system model, J. Sound Vib. 166 (1993) 539–556.

[44] R.W. Gregory, S.L. Harris, R.G. Munro, Dynamic behaviour of spur gears, Proc. Inst. Mech. Eng. 178 (1963) 207–218.

[45] P. Velex, On the Modelling of Spur and Helical Gear Dynamic Behaviour, (2012).

[46] R. Maliha, C.U. Doğruer, H.N. Özgüven, Nonlinear Dynamic Modeling of Gear-Shaft-Disk-Bearing Systems Using Finite Elements and Describing Functions, J. Mech. Des. 126 (2004) 534. doi:10.1115/1.1711819.

[47] R. Singh, H. Xie, R.J. Comparin, Analysis of automotive neutral grear rattle, J. Sound Vib. 131 (1989) 177–196.

[48] F. Pfeiffer, W. Prestl, Hammering in diesel-engine driveline systems, Nonlinear Dyn. 5 (1994) 477–492. doi:10.1007/BF00052455.

[49] S.N. Doğan, Loose part vibration in vehicle transmissions-Gear rattle, Turkish J. Eng. Environ. Sci. 23 (2000) 439–454.

[50] A. Kahraman, G.W. Blankenship, Experiments on nonlinear dynamic behavior of an oscillator with clearance and periodically time-varying parameters, J. Appl. Mech. 64 (1997) 217–226.

[51] C. Wang, S.R. Wang, B. Yang, G.Q. Wang, Dynamic modeling of double helical gears, J. Vib. Control. 24 (2018) 3989–3999. doi:10.1177/1077546317717885.

[52] M.R. Kang, A. Kahraman, An experimental and theoretical study of the dynamic behavior of double-helical gear sets, J. Sound Vib. 350 (2015) 11–29. doi:10.1016/j.jsv.2015.04.008.

[53] R.G. Parker, V. Agashe, S.M. Vijayakar, Dynamic Response of a Planetary Gear System Using a Finite Element/Contact Mechanics Model, J. Mech. Des. 122 (2002) 304. doi:10.1115/1.1286189.

[54] V. Abousleiman, P. Velex, A hybrid 3D finite element/lumped parameter model for quasi-static and dynamic analyses of planetary/epicyclic gear sets, Mech. Mach. Theory. 41 (2006) 725–748. doi:10.1016/j.mechmachtheory.2005.09.005.

[55] C.G. Cooley, R.G. Parker, S.M. Vijayakar, A Frequency Domain Finite Element

Approach for Three-Dimensional Gear Dynamics, J. Vib. Acoust. 133 (2011) 041004. doi:10.1115/1.4003399.

[56] A. Fidlin, Nonlinear oscillations in mechanical engineering, Springer Science & Business Media, 2005.

[57] D. Wagg, S.A. Neild, Nonlinear vibration with control, Springer, 2016.

[58] K. Worden, Nonlinearity in structural dynamics: detection, identification and modelling, CRC Press, 2019.

[59] G. Liu, R.G. Parker, Nonlinear dynamics of idler gear systems, Nonlinear Dyn. 53 (2008) 345–367. doi:10.1007/s11071-007-9317-z.

[60] T. Eritenel, R.G. Parker, An investigation of tooth mesh nonlinearity and partial contact loss in gear pairs using a lumped-parameter model, Mech. Mach. Theory. 56 (2012) 28–51.

[61] T. Eritenel, R.G. Parker, Nonlinear Vibration of Gears With Tooth Surface Modifications, J. Vib. Acoust. 135 (2013) 051005. doi:10.1115/1.4023913.

[62] M. Cirelli, P.P. Valentini, E. Pennestrì, A study of the non-linear dynamic response of spur gear using a multibody contact based model with flexible teeth, J. Sound Vib. 445 (2019) 148–167. doi:10.1016/j.jsv.2019.01.019.

[63] A. Kahraman, R. Singh, Interactions between time-varying mesh stiffness and clearance non-linearities in a geared system, J. Sound Vib. 146 (1991) 135–156.

[64] R.G. Parker, S.M. Vijayakar, T. Imajo, Non-linear dynamic response of a spur gear pair: modelling and experimental comparisons, J. Sound Vib. 237 (2000) 435–455.

[65] S. Theodossiades, S. Natsiavas, Non-linear dynamics of gear-pair systems with periodic stiffness and backlash, J. Sound Vib. 229 (2000) 287–310.

[66] G. Litak, M.I. Friswell, Vibration in gear systems, Chaos, Solitons & Fractals. 16 (2003) 795–800.

[67] S. Wei, Q.K. Han, X.J. Dong, Z.K. Peng, F.L. Chu, Dynamic response of a single-mesh gear system with periodic mesh stiffness and backlash nonlinearity under uncertainty, Nonlinear Dyn. 89 (2017) 49–60.

[68] J. Margielewicz, D. Gąska, G. Litak, Modelling of the gear backlash, Nonlinear Dyn. (2019). doi:10.1007/s11071-019-04973-z.

[69] Y. Yang, M. Xu, Y. Du, P. Zhao, Y. Dai, Dynamic analysis of nonlinear time-varying spur gear system subjected to multi-frequency excitation, J. Vib. Control. 25 (2019) 1210–1226. doi:10.1177/1077546318814951.

[70] J. fei Shi, X. feng Gou, L. yun Zhu, Modeling and analysis of a spur gear pair considering multi-state mesh with time-varying parameters and backlash, Mech. Mach. Theory. 134 (2019) 582–603. doi:10.1016/j.mechmachtheory.2019.01.018.

[71] P. Velex, V. Cahouet, Experimental and Numerical Investigations on the Influence of Tooth Friction in Spur and Helical Gear Dynamics, J. Mech. Des. 122 (2000) 515. doi:10.1115/1.1320821.

[72] G. Liu, R.G. Parker, Impact of tooth friction and its bending effect on gear dynamics, J. Sound Vib. 320 (2009) 1039–1063. doi:10.1016/j.jsv.2008.08.021.

[73] C. Siyu, T. Jinyuan, L. Caiwang, W. Qibo, Nonlinear dynamic characteristics of

geared rotor bearing systems with dynamic backlash and friction, Mech. Mach. Theory. 46 (2011) 466–478. doi:10.1016/j.mechmachtheory.2010.11.016.

[74] S. Li, A. Kahraman, A spur gear mesh interface damping model based on elastohydrodynamic contact behaviour, Int. J. Powertrains. 1 (2011) 4. doi:10.1504/IJPT.2011.041907.

[75] Y. Cui, Z. Liu, Y. Wang, J. Ye, Nonlinear Dynamic of a Geared Rotor System With Nonlinear Oil Film Force and Nonlinear Mesh Force, J. Vib. Acoust. 134 (2012) 041001. doi:10.1115/1.4005032.

[76] Y. Fang, X. Liang, M.J. Zuo, Effects of friction and stochastic load on transient characteristics of a spur gear pair, Nonlinear Dyn. 93 (2018) 599–609. doi:10.1007/s11071-018-4212-3.

[77] Z. Xiao, C. Zhou, S. Chen, Z. Li, Effects of oil film stiffness and damping on spur gear dynamics, Nonlinear Dyn. 96 (2019) 145–159. doi:10.1007/s11071-019-04780-6.

[78] W. Li, J. Sun, J. Yu, Analysis of dynamic characteristics of a multi-stage gear transmission system, JVC/Journal Vib. Control. 25 (2019) 1653–1662. doi:10.1177/1077546319830810.

[79] A. Kahraman, Planetary Gear Train Dynamics, J. Mech. Des. 116 (1994) 713. doi:10.1115/1.2919441.

[80] J. Lin, R.G. Parker, Analytical Characterization of the Unique Properties of Planetary Gear Free Vibration, J. Vib. Acoust. 121 (1999) 316–321. doi:10.1115/1.2893982.

[81] T. Eritenel, R.G. Parker, Modal properties of three-dimensional helical planetary gears, J. Sound Vib. 325 (2009) 397–420. doi:10.1016/j.jsv.2009.03.002.

[82] C.G. Cooley, R.G. Parker, Vibration Properties of High-Speed Planetary Gears With Gyroscopic Effects, J. Vib. Acoust. 134 (2012) 061014. doi:10.1115/1.4006646.

[83] L. Zhang, Y. Wang, K. Wu, R. Sheng, Q. Huang, Dynamic modeling and vibration characteristics of a two-stage closed-form planetary gear train, Mech. Mach. Theory. 97 (2016) 12–28. doi:10.1016/j.mechmachtheory.2015.10.006.

[84] L. Zhang, Y. Wang, K. Wu, R. Sheng, Three-Dimensional Modeling and Structured Vibration Modes of Two-Stage Helical Planetary Gears Used in Cranes, Shock Vib. 2017 (2017) 10–19. doi:10.1155/2017/9864959.

[85] W. Liu, Z. Shuai, Y. Guo, D. Wang, Modal properties of a two-stage planetary gear system with sliding friction and elastic continuum ring gear, Mech. Mach. Theory. 135 (2019) 251–270. doi:10.1016/j.mechmachtheory.2019.01.026.

[86] M. Inalpolat, A. Kahraman, Dynamic modelling of planetary gears of automatic transmissions, Proc. Inst. Mech. Eng. Part K J. Multi-Body Dyn. 222 (2008) 229–242. doi:10.1243/14644193JMBD138.

[87] W. Sun, X. Ding, J. Wei, X. Hu, Q. Wang, An analyzing method of coupled modes in multi-stage planetary gear system, Int. J. Precis. Eng. Manuf. 15 (2014) 2357–2366. doi:10.1007/s12541-014-0601-9.

[88] J. Wang, Y. Wang, Z. Huo, Analysis of dynamic behavior of multiple-stage planetary gear train used in wind driven generator, Sci. World J. 2014 (2014). doi:10.1155/2014/627045.

[89] H. Zhai, C. Zhu, C. Song, H. Liu, G. Li, F. Ma, Dynamic modeling and analysis for

transmission system of high-power wind turbine gearbox, J. Mech. Sci. Technol. 29 (2015) 4073–4082. doi:10.1007/s12206-015-0901-8.

[90] J. Wei, A. Zhang, D. Qin, T.C. Lim, R. Shu, X. Lin, F. Meng, A coupling dynamics analysis method for a multistage planetary gear system, Mech. Mach. Theory. 110 (2017) 27–49. doi:10.1016/j.mechmachtheory.2016.12.007.

[91] A. Zhang, J. Wei, D. Qin, S. Hou, Analytical coupling characterization of multi-stage planetary gear free vibration considering flexible structure, J. Vibroengineering. 19 (2017) 3994–4008. doi:10.21595/jve.2017.17767.

[92] A. Kahraman, Free torsional vibration characteristics of compound planetary gear sets, Mech. Mach. Theory. 36 (2001) 953–971. doi:10.1016/S0094-114X(01)00033-7.

[93] S. Dhouib, R. Hbaieb, F. Chaari, M.S. Abbes, T. Fakhfakh, M. Haddar, Free vibration characteristics of compound planetary gear train sets, Proc. Inst. Mech. Eng. Part C J. Mech. Eng. Sci. 222 (2008) 1389–1401. doi:10.1243/09544062JMES870.

[94] D.R. Kiracofe, R.G. Parker, Structured Vibration Modes of General Compound Planetary Gear Systems, J. Vib. Acoust. 129 (2007) 1. doi:10.1115/1.2345680.

[95] Y. Guo, R.G. Parker, Purely rotational model and vibration modes of compound planetary gears, Mech. Mach. Theory. 45 (2010) 365–377. doi:10.1016/j.mechmachtheory.2009.09.001.

[96] P. Sondkar, A. Kahraman, A dynamic model of a double-helical planetary gear set, Mech. Mach. Theory. 70 (2013) 157–174. doi:10.1016/j.mechmachtheory.2013.07.005.

[97] Z. Sheng, J. Tang, S. Chen, Z. Hu, Modal Analysis of Double-Helical Planetary Gears With Numerical and Analytical Approach, J. Dyn. Syst. Meas. Control. 137 (2015) 041012. doi:10.1115/1.4028788.

[98] S. Mo, Y. Zhang, Q. Wu, H. Houjoh, S. Matsumura, Research on natural characteristics of double-helical star gearing system for GTF aero-engine, Mech. Mach. Theory. 106 (2016) 166–189. doi:10.1016/j.mechmachtheory.2016.09.001.

[99] M. K Khoozani, M. Poursina, A. P Anaraki, Study of gyroscopic effects on the dynamics and vibrations of double-helical planetary gear set, Proc. Inst. Mech. Eng. Part K J. Multi-Body Dyn. 0 (2017) 1–25. doi:10.1177/1464419317725947.

[100] V. Abousleiman, P. Velex, S. Becquerelle, Modeling of Spur and Helical Gear Planetary Drives With Flexible Ring Gears and Planet Carriers, J. Mech. Des. 129 (2007) 95. doi:10.1115/1.2359468.

[101] X. Wu, R.G. Parker, Modal Properties of Planetary Gears With an Elastic Continuum Ring Gear, J. Appl. Mech. 75 (2008) 031014. doi:10.1115/1.2839892.

[102] R.G. Parker, X. Wu, Vibration modes of planetary gears with unequally spaced planets and an elastic ring gear, J. Sound Vib. 329 (2010) 2265–2275. doi:10.1016/j.jsv.2009.12.023.

[103] Z. Chen, Y. Shao, D. Su, Dynamic simulation of planetary gear set with flexible spur ring gear, J. Sound Vib. 332 (2013) 7191–7204. doi:10.1016/j.jsv.2013.07.026.

[104] Z. Fan, C. Zhu, C. Song, Dynamic Analysis of Planetary Gear Transmission System Considering the Flexibility of Internal Ring Gear, Iran. J. Sci. Technol. Trans. Mech. Eng. (2019). doi:10.1007/s40997-019-00290-3.

[105] J.L.M. Peeters, D. Vandepitte, P. Sas, Analysis of internal drive train dynamics in a wind turbine, Wind Energy. 9 (2006) 141–161. doi:10.1002/we.173.

[106] M. Zhao, J. Ji, Dynamic analysis of wind turbine gearbox components, Energies. 9 (2016) 1–18. doi:10.3390/en9020110.

[107] D.C. Fyler, M. Inalpolat, A Dynamic Model for Double-Planet Planetary Gearsets, J. Vib. Acoust. 138 (2016) 021006. doi:10.1115/1.4032181.

[108] F. Concli, L. Cortese, R. Vidoni, F. Nalli, G. Carabin, A mixed FEM and lumped-parameter dynamic model for evaluating the modal properties of planetary gearboxes †, J. Mech. Sci. Technol. 32 (2018) 3047–3056. doi:10.1007/s12206-018-0607-9.

[109] T.M. Ericson, R.G. Parker, Planetary gear modal vibration experiments and correlation against lumped-parameter and finite element models, J. Sound Vib. 332 (2013) 2350–2375. doi:10.1016/j.jsv.2012.11.004.

[110] A. Hammami, A.F. Del Rincon, F.V. Rueda, F. Chaari, M. Haddar, Modal analysis of back-to-back planetary gear: experiments and correlation against lumped-parameter model, J. Theor. Appl. Mech. (2015) 125. doi:10.15632/jtam-pl.53.1.125.

[111] A. Mbarek, A.F. Del Rincon, A. Hammami, M. Iglesias, F. Chaari, F. Viadero, M. Haddar, Comparison of experimental and operational modal analysis on a back to back planetary gear, Mech. Mach. Theory. 124 (2018) 226–247. doi:10.1016/j.mechmachtheory.2018.03.005.

[112] T.M. Ericson, R.G. Parker, Experimental measurement of the effects of torque on the dynamic behavior and system parameters of planetary gears, Mech. Mach. Theory. 74 (2014) 370–389. doi:10.1016/j.mechmachtheory.2013.12.018.

[113] J. Lin, R.G. Parker, Sensitivity of planetary gear natural frequencies and vibration modes to model parameters, J. Sound Vib. 228 (1999) 109–128.

[114] Y. Guo, R.G. Parker, Sensitivity of General Compound Planetary Gear Natural Frequencies and Vibration Modes to Model Parameters, J. Vib. Acoust. 132 (2010) 011006. doi:10.1115/1.4000461.

[115] Z. Cao, Y. Shao, M. Rao, W. Yu, Effects of the gear eccentricities on the dynamic performance of a planetary gear set, Nonlinear Dyn. 91 (2018) 1–15. doi:10.1007/s11071-017-3738-0.

[116] A. Mbarek, A. Hammami, A. Fernandez Del Rincon, F. Chaari, F. Viadero Rueda, M. Haddar, Effect of load and meshing stiffness variation on modal properties of planetary gear, Appl. Acoust. 147 (2019) 32–43. doi:10.1016/j.apacoust.2017.08.010.

[117] T. Sun, H.Y. Hu, Nonlinear dynamics of a planetary gear system with multiple clearances, Mech. Mach. Theory. 38 (2003) 1371–1390. doi:10.1016/S0094-114X(03)00093-4.

[118] A. Al-Shyyab, A. Kahraman, A non-linear dynamic model for planetary gear sets, Proc. Inst. Mech. Eng. Part K J. Multi-Body Dyn. 221 (2007) 567–576. doi:10.1243/14644193JMBD92.

[119] L. Xiang, Y. Zhang, N. Gao, A. Hu, J. Xing, Nonlinear Dynamics of a Multistage Gear Transmission System with Multi-Clearance, Int. J. Bifurc. Chaos. 28 (2018) 1850034. doi:10.1142/s0218127418500347.

[120] L. Xiang, N. Gao, A. Hu, Dynamic analysis of a planetary gear system with multiple nonlinear parameters, J. Comput. Appl. Math. 327 (2018) 325–340.

doi:10.1016/j.cam.2017.06.021.

[121] C. Xun, X. Long, H. Hua, Effects of random tooth profile errors on the dynamic behaviors of planetary gears, J. Sound Vib. 415 (2018) 91–110. doi:10.1016/j.jsv.2017.11.022.

[122] Z. Zhu, L. Cheng, R. Xu, R. Zhu, Impacts of Backlash on Nonlinear Dynamic Characteristic of Encased Differential Planetary Gear Train, Shock Vib. 2019 (2019) 1–15. doi:10.1155/2019/9347925.

[123] V.K. Ambarisha, R.G. Parker, Nonlinear dynamics of planetary gears using analytical and finite element models, J. Sound Vib. 302 (2007) 577–595. doi:10.1016/j.jsv.2006.11.028.

[124] C.-J. Bahk, R.G. Parker, Analytical Solution for the Nonlinear Dynamics of Planetary Gears, J. Comput. Nonlinear Dyn. 6 (2011) 021007. doi:10.1115/1.4002392.

[125] W. Kim, J.Y. Lee, J. Chung, Dynamic analysis for a planetary gear with time-varying pressure angles and contact ratios, J. Sound Vib. 331 (2012) 883–901. doi:10.1016/j.jsv.2011.10.007.

[126] Y. Guo, J. Keller, R.G. Parker, Dynamic analysis of wind turbine planetary gears using an extended harmonic balance approach, in: Proc. Int. Conf. Noise Vib. Eng., 2012: pp. 4329–4343.

[127] Y. Guo, J. Keller, R.G. Parker, Nonlinear dynamics and stability of wind turbine planetary gear sets under gravity effects, Eur. J. Mech. A/Solids. 47 (2014) 45–57. doi:10.1016/j.euromechsol.2014.02.013.

[128] W. Zhu, S. Wu, X. Wang, Z. Peng, Harmonic balance method implementation of nonlinear dynamic characteristics for compound planetary gear sets, Nonlinear Dyn. 81 (2015) 1511–1522. doi:10.1007/s11071-015-2084-3.

[129] J. Zhou, W. Sun, L. Yuan, Nonlinear Vibroimpact Characteristics of a Planetary Gear Transmission System, Shock Vib. 2016 (2016) 1–11. doi:10.1155/2016/4304525.

[130] K. Salagianni, P. Nikolakopoulos, S. Theodossiades, Dynamic and tribological study of a planetary gearbox with local nonlinearities, Proc. Inst. Mech. Eng. Part K J. Multi-Body Dyn. 231 (2017) 504–518. doi:10.1177/1464419317720602.

[131] P. Ma, M. Botman, Load Sharing in a Planetary Gear Stage in the Presence of Gear Errors and Misalignment, J. Mech. Transm. Autom. Des. 107 (1985) 4. doi:10.1115/1.3258694.

[132] A. Kahraman, Load sharing characteristics of planetary transmissions, Mech. Mach. Theory. 29 (1994) 1151–1165. doi:10.1016/0094-114X(94)90006-X.

[133] H. Ligata, A. Kahraman, A. Singh, An Experimental Study of the Influence of Manufacturing Errors on the Planetary Gear Stresses and Planet Load Sharing, J. Mech. Des. 130 (2008) 041701. doi:10.1115/1.2885194.

[134] H. Ligata, A. Kahraman, A. Singh, A Closed-Form Planet Load Sharing Formulation for Planetary Gear Sets Using a Translational Analogy, J. Mech. Des. 131 (2009) 021007. doi:10.1115/1.3042160.

[135] A. Singh, Load sharing behavior in epicyclic gears: Physical explanation and generalized formulation, Mech. Mach. Theory. 45 (2010) 511–530. doi:10.1016/j.mechmachtheory.2009.10.009.

[136] M. Shuai, Z. Yidu, W. Qiong, Research on multiple-split load sharing of two-stage star gearing system in consideration of displacement compatibility, Mech. Mach. Theory. 88 (2015) 1–15. doi:10.1016/j.mechmachtheory.2015.01.005.

[137] N. Leque, A. Kahraman, A Three-Dimensional Load Sharing Model of Planetary Gear Sets Having Manufacturing Errors, J. Mech. Des. 139 (2017) 033302. doi:10.1115/1.4035554.

[138] M. Li, L. Xie, L. Ding, Load sharing analysis and reliability prediction for planetary gear train of helicopter, Mech. Mach. Theory. 115 (2017) 97–113. doi:10.1016/j.mechmachtheory.2017.05.001.

[139] Y. Hu, D. Talbot, A. Kahraman, A Load Distribution Model for Planetary Gear Sets, J. Mech. Des. 140 (2018) 053302. doi:10.1115/1.4039337.

[140] S. Mo, T. Zhang, G. Jin, Z. Feng, J. Gong, S. Zhu, Dynamic Characteristics and Load Sharing of Herringbone Wind Power Gearbox, Math. Probl. Eng. 2018 (2018) 1–24. doi:10.1155/2018/7251645.

[141] R.G. Parker, A physical explanation for the effectiveness of planet phasing to suppress planetary gear vibration, J. Sound Vib. 236 (2000) 561–573. doi:10.1006/jsvi.1999.2859.

[142] R.G. Parker, J. Lin, Mesh Phasing Relationships in Planetary and Epicyclic Gears, J. Mech. Des. 126 (2004) 365. doi:10.1115/1.1667892.

[143] S.H. Gawande, S.N. Shaikh, Experimental Investigations of Noise Control in Planetary Gear Set by Phasing, J. Eng. (United States). (2014). doi:10.1155/2014/857462.

[144] A. Kahraman, H.N. Ozguven, D.R. Houser, J.J. Zakrajsek, Dynamic Analysis of Geared Rotors by Finite Elements, J. Mech. Des. 114 (1992) 507. doi:10.1115/1.2926579.

[145] A. Saxena, M. Chouksey, A. Parey, Modal analysis of geared rotor system using finite element method, in: Multi-Disciplinary Sustain. Eng. Curr. Futur. Trends, CRC Press, 2016: pp. 413–417. doi:10.1201/b20013-68.

[146] S. Chen, J. Tang, Y. Li, Z. Hu, Rotordynamics analysis of a double-helical gear transmission system, Meccanica. 51 (2016) 251–268. doi:10.1007/s11012-015-0194-0.

[147] S. Chen, J. Tang, C. Zhou, Z. Hu, Modal and whirling analysis of coupled lateral and torsional vibration of herringbone gear, Int. J. Dyn. Control. 2 (2014) 404–414. doi:10.1007/s40435-013-0042-9.

[148] Y. Zhang, Q. Wang, H. Ma, J. Huang, C. Zhao, Dynamic analysis of three-dimensional helical geared rotor system with geometric eccentricity, J. Mech. Sci. Technol. 27 (2013) 3231–3242. doi:10.1007/s12206-013-0846-8.

[149] J.S. Rao, T.N. Shiau, J.R. Chang, Theoretical analysis of lateral response due to torsional excitation of geared rotors, Mech. Mach. Theory. 33 (1998) 761–783. doi:10.1016/S0094-114X(97)00056-6.

[150] S.-T. Choi, S.-Y. Mau, Dynamic Analysis of Geared Rotor-Bearing Systems by the Transfer Matrix Method, J. Mech. Des. 123 (2002) 562. doi:10.1115/1.1415739.

[151] C.-F. Li, S.-H. Zhou, J. Liu, B.-C. Wen, Coupled lateral-torsional-axial vibrations of a helical gear-rotor-bearing system, Acta Mech. Sin. 30 (2014) 746–761. doi:10.1007/s10409-014-0063-4.

[152] Q. Gao, M. Tanabe, K. Nishihara, Contact-impact analysis of geared rotor systems, J. Sound Vib. 319 (2009) 463–475. doi:10.1016/j.jsv.2008.05.023.

[153] J.W. David, L.D. Mitchell, Linear dynamic coupling in geared rotor systems, J. Vib. Acoust. Stress. Reliab. Des. 108 (1986) 171–176.

[154] T.N. Shiau, J.S. Rao, J.R. Chang, S.-T. Choi, Dynamic Behavior of Geared Rotors, J. Eng. Gas Turbines Power. 121 (1999) 494–503.

[155] S. Zhou, Z. Ren, G. Song, B. Wen, Dynamic Characteristics Analysis of the Coupled Lateral-Torsional Vibration with Spur Gear System, Int. J. Rotating Mach. 2015 (2015) 1–14. doi:10.1155/2015/371408.

[156] Z. Hu, J. Tang, S. Chen, Analysis of coupled lateral-torsional vibration response of a geared shaft rotor system with and without gyroscopic effect, J. Mech. Eng. Sci. (2018) 1–14. doi:10.1177/0954406217753457.

[157] M. Li, H.Y. Hu, Dynamic analysis of a spiral bevel-geared rotor-bearing system, J. Sound Vib. 259 (2003) 605–624. doi:10.1006/jsvi.2002.5111.

[158] X. Hua, T.C. Lim, T. Peng, W.E. Wali, Dynamic analysis of spiral bevel geared rotor systems applying finite elements and enhanced lumped parameters, Int. J. Automot. Technol. 13 (2012) 97–107. doi:10.1007/s12239-012-0009-4.

[159] Z. Hu, J. Tang, S. Chen, Z. Sheng, Coupled translation-rotation vibration and dynamic analysis of face geared rotor system, J. Sound Vib. 351 (2015) 282–298. doi:10.1016/j.jsv.2015.04.033.

[160] Y. Wang, H.M.E. Cheung, W.J. Zhang, Finite element modelling of geared multi-body system, Commun. Numer. Methods Eng. 18 (2002) 765–778. doi:10.1002/cnm.526.

[161] H.Y. Qi, L. Liu, Finite Element Analysis for Vibration Characteristic on Gear Rotors, Appl. Mech. Mater. 273 (2013) 193–197. doi:10.4028/www.scientific.net/AMM.273.193.

[162] M. Kubur, A. Kahraman, D.M. Zini, K. Kienzle, Dynamic Analysis of a Multi-Shaft Helical Gear Transmission by Finite Elements: Model and Experiment, J. Vib. Acoust. 126 (2004) 398. doi:10.1115/1.1760561.

[163] K. V. S. Seshendra Kumar, B. S. K. SundaraSiva Rao, An Experimental Study of Whirling Characteristics of Gear-Pinion Rotor System, Int. J. Mech. Appl. 2 (2012) 10–13. doi:10.5923/j.mechanics.20120202.03.

[164] M. Yin, G. Chen, H. Su, Theoretical and experimental studies on dynamics of double-helical gear system supported by journal bearings, Adv. Mech. Eng. 8 (2016) 1–13. doi:10.1177/1687814016646977.

[165] A. Saxena, M. Chouksey, A. Parey, Measurement of FRFs of coupled geared rotor system and the development of an accurate finite element model, Mech. Mach. Theory. 123 (2018) 66–75. doi:10.1016/j.mechmachtheory.2018.01.010.

[166] Z. Wang, Y. Yuan, Z. Wang, Y. Guo, D. Wang, W. Liu, Lateral-Torsional Coupling Characteristics of a Two-Stage Planetary Gear Rotor System, Shock Vib. 2018 (2018). https://doi.org/10.1155/2018/4293475.

[167] Z. Hu, J. Tang, J. Zhong, S. Chen, Frequency spectrum and vibration analysis of high speed gear-rotor system with tooth root crack considering transmission error excitation, Eng. Fail. Anal. 60 (2016) 405–441. doi:10.1016/j.engfailanal.2015.11.021.

[168] Z. Hu, J. Tang, J. Zhong, S. Chen, H. Yan, Effects of tooth profile modification on dynamic responses of a high speed gear-rotor-bearing system, Mech. Syst. Signal Process. 76–77 (2016) 294–318. doi:10.1016/j.ymssp.2016.01.020.

[169] A. Kahraman, R. Singh, Non-linear dynamics of a geared rotor-bearing system with multiple clearances, J. Sound Vib. 144 (1991) 469–506. doi:10.1016/0022-460X(91)90564-Z.

[170] H.N. Özgüven, D.R. Houser, Dynamic analysis of high speed gears by using loaded static transmission error, J. Sound Vib. 125 (1988) 71–83. doi:10.1016/0022-460X(88)90416-6.

[171] H. Zhang, G. Wei, B. Wen, Q. Han, H. Hao, Meshing characteristics of geared rotor system in integrally geared compressor with unbalance excitation, J. Vib. Control. 25 (2019) 26–40. doi:10.1177/1077546318767559.

[172] L. Xiang, N. Gao, Coupled torsion–bending dynamic analysis of gear-rotor-bearing system with eccentricity fluctuation, Appl. Math. Model. 50 (2017) 569–584. doi:10.1016/j.apm.2017.06.026.

[173] W. Yu, C.K. Mechefske, M. Timusk, The dynamic coupling behaviour of a cylindrical geared rotor system subjected to gear eccentricities, Mech. Mach. Theory. 107 (2017) 105–122. doi:10.1016/j.mechmachtheory.2016.09.017.

[174] Y. Yang, J. Wang, X. Wang, Y. Dai, A general method to predict unbalance responses of geared rotor systems, J. Sound Vib. 381 (2016) 246–263. doi:10.1016/j.jsv.2016.06.031.

[175] H. Zhang, J. Zhai, Q. Han, W. Sun, Dynamics of a geared parallel-rotor system subjected to changing oil-bearing stiffness due to external loads, Finite Elem. Anal. Des. 106 (2015) 32–40. doi:10.1016/j.finel.2015.07.008.

[176] H.N. Özgüven, A non-linear mathematical model for dynamic analysis of spur gears including shaft and bearing dynamics, J. Sound Vib. 145 (1991) 239–260. doi:10.1016/0022-460X(91)90590-G.

[177] S. Chowdhury, R.K. Yedavalli, Dynamics of low speed geared shaft systems mounted on rigid bearings, Mech. Mach. Theory. 112 (2017) 123–144. doi:10.1016/j.mechmachtheory.2017.02.002.

[178] S. Chowdhury, R.K. Yedavalli, Vibration of high speed helical geared shaft systems mounted on rigid bearings, Int. J. Mech. Sci. 142–143 (2018) 176–190. doi:10.1016/j.ijmecsci.2018.04.033.

[179] Z. Hu, J. Tang, S. Chen, D. Lei, Effect of Mesh Stiffness on the Dynamic Response of Face Gear Transmission System, J. Mech. Des. 135 (2013) 071005. doi:10.1115/1.4024369.

[180] W. Shi, C.-W. Kim, C.-W. Chung, H.-C. Park, Dynamic Modeling and Analysis of a Wind Turbine Drivetrain Using the Torsional Dynamic Model, Int. J. Precis. Eng. Manuf. 14 (2013) 153–159. doi:10.1007/s12541-013-0021-2.

[181] H.-L. Yao, Y. Liu, Z.-H. Ren, B.-C. Wen, C.-F. Li, Research on Dynamic Modeling and Analysis of the Coupled Planetary Gear and Rotor System, in: P. Pennacchi (Ed.), Proc. 9th IFToMM Int. Conf. Rotor Dyn., Springer International Publishing, Cham, 2015: pp. 1323–1331. doi:10.1007/978-3-319-06590-8_108.

[182] S. Wei, J. Zhao, Q. Han, F. Chu, Dynamic response analysis on torsional vibrations of

wind turbine geared transmission system with uncertainty, Renew. Energy. 78 (2015) 60–67. doi:10.1016/j.renene.2014.12.062.

[183] H. Dong, C. Zhang, D. Wang, S. Xu, J. Qiu, Dynamic characteristics of gear box with PGT for wind turbine, Procedia Comput. Sci. 109 (2017) 801–808. doi:10.1016/j.procs.2017.05.331.

[184] C. Zhu, S. Chen, C. Song, H. Liu, H. Bai, F. Ma, Dynamic analysis of a megawatt wind turbine drive train, J. Mech. Sci. Technol. 29 (2015) 1913–1919. doi:10.1007/s12206-015-0413-6.

[185] J. Helsen, F. Vanhollebeke, B. Marrant, D. Vandepitte, W. Desmet, Multibody modelling of varying complexity for modal behaviour analysis of wind turbine gearboxes, Renew. Energy. 36 (2011) 3098–3113. doi:10.1016/j.renene.2011.03.023.

[186] X. Jin, L. Li, W. Ju, Z. Zhang, X. Yang, Multibody modeling of varying complexity for dynamic analysis of large-scale wind turbines, Renew. Energy. 90 (2016) 336–351. doi:10.1016/j.renene.2016.01.003.

[187] A. Tatar, C.W. Schwingshackl, Effect of a Planetary Gearbox on the Dynamics of a Rotor System, in: ASME Turbo Expo 2018 Turbomach. Tech. Conf. Expo., American Society of Mechanical Engineers, Oslo, 2018: pp. 1–11.

[188] J. Wei, P. Bai, D. Qin, T.C. Lim, P. Yang, H. Zhang, Study on vibration characteristics of fan shaft of geared turbofan engine with sudden imbalance caused by blade off, J. Vib. Acoust. 140 (2018) 41010.

[189] S. Adhikari, Damping models for structural vibration, (2001).

[190] P. Sondkar, Dynamic modeling of double-helical planetary gear sets, The Ohio State University, 2012.

[191] P. Lynwander, Gear drive systems: Design and application, CRC Press, 1983.

[192] D. Ewins, E. Gutierrez-Wing, Modal characterisation of rotating machines, in: IMAC-XIX A Conf. Struct. Dyn., 2001: pp. 1249–1256.

[193] I. Bucher, D.J. Ewins, Modal analysis and testing of rotating structures, Philos. Trans. R. Soc. London A Math. Phys. Eng. Sci. 359 (2001) 61–96.

[194] E. Anderson, Z. Bai, C. Bischof, J. Demmel, J. Dongarra, J. Du Croz, A. Greenbaum, S. Hammarling, A. McKenney, S. Ostrouchov, LAPACK usersguide: Release 1.0, Argonne National Lab., IL (United States), 1992.

[195] C. Moler, Matlab incorporates LAPACK, Increasing Speed Capab. Matrix Comput. MATLAB News Notes–Winter. (2000).

[196] H. Koruk, K.Y. Sanliturk, A novel definition for quantification of mode shape complexity, J. Sound Vib. 332 (2013) 3390–3403. doi:10.1016/j.jsv.2013.01.039.

[197] I. Bucher, RotFE 2.1 The Finite Element Rotor Analysis Package, Fac. Mech. Eng. Tech. Haifa, User Man. (2000).

[198] G. Genta, D. Bassani, C. Delprete, DYNROT: A Matlab toolbox for rotordynamics analysis, (1994).

[199] M.I. Friswell, J.E.T. Penny, S.D. Garvey, A.W. Lees, Dynamics of Rotating Machines Rotordynamics Software Manual, Elements. (2010) 1–19.

[200] J.E. Shigley, Shigley's mechanical engineering design, Tata McGraw-Hill Education,

2011.

[201] H. Li, J. Liu, J. Ma, Y. Shao, Effect of the radial support stiffness of the ring gear on the vibrations for a planetary gear system, J. Low Freq. Noise, Vib. Act. Control. (2019) 146134841984464. doi:10.1177/1461348419844642.

[202] J. Tan, C. Zhu, C. Song, Y. Li, X. Xu, Dynamic modeling and analysis of wind turbine drivetrain considering platform motion, Mech. Mach. Theory. 140 (2019) 781–808. doi:10.1016/j.mechmachtheory.2019.06.026.

[203] X. Qiu, Q. Han, F. Chu, Dynamic modeling and analysis of the planetary gear under pitching base motion, Int. J. Mech. Sci. 141 (2018) 31–45. doi:10.1016/j.ijmecsci.2018.03.037.

Appendix A

Lagrange`s equations

Lagrangian function is expressed as

$$L = T - V, \tag{A.1}$$

where T and V are the kinetic and potential energies respectively. Then, the Lagrange`s equations of the second kind can be written as

$$\frac{d}{dt}\left(\frac{\partial L}{\partial \dot{q}_i}\right) - \frac{\partial L}{\partial q_i} = 0 \ \ (i = 1, 2, \dots, n), \tag{A.2}$$

by using the kinetic and potential energies. Here, q_i is generalized coordinate. t and n represent time and number of degrees of freedom respectively.

Appendix B

Springer copyright agreement

SPRINGER NATURE LICENSE TERMS AND CONDITIONS

Jun 21, 2019

This Agreement between Imperial College London -- Ali Tatar ("You") and Springer Nature ("Springer Nature") consists of your license details and the terms and conditions provided by Springer Nature and Copyright Clearance Center.

License Number	4613751262980
License date	Jun 21, 2019
Licensed Content Publisher	Springer Nature
Licensed Content Publication	Springer eBook
Licensed Content Title	Comparison of Computational Generalized and Standard Eigenvalue Solutions of Rotating Systems
Licensed Content Author	Ali Tatar, Loic Salles, Alexander H. Haslam et al
Licensed Content Date	Jan 1, 2019
Type of Use	Thesis/Dissertation
Requestor type	academic/university or research institute
Format	print and electronic
Portion	full article/chapter
Will you be translating?	no
Circulation/distribution	<501
Author of this Springer Nature content	yes
Title	Effect of planetary gearboxes on the dynamics of rotating systems
Institution name	Imperial College London
Expected presentation date	Sep 2019
Requestor Location	Imperial College London Exhibition Road London, SW7 2AZ United Kingdom Attn: Imperial College London

Elsevier copyright agreement

Copyright Clearance Center RightsLink®

Home | Account Info | Help | LIVE CHAT

Title: Dynamic behaviour of three-dimensional planetary geared rotor systems

Author: Ali Tatar,Christoph W. Schwingshackl,Michael I. Friswell

Publication: Mechanism and Machine Theory

Publisher: Elsevier

Date: April 2019

Logged in as:
Ali Tatar
Imperial College London
Account #:
3001462950

LOGOUT

Please note that, as the author of this Elsevier article, you retain the right to include it in a thesis or dissertation, provided it is not published commercially. Permission is not required, but please ensure that you reference the journal as the original source. For more information on this and on your other retained rights, please visit: https://www.elsevier.com/about/our-business/policies/copyright#Author-rights

BACK | CLOSE WINDOW